THE UNIVERSITY OF CHICAGO

EVALUATING THE USE OF INTRACORTICAL MICROSTIMULATION FOR TACTILE RESTORATION OF BIONIC HANDS IN PATIENTS WITH SPINAL CORD INJURY

A DISSERTATION SUBMITTED TO

THE FACULTY OF THE DIVISION OF THE BIOLOGICAL SCIENCES

AND THE PRITZKER SCHOOL OF MEDICINE

IN CANDIDACY FOR THE DEGREE OF

DOCTOR OF PHILOSOPHY

COMMITTEE ON COMPUTATIONAL NEUROSCIENCE

BY

NATALYA SHELCHKOVA

CHICAGO, ILLINOIS

DECEMBER 2024

Table of Contents

List of Figures

List of Supplementary Figures

Acknowledgments

Bensmaia Lab Members:

Sliman Bensmaia, in honor and in memory
Charles Greenspon
Ashley van Driesche
Elizaveta Okorokova
Anton Sobinov
John Downey

Thesis Committee:

Stephanie Palmer
Nicholas Hatsopoulos
Jason Maclean
Lee Miller

Family:

Mom, for all the sacrifices you've made, your strength and resilience, and for teaching me how to persevere in the face of adversity.
Alex, my partner and best friend, for your support and kindness through this journey, and for being a source of laughter and joy.

ABSTRACT

The importance of sensation in motor control is often under-appreciated despite the severe deficits that occur when that signal is lost. Thus, restoring sensation in bionic limbs is a crucial step in the advancement of prosthetic design. In patients with spinal cord injuries, this is accomplished by implanting arrays into primary somatosensory cortex (S1) through which the sense of touch can be restored with the use of intracortical microstimulation (ICMS). When evoking artificial sensations, the location of contact with an object is one crucial piece of information that is necessary for proper object manipulation. First, I demonstrate that the use of ICMS in Brodmann's Area 1 of S1 is a viable way of communicating contact location in a bionic limb as the sensations evoked through ICMS are stable over time and demonstrate the feasibility of this in a digit discrimination task. Second, I investigate the connectivity between S1 and primary motor cortex (M1) using ICMS and establish that there are connections between these regions through causal activation of M1 via ICMS of S1. Furthermore, I demonstrate that this connectivity is somatotopic with single digit resolution. I then considered the functional consequences of these connections on the performance of bionic hands in motor tasks and found that the use of linear stimulation impaired the decoding of motor intent and disrupted performance while biomimetic stimulation allowed us to provide sensory feedback without disrupting performance. Finally, I discuss the importance of these findings for the design of better prosthetics and our understanding of sensorimotor interactions.

CHAPTER 1 : INTRODUCTION

Our ability to dexterously interact with objects is the result of the interplay that occurs between the sensory and motor systems. While it may be easy to imagine the motor deficits that occur when motor pathways are damaged, the motor deficits that occur when sensory pathways are damaged may be harder to appreciate. Lesion studies to S1 in monkeys have demonstrated deficits in texture, shape, and size discrimination of objects[1–3]. Inactivation experiments using muscimol have reported difficulties with arm and finger coordination[4,5], and the ability to apply and maintain precise forces on objects[6].

Damage does not need to occur at the cortical level to observe these behavioral impairments; they can arise from damage to the periphery or spinal cord. Indeed, in humans with large-fiber neuropathy (which results in a loss of cutaneous and proprioceptive information) deficits in fine manual behavior have also been observed; they are unable to perform complex multi-joint movements, struggle to maintain forces on objects, and are unable to perform fine dexterous behaviors such as writing or buttoning a shirt[7–9]. Even a temporary removal of sensory information, e.g. by using anesthetic to numb the fingertips, results in severe deficits in participants' ability to grasp and manipulate objects[10,11]. Furthermore, the benefits of sensory feedback are also observed in robotics; the addition of sensory feedback in robotic surgery results in improved force control and less blunt force damage to tissues being operated upon[12]. Finally, in neuroprosthetics, the addition of sensory feedback improves the ability of the user to perform motor tasks[13,14].

Given the importance of sensation to manual dexterity, it is crucial that we consider its restoration in the design of prosthetic devices. One method to restore sensation is the use of

electrical stimulation. Penfield demonstrated that stimulation of different parts of cortex can result in artificial visual percepts, movements, and tactile sensations[15]. To this day, the use of intracortical microstimulation (ICMS) delivered through electrodes implanted into the brain is the standard method for providing sensory feedback in neuroprosthetic devices[13,16,17]. In order to restore tactile sensations we implant electrodes into S1 and can leverage the known somatotopy to target specific areas of the body[18] (Figure 1.1). This is especially important for patients with spinal cord injuries as other less invasive approaches such as peripheral nerve stimulation are not viable.

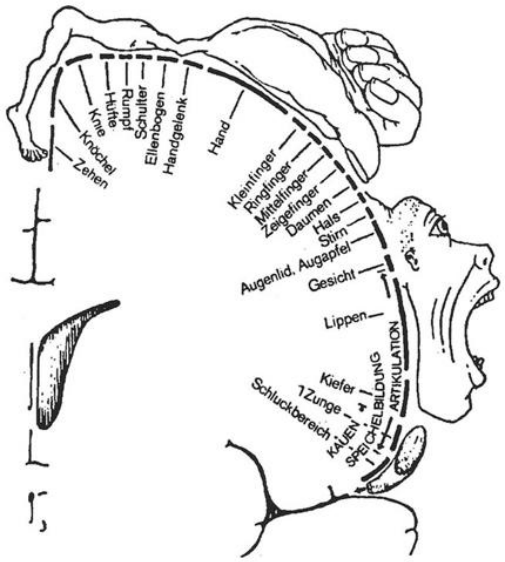

Figure 1.1. Somatotopy in primary somatosensory cortex. The sensory homunculus as described by Penfield; within S1 there exists a map of the body where neurons in each region are responsive to tactile events on distinct regions of the body. Adapted from Penfield and Rasmussen 1950.

With the goal of restoring tactile sensation through ICMS of S1, we must first consider its composition. First, S1 consists of four subregions, determined by differences in cytoarchitecture,

innervation, and responses[19] (Figure 1.2). For tactile sensation in particular, Areas 3b and 1 are most relevant, receiving exclusively tactile information, while Area 3a is the primary recipient of proprioceptive information and Area 2 receives a mixture of both. Additionally, we must consider surgical viability. In humans, Area 1 resides at the top of the gyrus, while Areas 3b and 2 are in the central and intraparietal sulci, respectively. Consequently, Area 1 is the only subregion that both facilitates the evocation of tactile signals and can be readily implanted

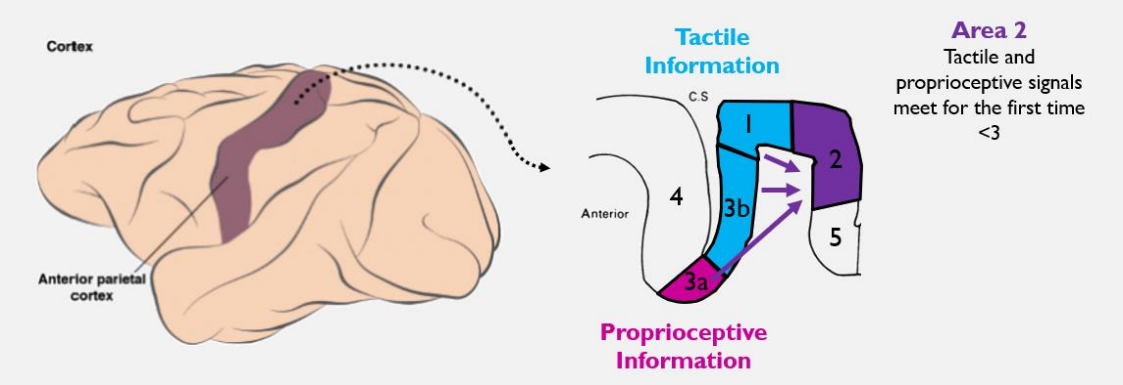

Figure 1.2. Primary somatosensory cortex consists of 4 regions. Area 3a is the primary recipient of proprioceptive information, arising from the muscles and joints. Areas 3b and 1 are tactile regions that receive tactile information, arising from the cutaneous mechanoreceptors which innervate the skin. Area 2 has both proprioceptive and tactile responses as it receives inputs from the other regions of S1. Adapted from Delhaye et al.

When ICMS is delivered through electrodes in Area 1, it produces a vivid tactile sensation, the location of which is defined as that electrode's projected field (PF)[17]. To convey contact location in an intuitive manner, we can map sensors on the robotic limb to electrodes whose projected field corresponds to the sensor location. To do so, experimenters collect subject reports about the location of the PF for each electrode and use that to generate these maps. However, to date there have been no studies quantifying the stability of these evoked percepts over time, and thus it is unclear if the associated mappings are stable and reliable or if

they must be repeated and, if so, at what frequency. We will address this question in Chapter 2 and show that PF location remains stable over many years and can be reliably used to convey contact location.

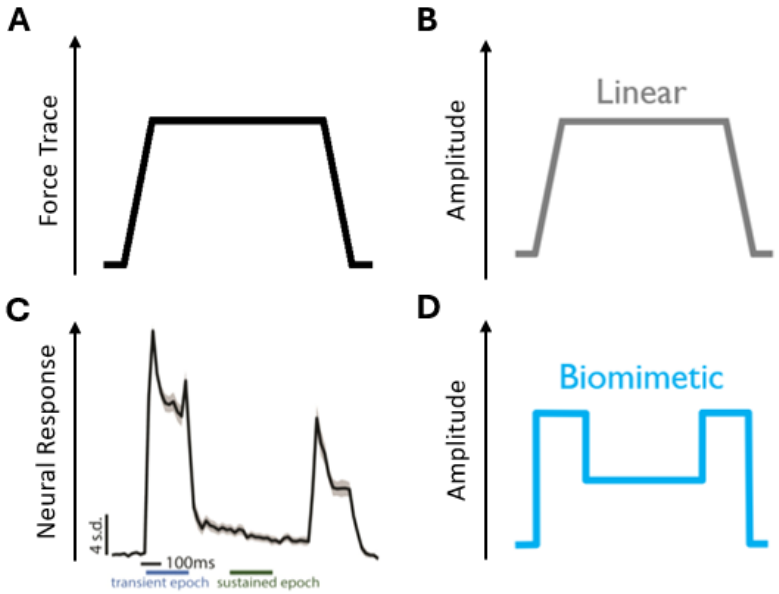

Figure 1.3. Intracortical microstimulation is used to restore feedback. A) Stereotyped force profile of a contact event. B) An example of a linear stimulation train, the amplitude of which can be determined by the experimenter or by inputs from a sensor. B) Indentations delivered to the digits have been used to study tactile responses in Area 1. D) An example of a biomimetic stimulation train, which has a higher amplitude at the onset and offset as seen in Area 1 neurons. Adapted from Callier, Suresh, and Bensmaia 2019.

When attempting to convey contact force, the salient feature we typically aim to reproduce is the intensity profile. A typical grasp is composed of three phases: initiation, maintenance, and release, which involve an increase, hold, and decrease in the force, respectively (Figure 1.3A). Consequently, we exploit the observation that the perceived intensity of the stimulus is directly related to the amplitude (current) and frequency of the ICMS train[17,20] and thus produce stimulation paradigms which use linear trains whose amplitude resemble a

step function or directly relate the stimulation level to the sensor readout (Figure 1.3B). However, whether this simple strategy is the most appropriate for evoking tactile sensations is unclear. Indeed, population recordings from BA1 to indentations on the digits show strong transients at the onset and offset of contact with lowered sustained response during the hold period[21] (Figure 1.3C). The biomimetic approach is thus to use stimulation trains that resemble these natural patterns of activation[22] (Figure 1.3D). In support of biomimetic stimulation, its implementation in peripheral nerve interfaces, where stimulation is delivered to the peripheral nerves via cuff electrodes, resulted in more natural sensations compared to linear trains[23,24]. One potential pitfall of using ICMS, linear or biomimetic, is that it is likely to disrupt our ability to decode motor intent, either through saturation of recording equipment or through unintentional activation of M1. Indeed, while sensory information is undoubtedly integrated by M1 and used for creating or updating movement plans, whether ICMS evoked activity in M1 will have useful or disruptive effects is unclear, though some work in humans has had promising results with bionic limb control[13], though they did not examine if this was because of ICMS-induced changes in M1 activity.

Anatomical tracing studies in monkeys have shown that there is reciprocal connectivity between M1 (specifically Area 4) and Area 1[25–30] (Figure 1.4) and suggested that the connected regions are somatotopically matched[31–33]. However, when somatotopy was established, the degree of overlap was not quantified, especially at the digit level. Furthermore, while electrical stimulation of S1 has been shown to elicit activity in motor neurons in mice[34], monkeys[35], and in humans[36], the functional consequences of this have not been investigated. There is currently active debate about the degree of somatotopy present in motor cortices, and therefore the

potential range of expectations that we might have about ICMS effect in motor cortex are broad. In Chapter 3, we demonstrate in humans that S1 and M1 are somatotopically connected with digit-level resolution. Furthermore, we demonstrate that the use of linear stimulation trains impedes the decoding of motor intent in closed loop motor tasks, while biomimetic stimulation allows us to provide sensory feedback without disrupting performance.

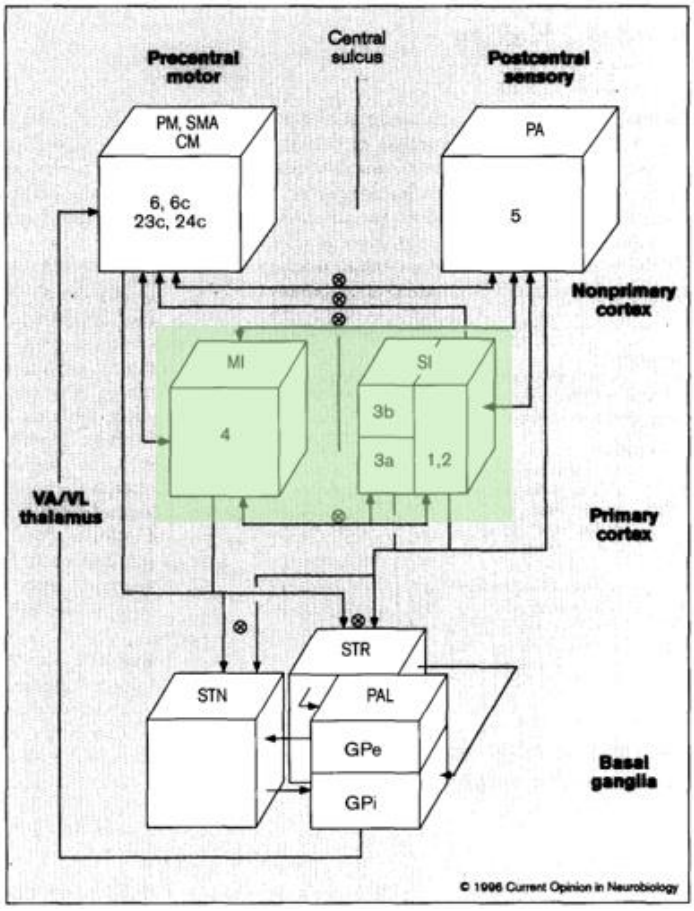

Figure 1.4. Sensory-motor connections are diverse and complex. S1 and M1 have reciprocal connectivity with one another as well as other structures across the brain. Adapted from Nelson 1996.

Finally, in Chapter 4 we discuss the implications of these findings for the design of better bionic limbs. The method for restoring sensation is not trivial and we need to better understand

how these sensory signals created through ICMS are used by the brain and our decoders during manual behavior.

1.1: References

1. Randolph, M. & Semmes, J. Behavioral consequences of selective subtotal ablations in the postcentral gyrus of Macaca mulatta. *Brain Research* **70**, 55–70 (1974).
2. Semmes, Josephine. & Turner, Blair. Effects of Cortical Lesions on Somatosensory Tasks. *Journal of Investigative Dermatology* **69**, 181–189 (1977).
3. Carlson, M. Characteristics of sensory deficits following lesions of brodmann's areas 1 and 2 in the postcentral gyrus ofMacaca mulatta. *Brain Research* **204**, 424–430 (1981).
4. Hikosaka, O., Tanaka, M., Sakamoto, M. & Iwamura, Y. Deficits in manipulative behaviors induced by local injections of muscimol in the first somatosensory cortex of the conscious monkey. *Brain Research* **325**, 375–380 (1985).
5. Goldring, A. B., Cooke, D. F., Pineda, C. R., Recanzone, G. H. & Krubitzer, L. A. Functional characterization of the fronto-parietal reaching and grasping network: Reversible deactivation of M1, areas 2, 5 and 7b in awake behaving monkeys. *Journal of Neurophysiology* (2022) doi:10.1152/jn.00279.2021.
6. Brochier, T., Boudreau, M.-J., Paré, M. & Smith, A. M. The effects of muscimol inactivation of small regions of motor and somatosensory cortex on independent finger movements and force control in the precision grip. *Experimental Brain Research* **128**, 31–40 (1999).
7. Sainburg, R. L., Ghilardi, M. F., Poizner, H. & Ghez, C. Control of limb dynamics in normal subjects and patients without proprioception. *Journal of Neurophysiology* **73**, 820–835 (1995).
8. Sanes, J. N., Mauritz, K. H., Evarts, E. V., Dalakas, M. C., & Chu, A. Motor deficits in patients with large-fiber sensory neuropathy. *Proceedings of the National Academy of Sciences* **81**, 979–982 (1984).
9. Rothwell, J. C. *et al.* Manual motor performance in a deafferented man. *Brain* **105**, 515–542 (1982).
10. Monzée, J., Lamarre, Y. & Smith, A. M. The Effects of Digital Anesthesia on Force Control Using a Precision Grip. *Journal of Neurophysiology* **89**, 672–683 (2003).

11. Johansson, R. S., Häger, C. & Bäckström, L. Somatosensory control of precision grip during unpredictable pulling loads. *Exp Brain Res* **89**, 204–213 (1992).

12. Wagner, C. R., Howe, R. D. & Stylopoulos, N. The Role of Force Feedback in Surgery: Analysis of Blunt Dissection. in *Proceedings of the 10th Symposium on Haptic Interfaces for Virtual Environment and Teleoperator Systems* 73 (IEEE Computer Society, USA, 2002).

13. Flesher, S. N. *et al.* A brain-computer interface that evokes tactile sensations improves robotic arm control. *Science* **372**, 831–836 (2021).

14. Valle, G., Petrini, F. M., Mijovic, P., Mijovic, B. & Raspopovic, S. A Computer-Brain Interface that Restores Lost Extremities' Touch and Movement Sensations. in *Brain-Computer Interface Research: A State-of-the-Art Summary 10* (eds. Guger, C., Allison, B. Z. & Gunduz, A.) 65–73 (Springer International Publishing, Cham, 2021). doi:10.1007/978-3-030-79287-9_7.

15. Penfield, W. & Boldrey, E. SOMATIC MOTOR AND SENSORY REPRESENTATION IN THE CEREBRAL CORTEX OF MAN AS STUDIED BY ELECTRICAL STIMULATION. *Brain* **60**, 389–443 (1937).

16. Torab, K. *et al.* Multiple factors may influence the performance of a visual prosthesis based on intracortical microstimulation: Nonhuman primate behavioural experimentation. *Journal of Neural Engineering* **8**, 035001–035001 (2011).

17. Flesher, S. N. *et al.* Intracortical microstimulation of human somatosensory cortex. *Science translational medicine* **8**, 361ra141 (2016).

18. Penfield, W. & Rasmussen, T. *The Cerebral Cortex of Man: A Clinical Study of Localization of Function*. (Macmillan, New York, 1950).

19. O'Connor, D. H., Krubitzer, L. & Bensmaia, S. Of mice and monkeys: Somatosensory processing in two prominent animal models. *Progress in Neurobiology* **201**, 102008 (2021).

20. Kim, S. *et al.* Behavioral assessment of sensitivity to intracortical microstimulation of primate somatosensory cortex. *PNAS* **112**, 15202–15207 (2015).

21. Callier, T., Suresh, A. K. & Bensmaia, S. J. Neural Coding of Contact Events in Somatosensory Cortex. *Cerebral Cortex* **29**, 4613–4627 (2019).

22. Okorokova, E. V., He, Q. & Bensmaia, S. J. Biomimetic encoding model for restoring touch in bionic hands through a nerve interface. *J. Neural Eng.* **15**, 066033 (2018).

23. Valle, G. *et al.* Biomimetic Intraneural Sensory Feedback Enhances Sensation Naturalness, Tactile Sensitivity, and Manual Dexterity in a Bidirectional Prosthesis. *Neuron* **100**, 37-45.e7 (2018).

24. George, J. A. *et al.* Biomimetic sensory feedback through peripheral nerve stimulation improves dexterous use of a bionic hand. *Science Robotics* **4**, (2019).

25. Jones, E. G., Coulter, J. D. & Hendry, S. H. C. lntracortical Connectivity of Architectonic Fields in the Somatic Sensory, Motor and Parietal Cortex of Monkeys. *Journal of Comparative Neurology* **181**, 291–348 (1978).

26. Vogt, B. A. & Pandya, D. N. Cortico-cortical connections of somatic sensory cortex (areas 3, 1 and 2) in the rhesus monkey. *Journal of Comparative Neurology* **177**, 179–191 (1978).

27. Jones, E. G., Burton, H. & Porter, R. Commissural and Cortico-Cortical 'Columns' in the Somatic Sensory Cortex of Primates. *Science* **190**, 572–574 (1975).

28. Darian-Smith, C., Darian-Smith, I., Burman, K. & Ratcliffe, N. Ipsilateral cortical projections to areas 3a, 3b, and 4 in the macaque monkey. *Journal of Comparative Neurology* **335**, 200–213 (1993).

29. Pons, T. P. & Kaas, J. H. Corticocortical connections of area 2 of somatosensory cortex in macaque monkeys: A correlative anatomical and electrophysiological study. *J. Comp. Neurol.* **248**, 313–335 (1986).

30. Jones, E. G. & Wise, S. P. Size, laminar and columnar distribution of efferent cells in the sensory-motor cortex of monkeys. *J of Comparative Neurology* **175**, 391–437 (1977).

31. Ghosh, S., Brinkman, C. & Porter, R. A quantitative study of the distribution of neurons projecting to the precentral motor cortex in the monkey (*M. fascicularis*). *J of Comparative Neurology* **259**, 424–444 (1987).

32. Jones, E. G. & Powell, T. P. S. Connexions of the Somatic Sensory Cortex of the Rhesus Monkey I: Ipsilateral Cortical Connexions. *Brain* **92**, 477–502 (1969).

33. Burton, H. & Fabri, M. Ipsilateral intracortical connections of physiologically defined cutaneous representations in areas 3b and 1 of macaque monkeys: Projections in the vicinity of the central sulcus. *J of Comparative Neurology* **355**, 508–538 (1995).

34. Petrof, I., Viaene, A. N. & Sherman, S. M. Properties of the primary somatosensory cortex projection to the primary motor cortex in the mouse. *Journal of Neurophysiology* **113**, 2400–2407 (2015).

35. Ruszala, B., Mazurek, K. A. & Schieber, M. H. Somatosensory cortex microstimulation modulates primary motor and ventral premotor cortex neurons with extensive spatial convergence and divergence. Preprint at https://doi.org/10.1101/2023.08.05.552025 (2023).

36. Osborn, L. E. *et al.* Intracortical microstimulation of somatosensory cortex generates evoked responses in motor cortex. in *2021 10th International IEEE/EMBS Conference on Neural Engineering (NER)* 53–56 (2021). doi:10.1109/NER49283.2021.9441123.

CHAPTER 2 : Quantifying the Stability of Intracortical Microstimulation Induced Percepts[1]

2.0: Contributions to the work

NDS and CMG collected the receptive field data together. NDS was responsible for analysis of sections 2.3.1 – 2.3.3. CMG contributed to sections 2.3.4 – 2.3.6.

2.1: Abstract

When we interact with objects, we rely on signals from the hand that convey information about the object and our interactions with it. A basic feature of these interactions, the locations of contacts between the hand and object, is often only available via the sense of touch. Information about locations of contact between a brain-controlled bionic hand and an object can be signaled via intracortical microstimulation (ICMS) of somatosensory cortex (S1), which evokes touch sensations that are localized to a specific patch of skin. To provide intuitive location information, tactile sensors on the robotic hand drive ICMS through electrodes that evoke sensations at skin locations matching sensor locations. This approach requires that ICMS-evoked sensations be focal, stable, and distributed over the hand. To systematically investigate the localization of ICMS-evoked sensations, we analyzed the projected fields (PFs) of ICMS-evoked sensations – their location and spatial extent – from reports obtained over multiple years from three participants implanted with microelectrode arrays in S1. First, we found that PFs vary widely in their size across electrodes, are highly stable within electrode, are distributed over large swaths of each participant's hand, and increase in size as the amplitude or frequency of ICMS increases.

[1] This article is available on bioRxiv: https://doi.org/10.1101/2023.06.23.545425

Second, while PF locations match the locations of the receptive fields (RFs) of the neurons near the stimulating electrode, PFs tend to be subsumed by the corresponding RFs. Third, multi-channel stimulation gives rise to a PF that reflects the conjunction of the PFs of the component channels. By stimulating through electrodes with largely overlapping PFs, then, we can evoke a sensation that is experienced primarily at the intersection of the component PFs. To assess the functional consequence of this phenomenon, we implemented multi-channel ICMS-based feedback in a bionic hand and demonstrated that the resulting sensations are more localizable than are those evoked via single-channel ICMS.

2.2: Introduction

When we interact with objects, signals from the hand convey information about the objects and about our interactions with them[1]. A basic feature of object interactions, the location on the hand of object contacts, is often only available via the sense of touch because some contacts are visually occluded and visual feedback, even when available, is a poor substitute for touch to guide object interactions[2]. Efforts are underway to restore tactile feedback via bionic hands by electrically activating touch neurons along the neuraxis[3]. Indeed, electrical activation of tactile nerve fibers evokes sensations experienced at a specific location on the skin, known as the projected field (PF)[4–9]. Similarly, intracortical microstimulation (ICMS) of somatosensory cortex (S1) typically evokes a sensation restricted to a specific patch of skin[10–13]. Force sensors on the bionic hand can thus be used to drive stimulation through electrodes in the nerve or in the brain that evoke sensations on the corresponding location on the phantom or deafferented hand, thereby intuitively conveying information about contact location.

The representation of the body in S1 is systematically organized, such that nearby body parts are encoded by the activity recorded from neighboring neuronal populations, with some discontinuities reflecting those in the body[14,15]. Stimulating through nearby electrodes has been shown to evoke sensations in nearby hand regions following the expected somatotopic organization[10,11]. Furthermore, the organization of S1 is consistent across individuals – with the hand representation featuring a systematic progression from the thumb to the little finger as one progresses in the medial posterior direction along the central sulcus. This organization facilitates electrode array placement because locating the respective S1 representations of a subset of digits informs the localization of the others. Pre-operative functional magnetic resonance imaging (fMRI), magnetoencephalography (MEG), or electroencephalography can be used to identify the digit representations and thus guide the placement of arrays of stimulating electrodes[11,16,17]. Critically, studies involving limited numbers of patients and electrodes have shown that PFs are relatively stable over time[11,18], suggesting that the somatotopic map is stable, even after deafferentation caused by spinal cord injury or amputation[19–21].

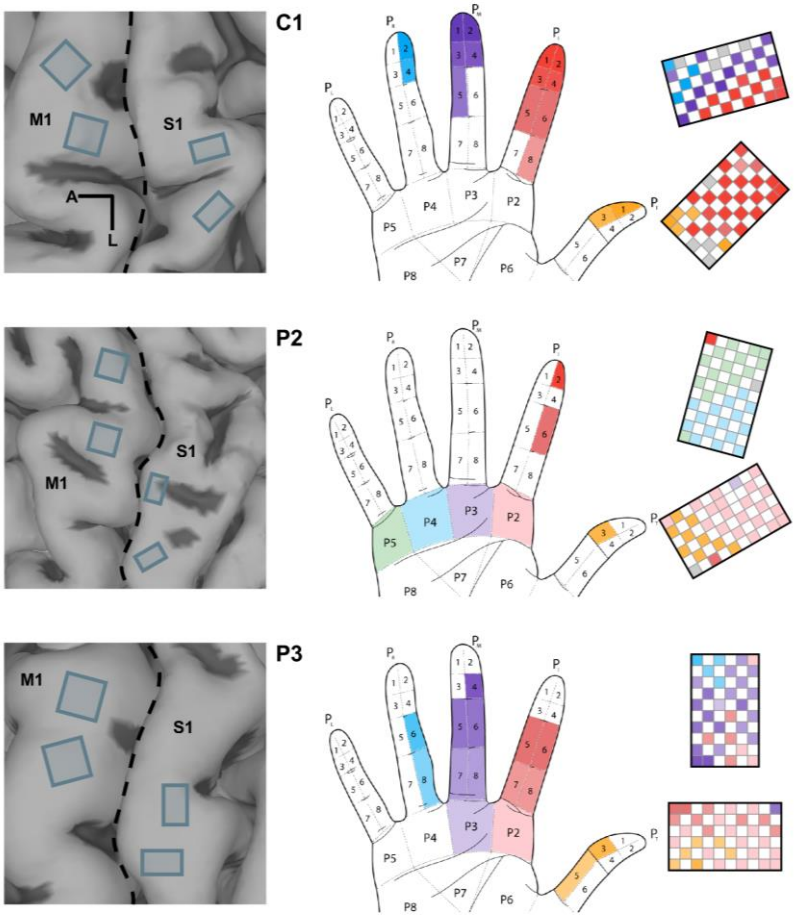

Figure 2.1. Array implant locations and sensation maps for all participants. *Left column*: Anatomical MRI with (subsequently implanted) arrays superimposed whose location is based on intra-operative photos. M1 and S1 denote primary motor cortex and somatosensory cortex (Brodmann's area 1), respectively. The central sulcus is indicated by the dashed line. *Middle and right columns*: The hand region on which ICMS-sensations are experienced along with the electrodes that evoked those sensations. Each row shows data from one participant.

Though electrical activation of S1 neurons has been shown to evoke focal sensations, these observations have been largely qualitative. The spatial extent, distribution, and stability of the evoked PFs have not been systematically evaluated[11,12,22]. To fill this gap, we quantitatively characterized the PFs of ICMS-evoked sensations in three human participants with cervical spinal

cord injury and gauged the degree to which they remained stable over a period of years. In an additional series of experiments with participants endowed with residual sensation, we also assessed the degree to which the PF of an electrode coincided with its receptive field (RF), defined as the patch of skin that, when touched, activates neurons around the electrode tip. First, we found that PFs are highly stable over time and cover large swaths of the hand (across two arrays in S1). Second, the locations of the PFs follow the expected somatotopic organization of the sensory homunculus. Third, increasing the amplitude or frequency of ICMS increases the size of the PF. Fourth, at the current levels tested, the PF of an electrode tends to be smaller than but largely subsumed by its RF. Fifth, ICMS delivered through multiple electrodes yields a PF reflecting a conjunction of the PFs of the individual electrodes; any overlapping regions of the PFs are thus more salient. Accordingly, stimulation through multiple electrodes with overlapping PFs enables improved localization of touches on a bionic hand compared to single-electrode stimulation. We discuss the implications of our findings for the development of sensitized brain-controlled bionic hands.

2.3: RESULTS

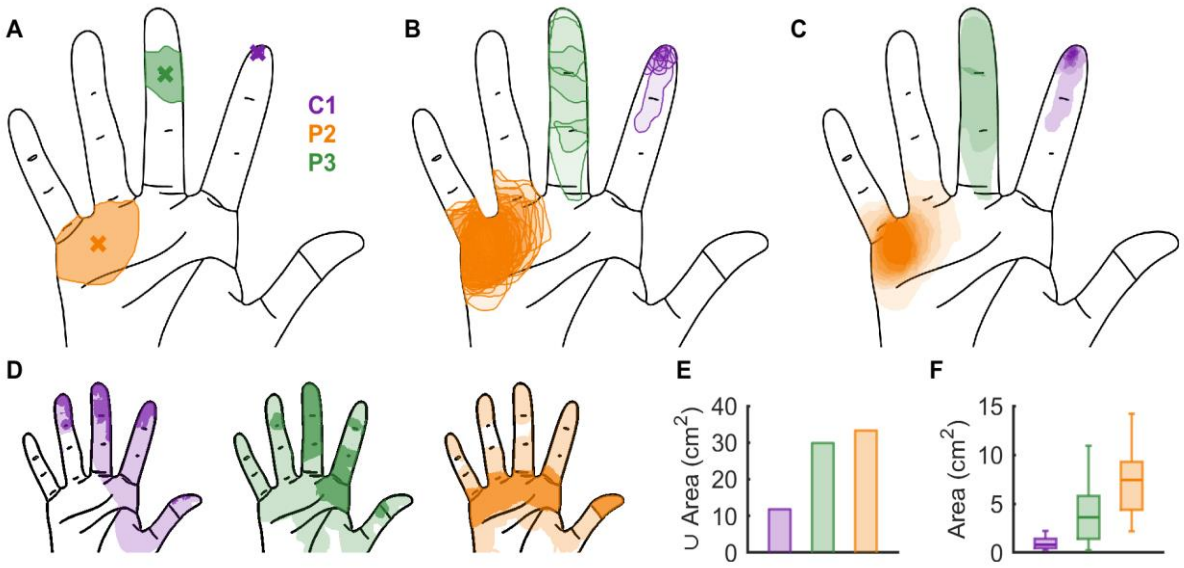

Figure 2.2. Projected field locations systematically vary in size and location across electrodes and participants. A| Example projected fields from one session from each participant. Crosses denote the respective centroids. **B|** The same projected fields as in panel A but across all sessions. **C|** The density function computed for the same electrodes across all sessions. **D|** Hand regions over which each participant reported a sensation across all electrodes. The lighter shade indicates pixels selected on <33% of sessions while the darker shade indicates pixels selected on >33% of sessions. **E|** The area of the hand over which a sensation was evoked (union of PFs across electrodes, after thresholding) for each participant. **F|** The distribution of individual PF sizes (after thresholding) for each participant.

Three participants were implanted with arrays of electrodes in the hand representation of S1 (Brodmann's area 1, Figure 2.1, Supplementary Figure S2.1), localized based on pre-operative fMRI or MEG. In participant C1, most of the sensations were experienced on the fingertips, in participant P2, on the palm, and in participant P3, on the medial phalanges and palm. To quantitatively characterize the PF of each electrode, we repeatedly delivered through it a 1-sec long ICMS pulse train (100 Hz, 60 µA), which was intense enough to reliably elicit a sensation for most electrodes (Supplementary Figure S2.2). After each stimulation bout, the participant drew the spatial extent of the PF on a digital representation of his hand, enabled by partial residual arm function. From

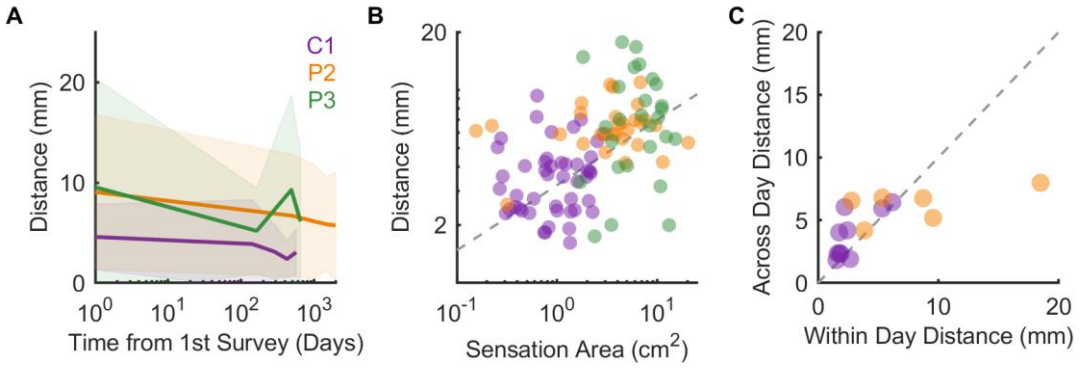

Figure 2.3. Projected field locations are stable over time. A| Distance between the centroid of the single-day PF and the aggregate centroid for each electrode, averaged across electrodes. The line denotes the mean and the shaded area the standard deviation. **B|** Mean distance between single day PF centroid and aggregate PF centroid for each electrode. Mean distance increases with the size of the PF. Dashed line denotes best fit. **C|** Mean centroid distance when reports were collected within a single day compared to that computed across years for a subset of electrodes. Dashed line denotes unity.

these images, we computed the area of skin over which the PF extended and its center of mass (centroid) (Figure 2.2A). This task was repeated regularly over several years (Figure 2.2B), allowing us to construct an aggregate PF for each stimulating channel by weighting each pixel on the hand by the proportion of times it was included in the reported PF over the duration of the study (Figure 2.2C). This allowed us to estimate the probability of a sensation being evoked on different parts of the hand for each channel and revealed that most PFs comprised a core region within which sensations were reliably evoked, surrounded by a diffuse shell over which sensations were less consistent. With this in mind, we applied a reliability criterion (33%) on the aggregate PFs and removed pixels that did not meet this criterion (see Supplementary Figure S2.3 for the justification of the threshold level). PFs for which no pixels met this threshold criterion were deemed too unreliable and excluded from further analysis, totaling around 25% for Participants C1 & P2 and ~60% for Participant P3. While the excluded PFs were typically reported on the same digit or hand

region (Figure 2.2 B, C - green), we reasoned that they were not sufficiently reliable to usefully convey location information.

Next, we examined how the PFs tiled the hands for each participant. While all participants reported a sensation over most of the hand on at least one occasion (Figure 2.2D, light shade), participant C1 predominantly experienced sensations on the tip of the digits, participant P2 on the pads and thumb, and participant P3 on both. The total area over which sensations were evoked (after thresholding) was 11.8, 33.3, and 29.9 cm^2 for C1, P2, and P3, respectively (Figure 2.2E). The size of the PF varied widely (median = 2.5 cm^2; $5^{th}/95^{th}$ percentiles = 0.3 / 11.3 cm^2) across electrodes and participants (Figure 2.2F), with C1 reporting the smallest PFs and P2 the largest. C1 had the most distal PFs and P2 had the most proximal ones, suggesting that PFs decrease in size as one progresses distally from the palm to the digit tips but confounded by the small sample of participants. Note that receptive fields (RFs) of neurons in S1 generally follow an analogous trend, where distal RFs are smaller than proximal ones[23]. Similarly, the size of ICMS-evoked phosphenes via ICMS of primary visual cortex increases as one proceeds toward the visual periphery[24].

2.3.1: Projected fields are highly stable over time

While PF field location has been reported to be stable over time[11], stability has not been systematically quantified. To fill this gap, we compared the location of the PFs at regular intervals across 2 to 7 years (for C1/P3 and P2, respectively; Figure 2.2B,C). First, we computed the degree to which PFs reported for an electrode on any given session matched the first ever reported PF on that electrode. We found that centroid distance between the initial PF and subsequent ones for a given electrode remained stable, with no significant change over the lifetime of the arrays for two of the three participants (C1 and P3, r = -0.03 and 0.12, p = 0.99 and 0.34, respectively), and a

slight but significant increase in the third participant, who had been implanted the longest (P2, $r = 0.23$, $p < 0.01$, Supplementary Figure S2.4A). In other words, we observed little to no progressive shift away from the first reported PF with subsequent reports. At the single electrode level, the slopes of the PF shifts over time (in mm per day) – some negative denoting trends toward the first reported PF after an initial increase – were always very shallow (median = 0.00 mm/day; Q_1, Q_3 = 0.00, 0.01 mm/day respectively) and their mean was only significantly different from zero for one participant (P2, $t(58) = 3.35$, $p < 0.01$**,** Supplementary Figure S2.4B). Second, we computed the distance between each single-day centroid and its corresponding aggregate centroid (Figure 2.3A) to determine how representative the aggregate PF was of any individual PF for a given electrode. Across all recording sessions, we found that the mean distance ranged from 3.5 to 8.7 mm (depending on the participant), but larger PFs tended to yield more variable centroids (Figure 2.3B, $r = 0.33$, $p < 0.01$), as might be expected. Furthermore, centroid distance was stable over time for one participant (P3, $r = -0.1$, $p = 0.77$) and *decreased* over time for the other two (C1 and P2, $r = -0.17$ for both, $p < 0.01$ for both), suggesting that the latter converged onto a more stable reporting of their PFs (over the years that these were measured).

Next, we assessed whether the fluctuations in reported PF reflected true changes in position over time or simply variability in the participants' reports. To this end, ICMS pulse trains were delivered through a subset of electrodes (n = 8 and 7 for C1 and P2, respectively), interleaved randomly, and the participant reported the PF of each. This procedure was then repeated multiple times throughout the day (6 and 5 times for participants C1 and P2, respectively), each time in a different order to reduce biases. We then assessed the degree to which the centroids of the reported PFs coincided. First, PFs were consistent between repeated reports for the two

participants tested (centroid distance: median = 3.5 mm, Q_1-Q_3, 1.6 – 4.8 mm). Second, the within- vs. across-day centroid distances for each electrode were highly correlated ($r = 0.68$, $p < 0.01$) and statistically equivalent (paired t-test, $t(15) = 0.1$, $p = 0.93$, Figure 2.3C). In other words, the change in PF reported within a session was equivalent to the change in PF reported over years of testing. We conclude that the bulk of the variability in PFs over time reflects variability in the reports rather than variability in the PFs themselves (assuming that PFs are stable within a day). The PF is thus highly stable over time and well described by the aggregate PF.

2.3.2: Projected fields progress systematically with location along the cortical surface

According to the canonical homunculus, the representations of digits and hand segments in S1 proceed systematically along the mediolateral axis, approximately parallel to the central sulcus, with the little finger represented medially and the thumb represented laterally[15]. Examination of the PF maps (Supplementary Figure S2.1) suggests that, within each array, the dominant digit or hand segment – where the PFs are predominantly located – also changes systematically along one axis, consistent with the geometry of the homunculus. To test this quantitatively, we projected the location of each electrode on each array onto a single axis and assessed the degree to which the identity of the digit could be inferred from the electrode's location along that axis (Figure 2.4A). By computing classification accuracy across a range of axes (spanning 180 degrees), we identified the axis along which the digit/hand segment gradients were most pronounced. We found that, for each array, a single axis could account for digit or hand segment dominance as well as if both coordinates were included (Supplementary Figure S2.5A) and

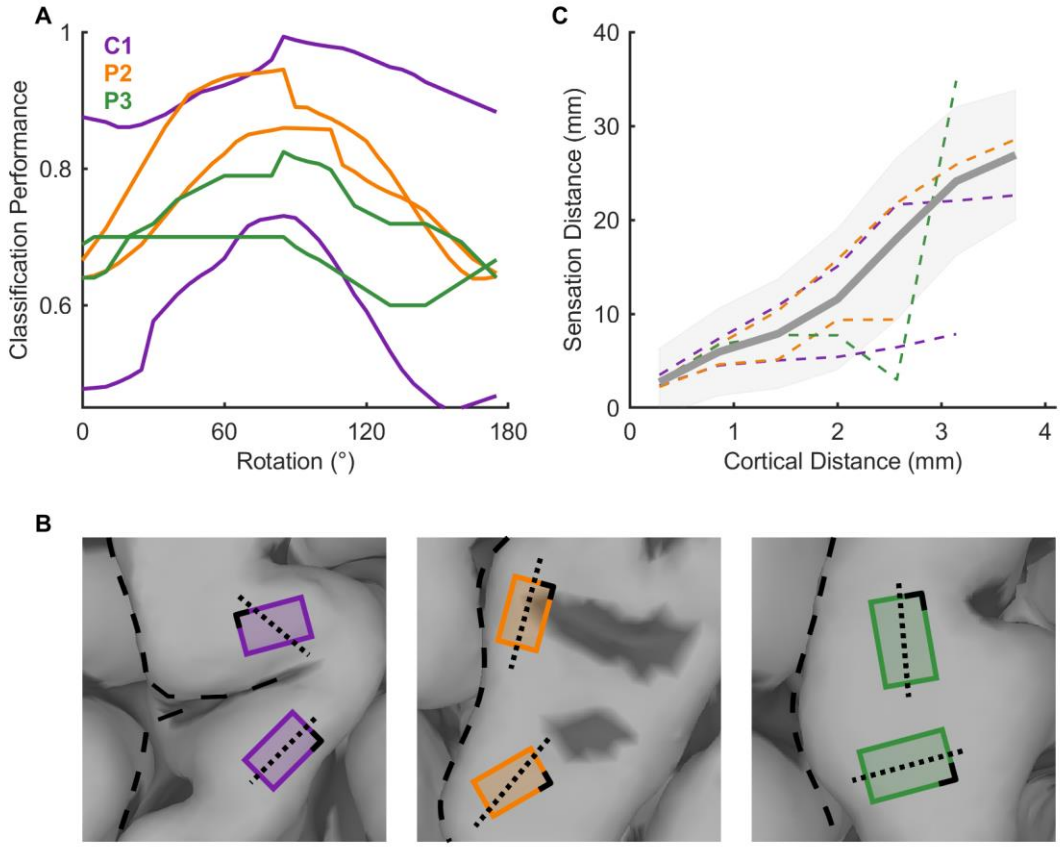

Figure 2.4. PFs progress systematically across electrodes. A| Classification performance vs. the angle of the projection axis, expressed relative to the local curvature of S1. The ability to infer digit or palmar segment identity based on position along a single axis depends on the angle of that axis. **B|** Optimal digit/palmar segment discrimination axis (perpendicular to the projection axis), superimposed on each S1 array (dotted line). The dashed line denotes the local curvature of S1, which, for C1, deviates from the curvature of the central sulcus. **C|** Within digit, the distance between two PF centroids is significantly correlated with the distance between the electrodes (n = 5892 pairs, $r = 0.69$, $p < 0.01$) and this relationship is observed for each array individually ($r > 0.4$, $p < 0.01$).

that this axis was approximately parallel to the local curvature of S1 for 5 out of the 6 arrays (Figure 2.4B, Supplementary Figure S2.5), consistent with the canonical homunculus. In the array that did not show this pattern (participant P3's lateral array), the axis was nearly perpendicular to the S1 curvature, but the PFs were largely confined to a single digit (the index finger), yielding comparable classification at all angles. Next, we examined whether the distance between PFs increased as the

distance between electrodes increased, restricting the analysis to pairs of electrodes with PFs on the same digit. We found that, as expected, centroid distance increased systematically with cortical distance (Figure 2.4C). A 2-mm shift in cortex corresponded to a ~10-mm shift in the PF on the skin, on average. The systematic relationship between cortical location and PF location is thus consistent with the canonical homunculus, in which S1 is characterized by strips that encode individual digits or palmar segments.

2.3.3: The projected field is determined by the receptive field of the activated neurons

To further examine the relationship between homunculus location and PF location, we leveraged the residual sensation in two of our participants (C1 and P3, Supplementary Figure S2.6) and compared the RF and PF of each electrode. Indeed, C1 has nearly normal sensation over the fingertips and some residual sensation over the rest of the volar surface of his hand. P3 has largely spared sensation on the thumb, some spared sensation on the index, and some residual sensation on D3 and D4, but his little finger is insensate. To map RFs, we applied gentle touches to the skin and monitored the multi-unit activity through speakers. As for the PFs, RFs were measured over multiple days with the experimenter blinded to electrode identity. Repeated mapping sessions (in participant C1) yielded very similar RFs (see Figure 2.5A left). We then compared the RF and PF of each electrode (Figure 2.5A). First, we found that, across electrodes and participants, the RF was 6.5 times as large as the PF (Figure 2.5B, ratio: $Q_2 = 6.5$, Q_1-$Q_3 = 3.8 – 14.3$) and PF size tended to scale with RF size, though this relationship was only significant for one of the two participants ($r = 0.15$ and 0.76, $p = 0.35$ and 0.011 for C1 and P3, respectively). Secondly, PFs were typically subsumed by the RF: On average, 93% of the reported PF fell within the measured RF (Figure 2.5C). In both participants, the RF included more hand segments (digits or palmar segments) than did

the PF. We verified that this phenomenon was not an artifact of our approach by examining the RFs and PFs characterized independently by another group in a third partially sensate participant using a different characterization method (Figure 2.5D, see Methods and ref[17]). We conclude that the PF of an electrode is determined by the RFs of the neurons around the electrode tip.

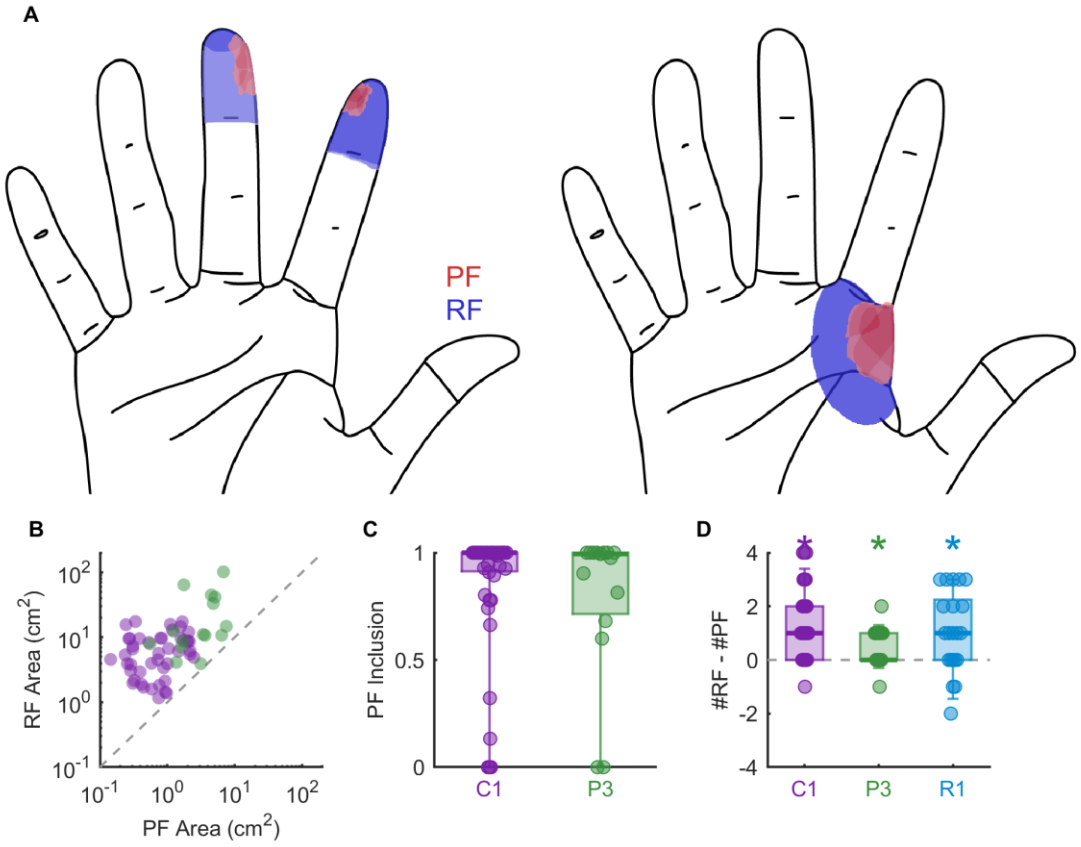

Figure 2.5. The projected field of an electrode is smaller than and circumscribed by its receptive field. A| Aggregate PF (red) and RF (blue) for two example electrodes from participant C1 (left) and P3 (right), respectively. The hue of each denotes the proportion of times a pixel was included in the PF or RF. **B|** Size of the RF vs. size of the PF for electrodes from which both were obtained in participants C1 and P3. Receptive fields were larger for both participants (paired t-test, $p < 0.01$ for both). Dashed line shows unity. **C|** Proportion of the PF that fell within the RF for all tested electrodes. The median proportion was 1 for both with 25th percentiles of 0.83 and 0.72 for C1 and P3, respectively, suggesting that PFs tended to be completely subsumed by the RF. **D|** Number of regions (digits and palm) encapsulated by each electrode's RF minus the number of regions encapsulated by its PF for 3 participants (N = 62, 25, 21 for participants C1, P3, and R1, respectively). Multiple electrodes are shown for each participant. RFs spanned more hand regions than PFs in all 3 participants (Wilcoxon rank sum test, $p < 0.01$, Holm-Bonferroni corrected).

2.3.4: Projected fields grow larger with more intense ICMS

Next, we examined the degree to which PFs were dependent on ICMS amplitude and frequency. First, we found that the size of the PF increased threefold as amplitude increased from 40 to 80 µA, with ICMS frequency fixed at 100 Hz (

Figure 2.6A, median (Q_1-Q_3)= 170% (142-330%), 2-way ANOVA, $F(2,11) = 6.26$, $p < 0.01$). Second, PFs grew systematically as frequency increased from 50 to 200 Hz, with amplitude fixed at 60 µA (Figure 2.6B, median (Q_1-Q_3)= 129% (121-185%), 2-way ANOVA (2,11), $F = 7.43$, $p < 0.01$). Because the perceived magnitude increases with both ICMS frequency and amplitude for the electrodes tested (3-way ANOVA (2,2,11), $F = 19.61$ and 42.35 respectively, $p < 0.01$ for both), we assessed the relationship between PF size and sensation magnitude. We found that the size of the reported PF could be accurately predicted from the reported magnitude of the evoked sensation, across ICMS frequencies and amplitudes (Figure 2.6C, $r = 0.77$, $p < 0.01$). The effect of ICMS intensity on PF size is qualitatively consistent with the proposed neural determinants of the PF. Each volume of cortex maps onto a patch of skin; the greater the volume of cortex activated (amplitude modulation[25,26]) or the number of activated neurons within that cortical volume (frequency modulation[27]), the greater the corresponding swath of skin.

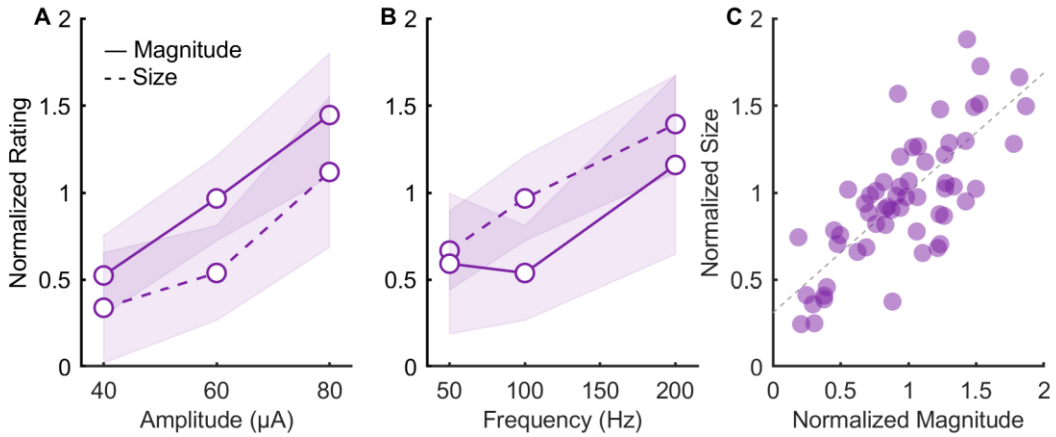

Figure 2.6. PF size and sensory magnitude increase with ICMS amplitude and frequency. A| Normalized ratings of sensory magnitude and PF size vs. ICMS amplitude (with frequency fixed at 100 Hz). The size of the PF for each electrode and condition was normalized by the mean PF across conditions. B| Normalized ratings of sensory magnitude and PF size vs. ICMS frequency (with amplitude fixed at 60 μA). Both frequency and amplitude significantly impact perceived size and intensity (2-way ANOVA, $p < 0.01$ for all). C| The effect of ICMS amplitude and frequency on PF size can be accounted for by the latter's impact on sensory magnitude ($r = 0.77$, $p < 0.01$). Data from participant C1.

2.3.5: Projected fields are superimposed with multi-electrode ICMS

Next, we examined the impact of simultaneously stimulating through multiple electrodes on reported PFs. We wished to assess the degree to which the composite PFs were a conjunction of the component PFs. To this end, we simultaneously delivered ICMS through pairs of electrodes and compared the reported PFs to those when ICMS was delivered through the individual electrodes that formed the pairs (Figure 2.7A, B). In some cases, the electrodes in the pair had PFs that largely overlapped, so we could assess how the two sensations were integrated. In other cases, the electrodes in the pair had non-overlapping PFs, so we could investigate whether the two sensations would interfere or interact with one another. Single and multi-electrode trials were

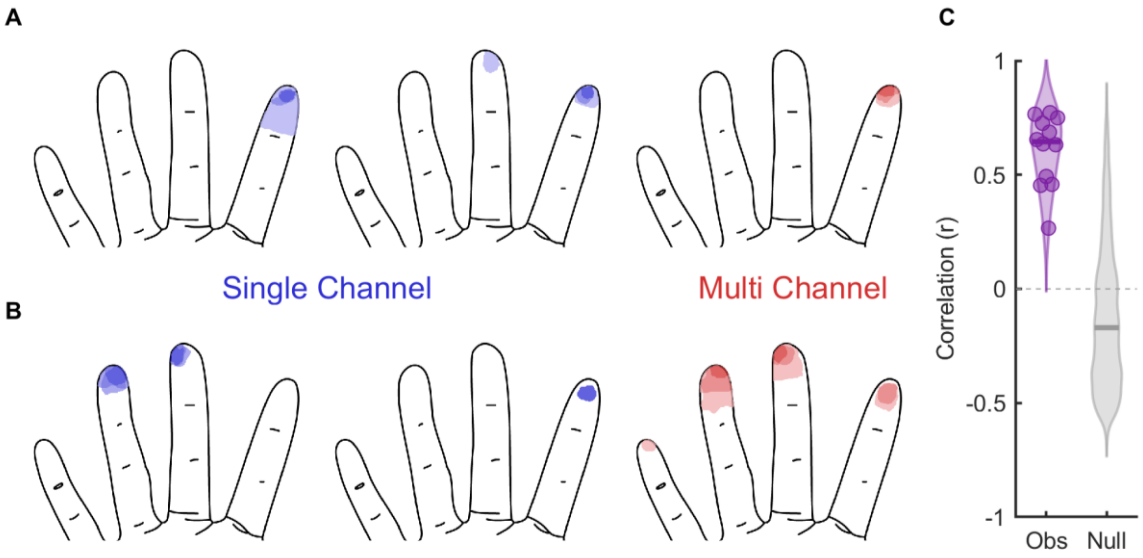

Figure 2.7. Projected fields with multi-channel stimulation are additive. A, B| Two example projected fields predicted from the union of two individual channels versus the reported field when the two channels were stimulated simultaneously. **C|** Correlation between the additive model and observed projected field versus a null model where two random channels were chosen. The additive model significantly outperformed the null model (2-sample Kolmogorov-Smirnov test, $D = 0.86$, $p < 0.01$). Data from participant C1.

interleaved to limit biases in the PF reports. Examination of the single-electrode and multi-electrode PFs suggests that the latter reflect a superimposition of the former. We tested this by computing the pixel-wise correlation between the sum of the individual PFs and the multi-electrode PF. We found the summed PFs of the component electrodes were highly predictive of the multi-electrode PF (mean $r = 0.61$, Figure 2.7C). We conclude that PFs combine approximately additively when ICMS is delivered through multiple electrodes.

2.3.6: Multi-electrode ICMS evokes more localizable sensations than does single-electrode ICMS

As discussed above, the circumscription and systematic localization of PFs can be exploited to convey information about (bionic) hand locations at which contact with an object is

established[11,28]. Given that multi-electrode PFs reflect a superimposition of their component PFs, we reasoned that more focal and thus more easily localizable sensations might be evoked via multi-electrode stimulation. To test this possibility, we mapped force sensors on the bionic hand (Ability Hand, Psyonic) to electrodes with matching PFs. For example, sensors on the prosthetic thumb tip drove stimulation through electrodes with PFs on the thumb tip. In some cases, each sensor drove stimulation through a single electrode; in other cases, sensor output drove a quartet of electrodes (at 60 μA) whose PFs largely overlapped. For these, the overlapping component matched the sensor location. We then randomly touched different bionic digits and had the (blindfolded) participant report which finger was touched (Figure 2.8A). Touches to single digits were randomly interleaved with touches to two digits. We also repeated the same experiment, except that digit(s) were selected by the experimenter on the experimental computer (rather than by physically touching the bionic hand). Results from these two paradigms – one with and one without the bionic hand – were similar and thus combined (Supplementary Figure S2.7A). With either single or multi electrode ICMS, the participant reported the expected digit(s) – corresponding to the PF of the electrode(s) – on the majority of trials. Compared to multi-channel ICMS, however, single-electrode stimulation more often failed to elicit a localizable sensation (30%

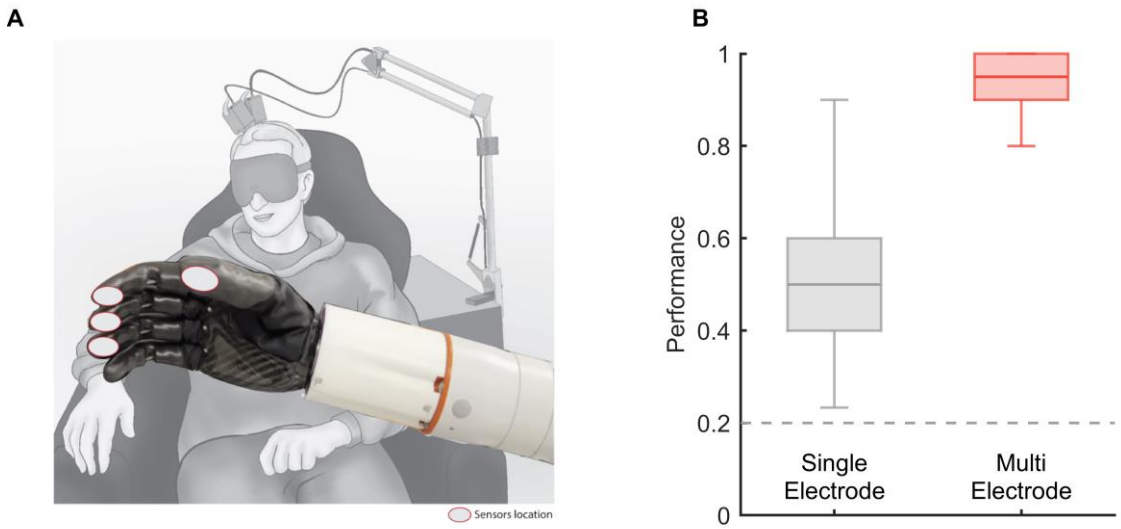

Figure 2.8 Multi-channel ICMS evokes more localizable sensations than does single-electrode ICMS. A| Task setup for robotic digit localization task. The participant was blindfolded while an experimenter randomly squeezed individual prosthetic digits or pairs of digits. **B|** Consolidated performance of robotic and open loop localization tasks. Multi-electrode stimulation evokes more localizable sensations (2-sample t-test, $t(236) = 21.6$, $p < 0.01$) Note that trials where the participant failed to detect stimulation are excluded here to reduce confounding localization performance with detectability. Data from participant C1.

vs. 0%) and more often elicited a sensation reported on the wrong digit (42% vs. 7%) (Figure 2.8A). The difference in performance for single- vs. multi-electrode stimulation was more pronounced on blocks in which multiple digits were touched, but in both cases multi-electrode stimulation significantly outperformed single-electrode stimulation (Wilcoxon rank sum test, $Z = 8.80$, $p < 0.01$ and $Z = 9.02$, $p < 0.01$). Multi-channel stimulation thus gives rise to more reliably localizable sensations than does its single-electrode counterpart.

2.4: Discussion

2.4.1: PFs are highly stable over time

PFs remained stable over the testing period, which spanned ~2 years for participants C1 and P3 and ~7 years for participant P2. Indeed, the variability in the PF overlap and centroid distance across repeated tests on the same electrode were equivalent within and across sessions. Given that the PF location largely coincides with RF location, this stability suggests that the somatosensory homunculus is highly stable, consistent with fMRI studies with amputees[19] and people with tetraplegia[20,29]. Moreover, the participants varied in their residual sensations, where participants C1 had spared sensation over most of his hand, P3 over all but the little finger, and P2 only on the thumb and index. Across participants, the PFs were indistinguishable in their size and relative locations whether these were on sensate or insensate patches of skin, suggesting that the homunculus remains stable regardless of the degree of residual sensation. Furthermore, recent results with intraneural electrodes implanted in the human nerves suggested that the PF changes observed over time are most likely caused by the foreign body reactions and their impact on the coupling between nerve and electrode[30]. Indeed, deliberate attempts to modify the PFs of electrodes implanted in the nerves – which leverage any subcortical plasticity – failed to systematically change the PF location[18], further evidence for the stability of body maps in adulthood[21].

2.4.2: The projected field of an electrode is subsumed by its receptive field

Since the PF of an electrode is determined by its location on the somatosensory homunculus, the spatial extent of the PF is expected to be determined by the spatial extent of activation across the cortical surface. Consistent with this, increases in ICMS amplitude or frequency lead to increases in the volume of activated neurons and/or density of activated neurons within a volume[25–27,31] and concomitant increases in PF area. Furthermore, the PF of an

electrode is, on average, a sixth to a seventh the size of its RF. If we assume that the spatial extent of a PF is determined by the activated cortical area, ICMS at 60 μA activates the somata of neurons over a span of around 1 mm[25] (Supplementary Figure S2.8A). The RF size is determined by (1) the area over which neurons contribute to the multiunit activity on a given electrode (~150 μm radius) and (2) the area of cortex that is activated by a touch (Supplementary Figure S2.8B). Regarding the latter, a punctate indentation applied to the skin evokes neuronal activity on two spatial scales (Supplementary Figure S2.8C). Contact initiation evokes a transient response over a wide swath of cortex (spanning ~15 electrodes on the array), with RFs spanning multiple digits. Contact maintenance is associated with a much more spatially restricted sustained response (spanning ~2 electrodes). RFs, mapped by touching the skin lightly and repetitively, reflect the transient response. If responses to contact transients determined the spatial extent of a tactile experience, a touch on a single digit would evoke a sensation on multiple digits. Accordingly, the spatial extent of a tactile sensation is more likely determined by the cortical population that remains active during maintained contact, the so-called hotzone[32]. For a punctate indentation, the hotzone spans 1 to 2 electrodes. At a first approximation, then, the area of cortex activated by ICMS is on the same order of magnitude as the hotzone, and much smaller than the transiently activated cortical area (Supplementary Figure S2.8D). Note, however, that the spatial extent of a sensation is not only determined by the spatial extent of the activated cortex but also by the spatial pattern of that activation. A punctate indentation produces a response that is spatially graded, peaking at the hotzone and dropping off smoothly around it[32]. While the ICMS-evoked activation also decreases with distance from the electrode tip[33], the pattern is almost certainly different. This difference likely underlies the fact that ICMS-evoked sensations have more diffuse borders than do their

natural tactile counterparts. The relationship between the spatial pattern of cortical activation and the evoked sensation remains to be conclusively elucidated.

2.4.3: Multi-electrode stimulation evokes more localizable sensations

Mapping sensors on the bionic hand to somatotopically matched electrodes in S1 yields intuitive feedback about the locations on the bionic hands at which contacts with an object occur. Indeed, contact with the prosthetic thumb tip, for example, leads to a sensation experienced on the thumb tip. Here, we show that this mapping is even more effective if the sensor output drives ICMS through multiple electrodes, whose common PF matches the sensor location. For example, if multiple electrodes have PFs that include the thumb, their aggregate PF will be dominated by the thumb. Multi-electrode ICMS thus results in sensations that not only are more tangible but also more readily localizable to the hand regions corresponding to the PF overlap. While the same outcome might be achieved by increasing the amplitude of ICMS delivered through a single electrode, resulting in a more salient PF core despite the concomitant increase in PF area, multi-channel ICMS enables improved localizability within the safety limits of ICMS, capped at 100 μA[34]. In addition to the improvement in localization, multi-channel ICMS also leads to an improvement in force feedback compared to its single-channel counterpart, as evidenced by a greater number of discriminable steps of force within the safe and perceptible range of amplitudes[35]. Moreover, multi-channel ICMS robustly evokes somatosensory sensations at significantly shorter latencies than does single-electrode ICMS[22,36]. On the other hand, multi-electrode ICMS of S1 has a stronger deleterious effect on the ability to decode motor intent by evoking more activity in M1 than does single-electrode ICMS[37]. Indeed, the intermixing of motor and sensory signals is liable to disrupt the decoders, particularly if these are not trained in the presence of ICMS-based feedback. This

disruption, however, can be minimized by implementing biomimetic feedback – which emphasizes contact transients at the expense of maintained contact[3,38]. Overall, then, multi-electrode stimulation leads to more effective tactile feedback for bionic hands.

2.4.4: Implanted arrays should consist of distributed clusters of electrodes

As the majority of our interactions with objects involve the digit tips[39], ICMS-tactile feedback emphasizes fingertip sensations over more proximal ones. Implants in S1 often consist of 6x10 arrays of electrodes with every other electrode wired in a checkerboard pattern (Figure 2.1). The placement of the arrays is based on the identification of distinct digit-specific patches of activity using fMRI or MEG. Individual arrays are then placed near the border of two digits to maximize coverage.

While the aforementioned imaging technologies yield reliable localization of the individual digit representations in S1 (e.g. digit 2 vs. digit 3), localization of the digit tips (vs the digit bases) is far less clear. In fact, the location of the digit tip representation in postcentral gyrus is unclear. In humans and monkeys, RFs progress from digit tip to base as one progresses caudally through Brodmann's area 3b from its border with area 3a[14,40–42]. The RF progression reverses at the border with area 1, proceeding from base to tip, then reverses again at the border with area 2. Given that digit tip representations in area 3b are deep in the central sulcus, the only access to digit tip representations is at the area 1/2 border with the arrays currently approved for human use, which cannot access deep structures. As much of area 2 may be in the anterior bank of the intraparietal sulcus (IPS) in humans[43], the digit tip representations are likely to be near the IPS, though this does not seem to always be the case. While implanting larger arrays may improve the coverage, implanting more arrays rather than larger ones might improve the chances that all digits are

represented. Ideally, clusters of electrodes (4 or 9 electrodes) would be implanted in the center of the presumptive digit tip representations, near the IPS (Supplementary Figure S2.9). With an inter-electrode spacing of 400 µm, the clusters would activate populations of neurons with largely overlapping RFs yet different electrodes would activate largely non-overlapping neuronal populations as the electric fields at each electrode would be largely nonoverlapping over the range of safe ICMS amplitudes. This configuration can scale up as the robotics, sensorization, and algorithms improve, with each cluster matched to a sensor on the hand.

2.5: Methods

2.5.1: Participants

This study was conducted under an Investigational Device Exemption from the U.S. Food and Drug Administration and approved by the Institutional Review Boards at the Universities of Pittsburgh and Chicago. The clinical trial is registered at ClinicalTrials.gov (NCT01894802). Informed consent was obtained before any study procedures were conducted. Participant C1 (m), 57 years old at the time of implant, presented with a C4-level ASIA D spinal cord injury (SCI) that occurred 35 years prior to implant. Participant P2 (m), 28 years old at the time of implant, presented with a C5 motor/C6 sensory ASIA B SCI that occurred 10 years prior to implant. Participant P3 (m), 28 years old at the time of implant, presented with a C6 ASIA B SCI that occurred 12 years prior to implant. Participant R1 (m), who performed a subset of experiments, was enrolled under a separate IRB and IDE-approved clinical trial (NCT3898804). R1 presented with a C3/C4 ASIA B SCI that occurred 5 years prior to implant, and his cortical implants are described in detail in[17].

2.5.2: Residual sensation

Participant C1 had retained sensation over the entire volar surface of the hand, with nearly normal detection thresholds (measured with van Frey hairs) on the digit tips, and elevated thresholds over the rest of the hand (Supplementary Figure S2.6). Participant P2 had retained sensation over the thumb, index finger, and underlying palm, albeit with elevated thresholds, but the rest of his hand was insensate. Participant P3 had nearly normal thresholds on the thumb and most of the index finger, higher thresholds on the middle finger, was nearly insensate on the ring finger and completely insensate on the little finger.

2.5.3: Cortical implants

We implanted four microelectrode arrays (Blackrock Neurotech, Salt Lake City, UT, USA) in each participant (C1, P2, P3). The two arrays (one medial and one lateral array) in Brodmann's area 1 of S1 were 2.4 mm x 4 mm with sixty 1.5-mm long electrode shanks wired in a checkerboard pattern such that 32 electrodes could be stimulated. The two arrays in primary motor cortex were 4 mm x 4 mm with one-hundred 1.5-mm long electrode shanks wired such that 96 (C1 and P3) or 88 (P2) electrodes could be used to monitor neural activity. The inactive shanks were located at the corners of these arrays. Two percutaneous connectors, each connected to one sensory array and one motor array, were fixed to the participant's skull. We targeted array placement during surgery based on functional neuroimaging (fMRI) or magnetoencephalography (MEG) of the participants attempting to make movements of the hand and arm (all participants) and imagining feeling sensations on their fingertips (participant P2), within the constraints of anatomical features such as blood vessels and cortical topography. Participant R1 was implanted with two 64-channel arrays (8 x 8) in Brodmann's area 1, with PFs primarily on the index and middle fingers (see ref[17] for details).

2.5.4: Intracortical microstimulation

ICMS was delivered via a CereStim 96 (Blackrock Neurotech). Each stimulating pulse consisted of a 200-µs cathodic phase followed by a half-amplitude 400-µs anodic phase (to maintain charge balance), the two phases separated by 100 µs. For multi-channel stimulation, the same pulse train was delivered to all channels simultaneously and synchronously.

2.5.5: Projected field mapping and quantification

To map a PF, ICMS was delivered through one or more electrodes (60 µA, 100 Hz, 1 second unless otherwise specified), and the participant reported whether a sensation was evoked. The participant could request as many repetitions of the stimulus as desired. During or after the stimulation, the participants drew the spatial extent of the sensation on a digital representation of the hand using a stylus.

Periodically (every 1-3 months), this procedure was repeated for every electrode on both sensory arrays, with electrodes interleaved in random order, across a span of approximately 800, 2750, and 750 days for participants C1, P2, and P3, respectively. From these digital images, we counted the number of pixels subsumed by the PF, computed its area and centroid (center of mass). To gauge the validity of the computed center of mass, one participant also marked, on a subset of electrodes in one session, the center of the PF on the picture of their hand. We found that the estimated centroids matched the reported centroids with sub-millimeter accuracy (median = 0.71 mm, Q_1, Q_3 = 0.52, 1.33 mm).

In a fourth participant (R1), the PF mapping procedure differed slightly. On each experimental block, a group of 5 electrodes were randomly selected, and each electrode was stimulated approximately 5 times (n = 4-7 times, mean = 5.12) in randomized order within the

block. The participant verbally reported the hand segments on which the sensation was experienced (distal and medial finger pads, e.g.), each segment numbered on a digital representation of the hand[17]. ICMS was identical as that for the other participants, except that pulse amplitude was 80 μA. Skin locations included in the reported PF on at least 60% of trials for a given electrode were included in its PF.

2.5.6: Aggregate projected fields

Having established that day-to-day variations in PF location were essentially random and primarily reflected noise in the reports, we constructed an estimate of each PF that weighted skin regions according to the frequency with which these were included in the single-day PF reports. Specifically, we computed the proportion of times a given pixel was included in the single-day PF. We then eliminated pixels that were included on fewer than 25% of single-day reports and normalized the remaining proportions such that they summed to one. For some electrodes, this criterion eliminated all of the pixels. These electrodes were not included in subsequent analysis and are reported as having no reliable PF. In the computation of the aggregate centroid, each pixel was weighted according to its value (normalized proportion). When aggregate centroids spanned multiple hand segments, the one with the largest summed pixel values was identified as the dominant one. The size of the aggregate field was the total number of pixels that exceeded the threshold.

2.5.7: Projected field stability

We gauged projected field stability in three ways. First, we computed the distance between each single-day PF centroid and the centroid of the first reported PFs. Because this measure was susceptible to an anomalous report on the first session, we also computed the

distance between the PF centroid on any given session and the centroid of the aggregate PF. Third, we measured the proportion of all unique pixels reported for a given electrode that exceeded each of several thresholds, reasoning that stable PFs would be consistent across a wide range of thresholds.

2.5.8: PF PROGRESSION OVER THE CORTICAL SURFACE

To test the degree to which PF progressions follow the canonical homunculus, we assessed how well we could identify the dominant hand segment for an electrode given that electrode's location. In brief, we used the row and column coordinates of the array as the X and Y coordinates in Cartesian space, whose origin was the center of the array. We then projected the coordinates onto each of 72 axes, spanning the range from 0 to 360 degrees in increments of 5 degrees. For example, for the 0-degree axis, the coordinate would be identical to the X coordinate (row). For each axis, we then applied a linear discriminant classifier with the projected coordinates as inputs and the dominant hand segments (digit, e.g.) as output classes (MATLAB's *fitcdiscr*). To further test the degree to which PFs progress somatotopically, we computed, for each pair of electrodes, the distance between their respective aggregate centroids and assessed the relationship between PF centroid distance and the physical distance between the electrodes over the cortical surface.

2.5.9: RECEPTIVE FIELD MAPPING

To map the extent of the receptive fields of the multi-unit around each electrode, we lightly brushed the skin of the hand using cotton swabs or Von Frey hairs while monitoring the multi-unit response using a speaker. One experimenter stimulated the hand while the other experimenter selected the electrode to be mapped (unknown to the first). In the case of participant C1, where 3 sessions were completed, the electrode order was randomized across sessions. The RF was

reported on the same tablet interface used for PFs so that the same analytical protocols could be applied to both types of fields. An aggregate RF was produced for participant C1 with a cutoff of 33% (the pixel must have been present on 1/3 of observations) using the method described above for PFs. Measured RFs were nearly identical across sessions in the one participant for whom these were measured repeatedly over multiple sessions. For participant R1, a trapezoidal indentation was delivered to the distal finger pad of each digit using a tactile linear actuator (LCA25-025-6MSD6, SMAC, Carlsbad, California, USA) while recording the neuronal activity evoked in S1. Each indentation was presented 60 times at a constant amplitude. Because the neuronal signal was weak, we computed spike band power – the root mean square of the filtered signal in 1 ms bins – to quantify the strength of the neural response. The spike band power was normalized within trials by z-scoring the signal during the 2 second stimulus by the 2 second pre-stimulus interval, then the normalized metric was trial averaged for each indenter location. Electrodes with peak normalized spike band power greater than 1.5 standard deviations above baseline were considered responsive to indentation at the specific location. While this RF mapping approach involved a much more controlled and systematic mechanical stimulus than that used in the other three participants (P2, P3, C1), it suffers from the poor coverage, able only to detect neuronal responses evoked by stimulation of the distal digit tips.

2.5.10: LOCALIZATION TASK

To assess the degree to which ICMS conveys information about the location of contact between bionic hand and objects, we implemented a sensory encoding algorithm that linked sensors on the robotic hand (Ability Hand, Psyonic, CA, USA) and somatotopically matched electrodes in S1. For example, the output of a sensor on the index fingertip drove ICMS delivered

through one or more electrodes with PFs on the index fingertip. Then, on each trial, the experimenter squeezed one or more digits and the participants task was to report which digits were squeezed. Single-digit and two-digit trials were randomly interleaved and the participant was warned that one or two fingers might be squeezed on any given trial. On some experimental blocks, the digit(s) were selected by the experimenter, and an automated protocol randomly selected stimulating channels corresponding to the selected digits for testing, allowing for greater flexibility to test different channels. Sensor output drove ICMS (at 100 Hz) through a single electrode with a PF on the corresponding digit or through multiple electrodes, all with PFs that were predominantly on that digit. The amplitude of the ICMS was proportional to the sensor output and capped at 60 μA; for multi-electrode stimulation, the same ICMS was delivered to all the channels simultaneously. For computer controlled trials, selection of digit triggered a 1-sec, 100-Hz, 60-μA ICMS pulse train delivered through 1 or 4 electrodes. We could then compare the participant's performance with single vs. multi-channel stimulation on the single- vs. multi-digit task. The participant reported the location of the sensation (individual digits, combinations of digits, or no sensation) at the end of the stimulus. On single-digit trials, the participant received full credit if he correctly identified the digit where the aggregate PF was located; on multi-digit trials, he received half credit for each correctly identified digit.

2.6: References

1. Johansson, R. S. & Flanagan, J. R. Coding and use of tactile signals from the fingertips in object manipulation tasks. *Nature Reviews Neuroscience* **10**, 345–359 (2009).
2. Cabibihan, J.-J., Alhaddad, A. Y., Gulrez, T. & Yoon, W. J. Influence of Visual and Haptic Feedback on the Detection of Threshold Forces in a Surgical Grasping Task. *IEEE Robotics and Automation Letters* **6**, 5525–5532 (2021).
3. Bensmaia, S. J., Tyler, D. J. & Micera, S. Restoration of sensory information via bionic hands. *Nature Biomedical Engineering* 1–13 (2020) doi:10.1038/s41551-020-00630-8.
4. Ochoa, J. & Torebjörk, E. Sensations evoked by intraneural microstimulation of single mechanoreceptor units innervating the human hand. *The Journal of Physiology* **342**, 633–654 (1983).
5. Ortiz-Catalan, M., Mastinu, E., Sassu, P., Aszmann, O. & Brånemark, R. Self-Contained Neuromusculoskeletal Arm Prostheses. *New England Journal of Medicine* **382**, 1732–1738 (2020).
6. Overstreet, C. K., Cheng, J. & Keefer, E. Fascicle specific targeting for selective peripheral nerve stimulation. *J. Neural Eng.* (2019) doi:10.1088/1741-2552/ab4370.
7. Petrini, F. M. *et al.* Six-Month Assessment of a Hand Prosthesis with Intraneural Tactile Feedback. *Annals of Neurology* **85**, 137–154 (2019).
8. Tan, D. W. *et al.* A neural interface provides long-term stable natural touch perception. *Science Translational Medicine* **6**, 257ra138-257ra138 (2014).
9. Wendelken, S. *et al.* Restoration of motor control and proprioceptive and cutaneous sensation in humans with prior upper-limb amputation via multiple Utah Slanted Electrode Arrays (USEAs) implanted in residual peripheral arm nerves. *J NeuroEngineering Rehabil* **14**, 121 (2017).
10. Fifer, M. S. *et al.* Intracortical Microstimulation Elicits Human Fingertip Sensations. *medRxiv* 2020.05.29.20117374 (2020) doi:10.1101/2020.05.29.20117374.
11. Flesher, S. N. *et al.* Intracortical microstimulation of human somatosensory cortex. *Science translational medicine* **8**, 361ra141 (2016).

12. Salas, M. A. *et al.* Proprioceptive and cutaneous sensations in humans elicited by intracortical microstimulation. *eLife Sciences* **7**, e32904 (2018).

13. Tabot, G. A. *et al.* Restoring the sense of touch with a prosthetic hand through a brain interface. *Proceedings of the National Academy of Sciences* **110**, 18279–18284 (2013).

14. Delhaye, B. P., Long, K. H. & Bensmaia, S. J. Neural Basis of Touch and Proprioception in Primate Cortex. *Comprehensive Physiology* **8**, 1575–1602 (2018).

15. Penfield, W. & Boldrey, E. SOMATIC MOTOR AND SENSORY REPRESENTATION IN THE CEREBRAL CORTEX OF MAN AS STUDIED BY ELECTRICAL STIMULATION. *Brain* **60**, 389–443 (1937).

16. Foldes, S. T. *et al.* Case Study: Mapping Evoked Fields in Primary Motor and Sensory Areas via Magnetoencephalography in Tetraplegia. *Frontiers in Neurology* **12**, (2021).

17. Herring, E. Z. *et al.* Reconnecting the Hand and Arm to the Brain: Efficacy of Neural Interfaces for Sensorimotor Restoration after Tetraplegia. *medRxiv* 2023.04.24.23288977 (2023) doi:10.1101/2023.04.24.23288977.

18. Ortiz-Catalan, M., Mastinu, E., Greenspon, C. & Bensmaia, S. Chronic use of a sensitized bionic hand does not remap the sense of touch. *Cell Reports* (2020).

19. Kikkert, S. *et al.* Revealing the neural fingerprints of a missing hand. *eLife* **5**, 1–19 (2016).

20. Kikkert, S., Pfyffer, D., Verling, M., Freund, P. & Wenderoth, N. Finger somatotopy is preserved after tetraplegia but deteriorates over time. *eLife* **10**, e67713 (2021).

21. Makin, T. R. & Bensmaia, S. J. Stability of Sensory Topographies in Adult Cortex. *Trends in cognitive sciences* **21**, 195–204 (2017).

22. Bjånes, D. A. *et al.* Multi-channel intra-cortical micro-stimulation yields quick reaction times and evokes natural somatosensations in a human participant. 2022.08.08.22278389 Preprint at https://doi.org/10.1101/2022.08.08.22278389 (2022).

23. Sur, M., Merzenich, M. M. & Kaas, J. H. Magnification, receptive-field area, and 'hypercolumn' size in areas 3b and 1 of somatosensory cortex in owl monkeys. *Journal of Neurophysiology* **44**, 295–311 (1980).

24. Bosking, W. H. *et al.* Saturation in Phosphene Size with Increasing Current Levels Delivered to Human Visual Cortex. *J. Neurosci.* **37**, 7188–7197 (2017).

25. Kumaravelu, K., Sombeck, J., Miller, L. E., Bensmaia, S. J. & Grill, W. M. Stoney vs. Histed: Quantifying the spatial effects of intracortical microstimulation. *Brain Stimulation* **15**, 141–151 (2022).

26. Stoney, S. D., Thompson, W. D. & Asanuma, H. Excitation of pyramidal tract cells by intracortical microstimulation: effective extent of stimulating current. *Journal of Neurophysiology* **31**, 659–669 (1968).

27. Sombeck, J. T. *et al.* Characterizing the short-latency evoked response to intracortical microstimulation across a multi-electrode array. *Journal of Neural Engineering* **19**, 026044 (2022).

28. Flesher, S. N. *et al.* A brain-computer interface that evokes tactile sensations improves robotic arm control. *Science* **372**, 831–836 (2021).

29. Andersen, R. A. & Aflalo, T. Preserved cortical somatotopic and motor representations in tetraplegic humans. *Current Opinion in Neurobiology* **74**, 102547 (2022).

30. Valle, G. *et al.* Multifaceted understanding of human nerve implants to design optimized electrodes for bioelectronics. *Biomaterials* **291**, 121874 (2022).

31. Dadarlat, M. C., Sun, Y. J. & Stryker, M. P. Spatiotemporal recruitment of inhibition and excitation in the mammalian cortex during electrical stimulation. *bioRxiv* 2022.06.03.494729 (2022) doi:10.1101/2022.06.03.494729.

32. Callier, T., Suresh, A. K. & Bensmaia, S. J. Neural Coding of Contact Events in Somatosensory Cortex. *Cerebral cortex (New York, N.Y. : 1991)* 1–15 (2019) doi:10.1093/cercor/bhy337.

33. Merrill, D. R., Bikson, M. & Jefferys, J. G. R. Electrical stimulation of excitable tissue: design of efficacious and safe protocols. *Journal of Neuroscience Methods* **141**, 171–198 (2005).

34. Rajan, A. T. *et al.* The effects of chronic intracortical microstimulation on neural tissue and fine motor behavior. *J. Neural Eng.* **12**, 066018 (2015).

35. Greenspon, C. M. *et al. Biomimetic Multi-Channel Microstimulation of Somatosensory Cortex Conveys High Resolution Force Feedback for Bionic Hands*. http://biorxiv.org/lookup/doi/10.1101/2023.02.18.528972 (2023) doi:10.1101/2023.02.18.528972.

36. Sombeck, J. T. & Miller, L. E. Short reaction times in response to multi-electrode intracortical microstimulation may provide a basis for rapid movement-related feedback. *J. Neural Eng.* **17**, 016013 (2019).

37. Shelchkova, N. D. *et al.* Microstimulation of human somatosensory cortex evokes task-dependent, spatially patterned responses in motor cortex. 2022.08.10.503543 Preprint at https://doi.org/10.1101/2022.08.10.503543 (2022).

38. Okorokova, E. V., He, Q. & Bensmaia, S. J. Biomimetic encoding model for restoring touch in bionic hands through a nerve interface. *J. Neural Eng.* **15**, 066033 (2018).

39. Christel, M.I., Ktizel, S., & Niemitz, C. How Precisely Do Bonobos (Pan paniscus) Grasp Small Objects? *International journal of primatology* **19**, 165–194 (2020).

40. Blankenburg, F., Ruben, J., Meyer, R., Schwiemann, J. & Villringer, A. Evidence for a Rostral-to-Caudal Somatotopic Organization in Human Primary Somatosensory Cortex with Mirror-reversal in Areas 3b and 1. *Cerebral Cortex* **13**, 987–993 (2003).

41. Rosa M. Sanchez-Panchuelo *et al.* Within-Digit Functional Parcellation of Brodmann Areas of the Human Primary Somatosensory Cortex Using Functional Magnetic Resonance Imaging at 7 Tesla. *J. Neurosci.* **32**, 15815 (2012).

42. Roux, F.-E., Djidjeli, I. & Durand, J.-B. Functional architecture of the somatosensory homunculus detected by electrostimulation. *J Physiol* **596**, 941–956 (2018).

43. Geyer, S., Schleicher, A. & Zilles, K. Areas 3a, 3b, and 1 of Human Primary Somatosensory Cortex: 1. Microstructural Organization and Interindividual Variability. *NeuroImage* **10**, 63–83 (1999).

2.7: Appendix: Chapter 2 Supplementary Figures

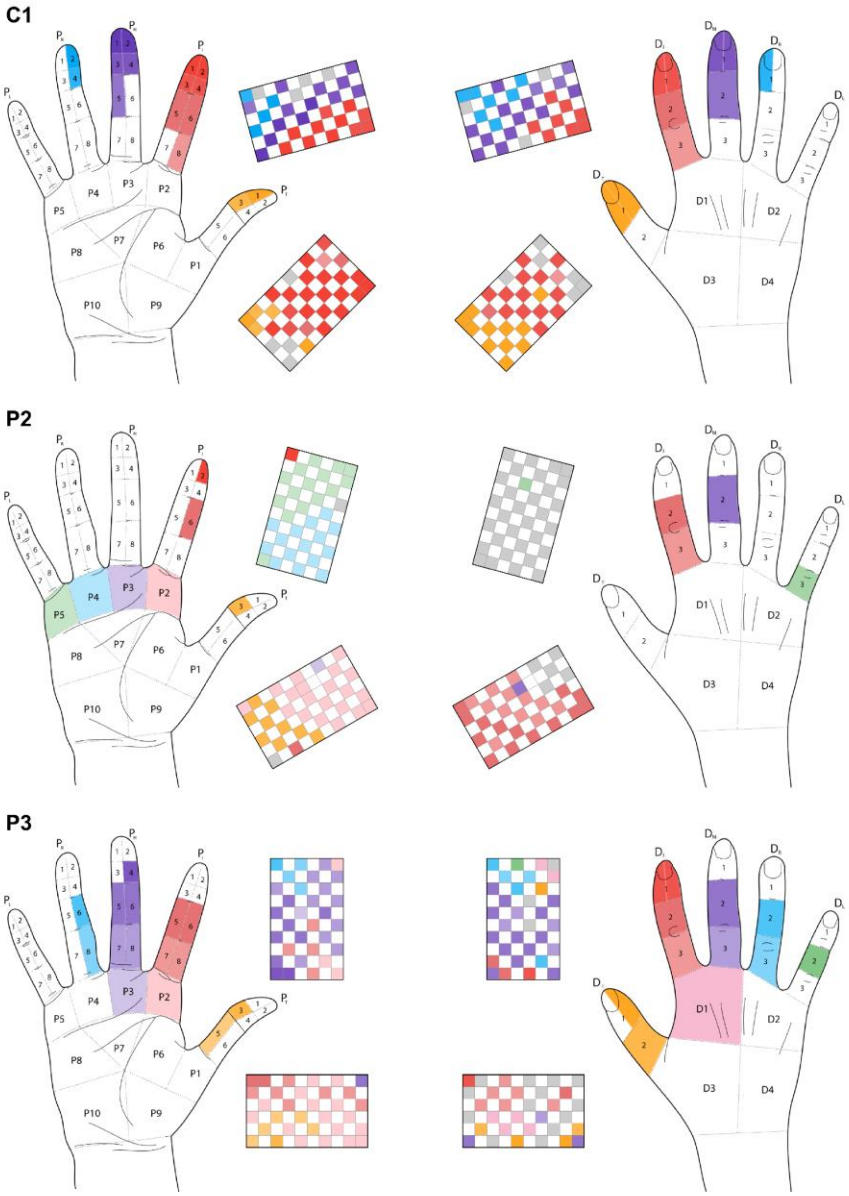

Supplementary Figure S2.1. Palmar and dorsal projected field maps for all participants. The hand diagrams show the distributions of the locations of the sensations evoked by ICMS any electrode on the palmar (left) and dorsal (right) surface of the hand. The array diagrams show the dominant hand segment for each electrode. All array rotations are approximately aligned such that up is medial and anterior is left.

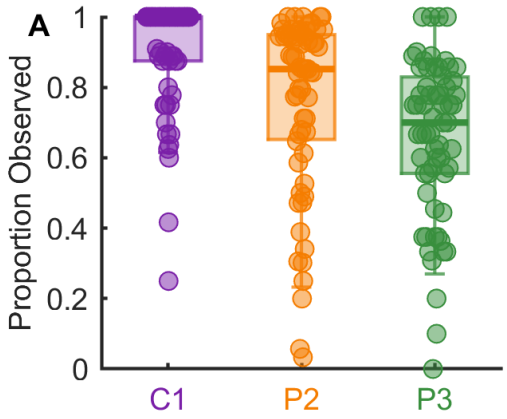

Supplementary Figure S2.2. Incidence of evoked sensations. Proportion of times that ICMS (at 100 Hz, 60 µA) through a given electrode evoked a sensation in the three participants.

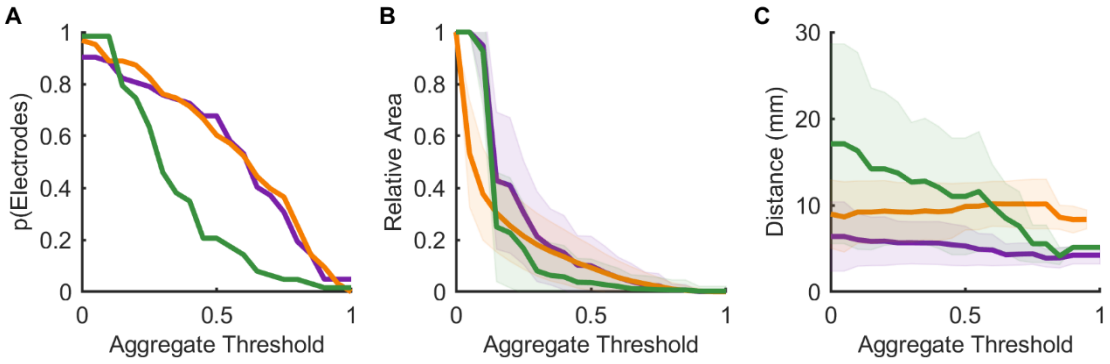

Supplementary Figure S2.3. Thresholding the aggregate PFs to assess stability. A| The proportion of electrodes for which any pixel exceeds the criterion decreases as the threshold increases. B| The area of the aggregate PF drops dramatically as the threshold increases to 0.25 and then decrease more slowly. C| The variability in the PF (Euclidean distance of each observation's centroid from the aggregate centroid) changes only marginally as threshold increases.

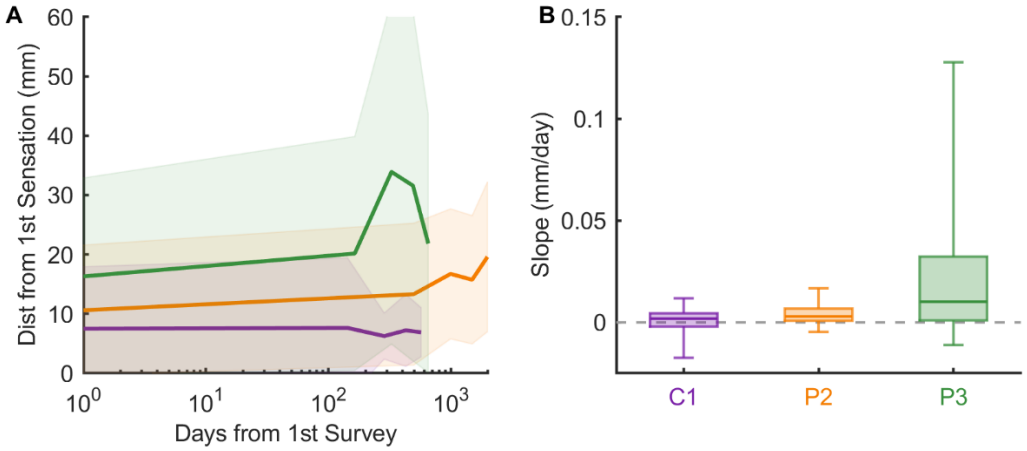

Supplementary Figure S2.4. Sensations are stable over time. A| The mean distance between the first centroid and subsequent ones is stable. B| The distribution of slopes computed from the data shown in panel A for individual electrodes grouped by participant.

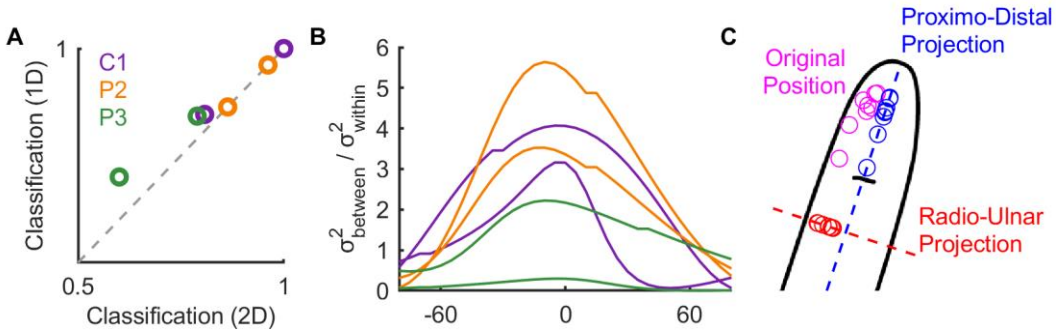

Supplementary Figure S2.5. Percepts are distributed along anatomical axes within S1. A| Digit classification when using either both axes (row & column) or the best single projected axis. B| Within class variance divided by across class variance for digit discrimination LDA as a function of rotation relative to the central sulcus. C| Example projections of percept centroids in their original position (magenta) when projected along either the proximo-distal (blue) or radio-ulnar (red) axes.

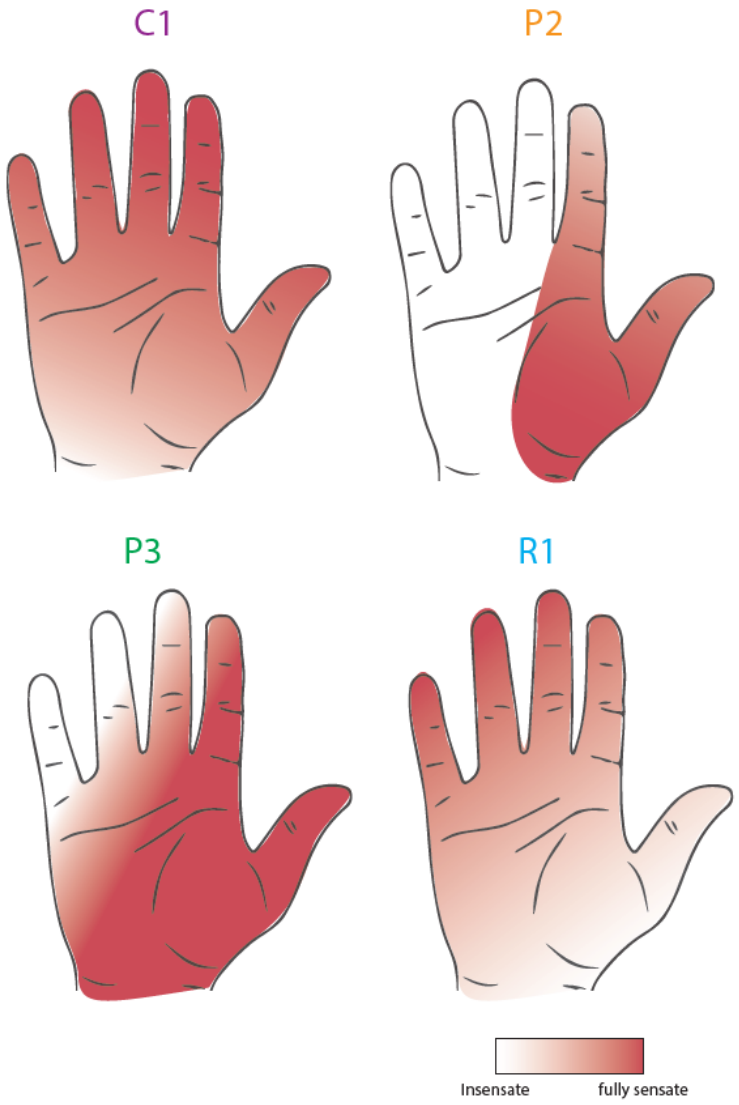

Supplementary Figure S2.6. Residual touch sensation for each participant.

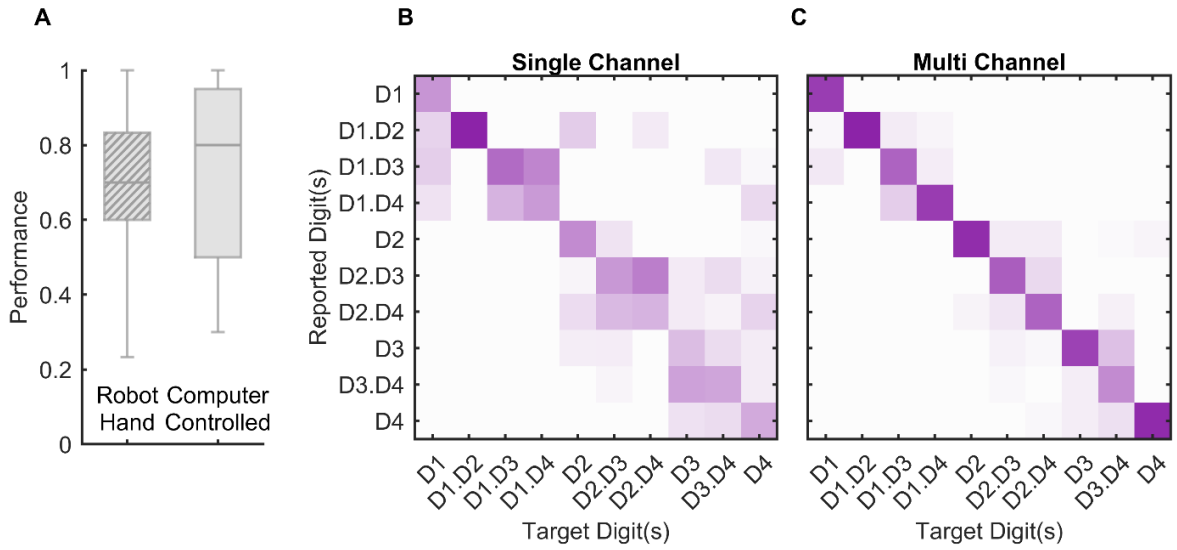

Supplementary Figure S2.7. Multi-electrode ICMS leads to improved localization. A| Performance on the localization task when stimuli were triggered via the robotic hand or the computer. Overall performance was statistically equivalent (2-sample t-test, $t(236) = 0.58$, $p = 0.56$). B| Confusion matrices for single and multi-channel stimulation. Data from participant C1.

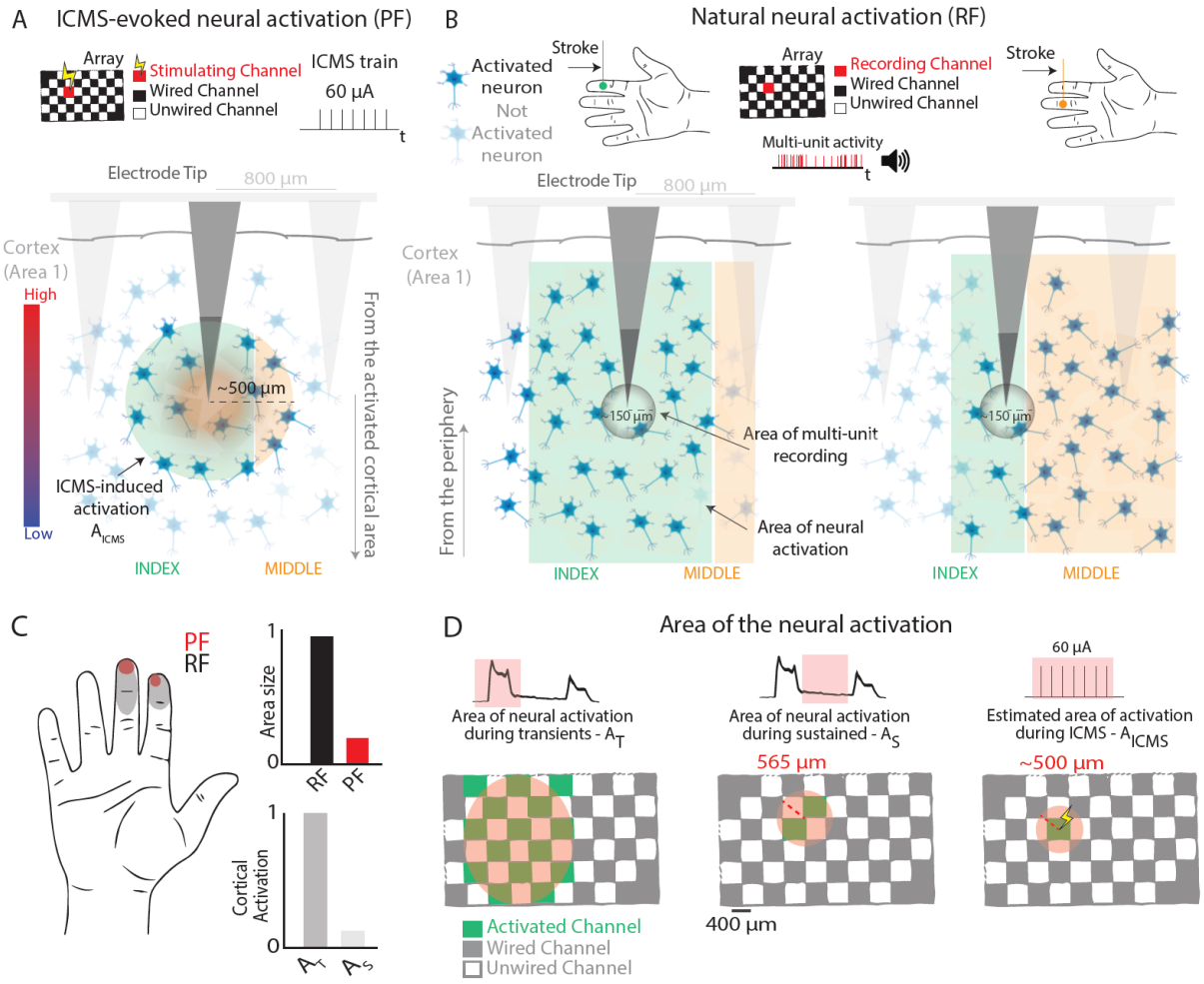

Supplementary Figure S2.8. Cortical activation during natural touch and ICMS. A| Illustration of cortical activation by ICMS and B| during RF mapping for a given electrode. The cortical activation by touch is much wider than that by ICMS. C| Considering the differences in cortical activation during transient and sustained phases of contact, the area of cortex activated by ICMS (A_{ICMS}) is on the same spatial scale as the hotzone (cortical activation during sustained contact - A_S), but systematically smaller than the transiently activated cortical area (- A_T), at a first approximation.

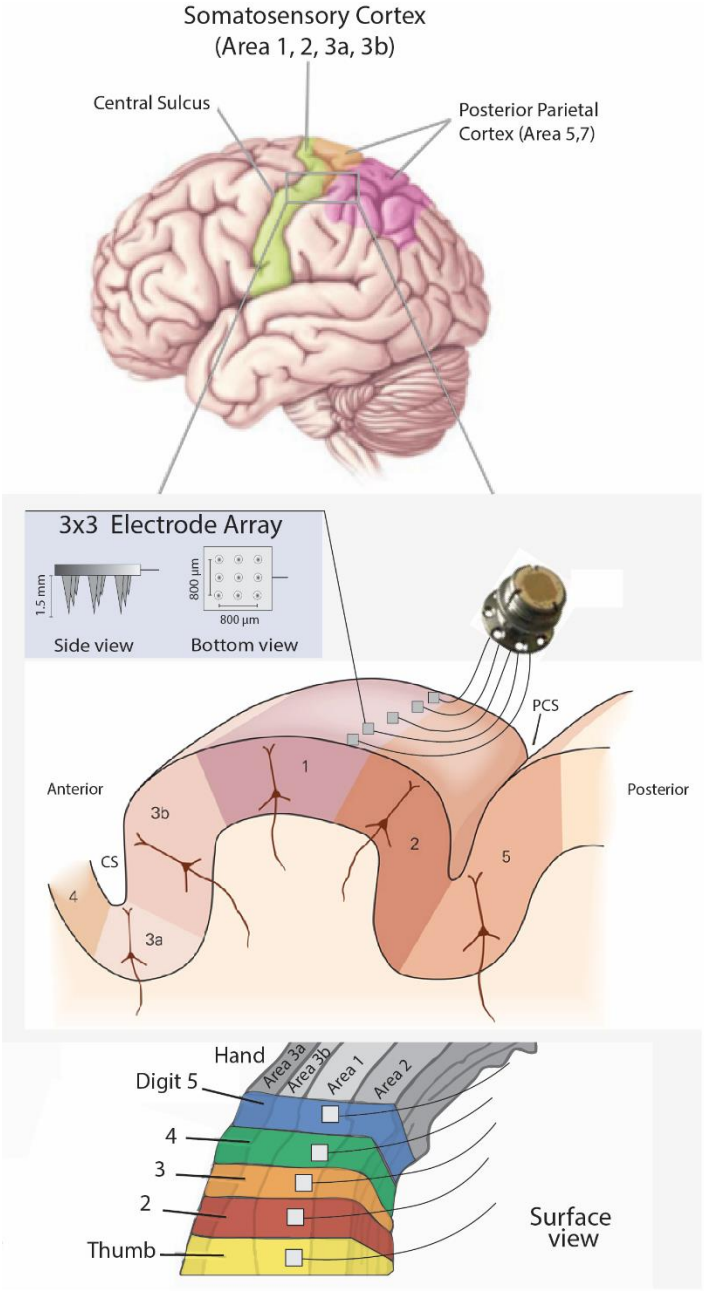

Supplementary Figure S2.9. Proposed design of the neural interface. Five 3 x 3 arrays are implanted in Brodmann's area 1 near its border with area 2, each centered on the respective representations of the five digits, identified using fMRI, MEG, or ECog.

CHAPTER 3 : The Relationship Between Somatotopy and Functional Connectivity[2]

3.0: Contributions to the work

NDS collected the data and wrote analysis for sections 3.3.1-3.3.3. CMG wrote the experimental protocols for the stimulation experiments and contributed to the mentorship and analysis design with NDS. JD collected data and wrote analysis for sections 3.3.4-3.3.5.

3.1: Abstract

The primary motor (M1) and somatosensory (S1) cortices play critical roles in motor control but the signaling between these structures is poorly understood. To fill this gap, we recorded – in three participants in an ongoing human clinical trial (NCT01894802) for people with paralyzed hands – the responses evoked in the hand and arm representations of M1 during intracortical microstimulation (ICMS) in the hand representation of S1. We found that ICMS of S1 activated some M1 neurons at short, fixed latencies consistent with monosynaptic activation. Additionally, most of the ICMS-evoked responses in M1 were more variable in time, suggesting indirect effects of stimulation. The spatial pattern of M1 activation varied systematically: S1 electrodes that elicited percepts in a finger preferentially activated M1 neurons excited during that finger's movement. Moreover, the indirect effects of S1 ICMS on M1 were context dependent, such that the magnitude and even sign relative to baseline varied across tasks. We tested the implications of these effects for brain-control of a virtual hand, in which ICMS conveyed tactile feedback. While ICMS-evoked activation of M1 disrupted decoder performance,

[2] This chapter is published at Nature Communications: https://doi.org/10.1038/s41467-023-43140-2

this disruption was minimized using biomimetic stimulation, which emphasizes contact transients at the onset and offset of grasp, and reduces sustained stimulation.

3.2: Introduction

Manual interactions with objects involve the integration of sensory signals – about the state of the hand and its interactions with objects – and motor signals – about intended actions. Dexterous hand use relies on both somatosensory and motor cortices as evidenced by the severe deficits in manual dexterity that follow lesions to either of these brain regions[1,2]. However, many of the cortical mechanisms of sensorimotor integration remain to be elucidated. Brodmann's area 1 of somatosensory cortex (S1) has been shown to send projections, albeit sparse ones, to primary motor cortex (M1)[3–5], and this direct sensorimotor pathway has been hypothesized to play a key role in integrating sensory signals with signals involved in motor execution. ICMS of human S1 has been shown to evoke responses in M1 local field potentials[6,7], and bipolar surface stimulation of monkey S1 evokes responses in M1 neurons[8], both consistent with the identified anatomical pathway. However, the modulation of single-cell responses in M1 to S1 stimulation and the function of the signals passed from S1 to M1 remain to be elucidated.

To fill this gap, we delivered – in three human participants whose hands were paralyzed as a result of a spinal cord injury – intracortical microstimulation (ICMS) to the hand representation of S1 while we recorded the responses evoked in the hand and arm representation of M1. First, we quantified the prevalence and temporal characteristics of ICMS-evoked activation. Second, we characterized the spatial pattern of activation in M1 and its relationship to the location of the stimulating electrode. Third, we compared ICMS-evoked M1

activity in different task conditions. Finally, we assessed the consequence of the ICMS-evoked activity on our ability to infer on-going motor intent from M1 signals.

3.3: Results

ICMS pulse trains varying in frequency and amplitude were delivered under two conditions: a passive condition in which the participants watched videos and an active condition in which they attempted to reach toward, grasp, and transport a virtual object, a task commonly used to calibrate decoders[9].

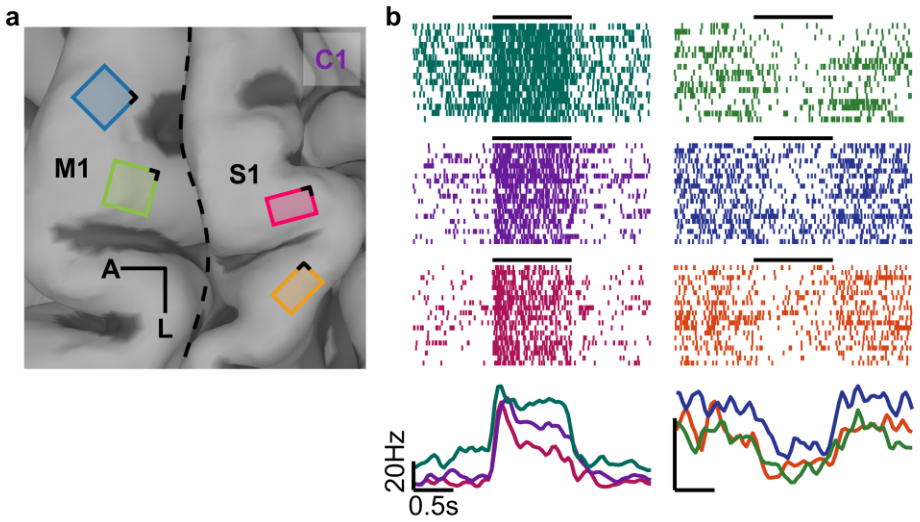

Figure 3.1. Array placements and interactions. A| Four NeuroPort electrode arrays (Blackrock Neurotech, Inc.) were implanted in the hand and arm representations of motor cortex (M1) and the hand representation of somatosensory cortex (Brodmann's area 1, S1). Here, the implant locations are shown for participant C1. The implant locations for the other two participants are shown in Supplementary Figure 1. Black lines indicate the posterior-medial corner of each array, which is used as a reference in later figures. B| M1 responses to ICMS trains delivered to S1. Responses of three example motor channels (spike rasters above and averaged, smoothed firing rates below) that were excited by ICMS (left) and three that were inhibited by ICMS (right). Black horizontal lines indicate the period of ICMS. The green rasters are from participant P3, the purple ones from participant C1.

3.3.1: Motor cortex responds to stimulation of somatosensory cortex

First, we examined the responses of M1 neurons to 60-μA, 100-Hz, 1-sec ICMS pulse trains delivered through individual electrodes in S1 in the passive condition (see Figure 3.1A and Supplementary Figure S3.1 for array locations). We found that, ICMS of S1 modulated activity on a majority of M1 channels (Figure 3.1B and Figure 3.2). For some pairs of M1/S1 channels, the M1 activity increased (Figure 3.1B, left), for other pairs, it decreased (Figure 3.1B, right). Most modulated M1 channels exhibited both increases and decreases in ICMS-evoked activity, depending on the stimulation channel (48%, 90%, and 98% for C1, P2 and P3 respectively). We verified that these effects were not electrical artifacts by confirming that they were also observed in the responses of sorted single units **(**Supplementary Figure S3.2 and Supplementary Figure S3.3). The prevalence and strength of these effects varied across participants: The effects were stronger and more prevalent in participant C1 than in the other two (P2 and P3, Figure 3.2, Supplementary Figure S3.4). The participants also differed in the sign of the ICMS-induced modulation, with primarily excitatory responses in C1 (94.2%) and a more even mix in P2 and P3 (39.3% and 46.0% excitatory, respectively).

3.3.2: Stimulation of somatosensory cortex can directly activate neurons in motor cortex

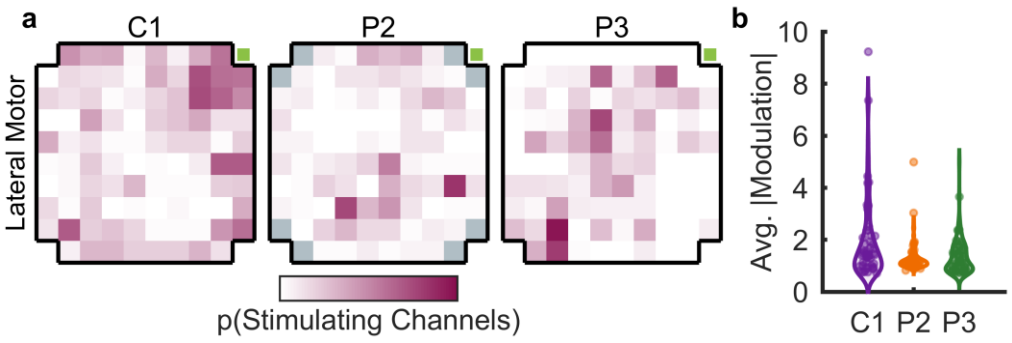

Figure 3.2. Prevalence of ICMS-evoked activity in motor cortex. A| Proportion of stimulating channels that significantly modulated each motor channel on the lateral motor array of each participant (range: 0 - 0.7). In P2, grey squares indicate channels that are not wired. The majority of M1 channels could be modulated by ICMS through at least one S1 channel. The green square indicates the posterior-medial corner of the array (see Figure 3.1A and Supplementary Figure S3.1). B| ICMS-driven modulation of activity in individual M1 channels, averaged across stimulating channels. Modulation is the ICMS-driven change in the response, normalized by baseline activity.

Next, we examined whether the ICMS-evoked activation of M1 was temporally locked to the stimulation pulses at a short latency, suggesting direct input from S1. To this end, we computed the pulse-triggered average for each pair of stimulating and recording electrodes. We found M1 channels with responses that were systematically locked to the stimulation pulses (Figure 3.3A; Supplementary Figure S3.5). For most of these channels, the evoked neural activity occurred between 2 and 6 ms after pulse onset with millisecond or even sub-millisecond jitter across pulses (Figure 3.3B; Supplementary Figure S3.6). To eliminate the possibility that the response latency was longer than the inter-pulse duration, we measured the latency with pulse trains at different frequencies (25, 50, and 100 Hz) and found the latency to be consistent (Supplementary Figure S3.7). Of the M1 channels that were modulated by ICMS delivered to S1, 37%, 0.6%, and 32% exhibited this pulse-locked response in C1, P2, and P3, respectively. In contrast to these channels, which seem to receive direct input from S1, most channels exhibited

large and significant ICMS-evoked shifts in firing rate with no pronounced peak in the pulse-triggered average (Figure 3.3C; Supplementary Figure S3.8). Thus, while some of the ICMS-evoked activity in M1 seems to be triggered through direct, possibly monosynaptic connections from S1, most of it seems to reflect more indirect effects.

3.3.3: The spatial pattern of activation in motor cortex varies systematically across stimulating electrodes

Next, we examined the spatial patterns of activity evoked over the M1 surface (both direct and indirect) by ICMS in S1 and assessed whether the patterns differed systematically across stimulating electrodes. We found that different stimulating electrodes evoked different spatial patterns of activation in M1 (Supplementary Figure S3.9). Moreover, these patterns changed systematically: neighboring stimulating electrodes tended to produce more similar patterns of M1 activation than did distant stimulating electrodes, which sometimes produced entirely non-overlapping patterns. This was particularly pronounced when comparing the spatial pattern of M1 activation evoked by electrodes in different S1 arrays: M1 activation patterns evoked by two electrodes on the same S1 array were significantly more correlated than the patterns evoked by two electrodes on different arrays ($p < 0.001$, Wilcoxon Rank-Sum test for each of the three participants, Supplementary Figure S3.9). Within array, the correlation decreased as the distance between the two S1 channels increased (Supplementary Figure S3.10). While the trends were similar, P2 showed lower correlations in ICMS-evoked spatial patterns across all M1/S1 pairs.

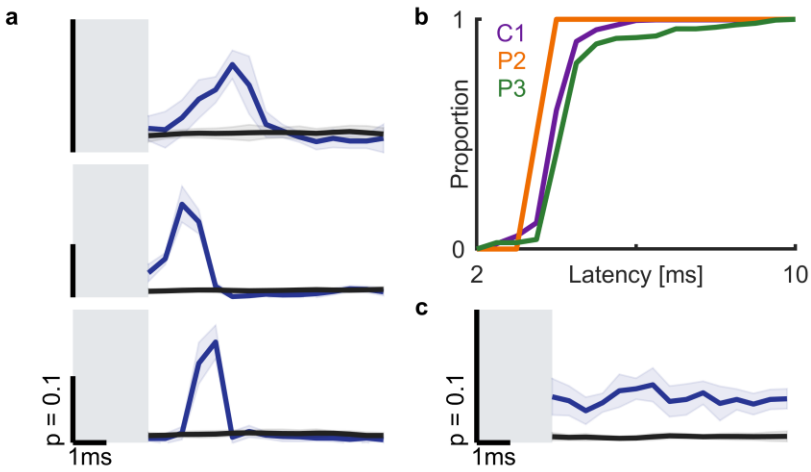

Figure 3.3. Short-latency, pulse-locked responses in M1. A| Pulse-triggered average of the responses of three motor channels to ICMS at 100 Hz. On a subset of channels, such as these, responses were tightly locked to each pulse with millisecond or even sub-millisecond jitter across pulses. Blue line denotes the response during stimulation, black line the response during baseline (sham stimulation), grey box indicates blanked recording time to eliminate the stimulation artifact. Error bars represent bootstrapped standard error. Scale bar indicates a 10% probability of a spike occurring in a 0.5-ms bin. B| Cumulative distribution of the latency of the peak pulse-locked, direct, response. Latencies tended to be shorter than 6 ms. C| Pulse-triggered average of the response of a motor channel whose activity increases with stimulation but is not pulse locked. Error bars represent bootstrapped standard error.

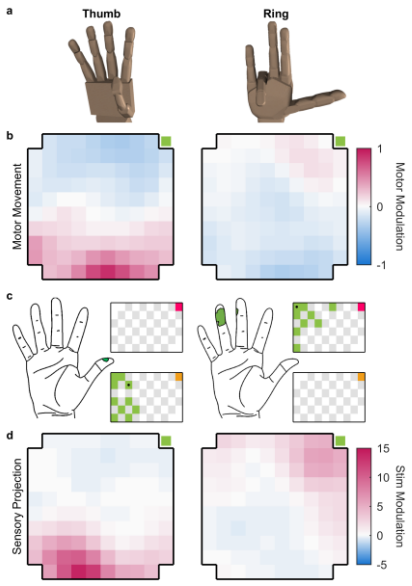

Figure 3.4. Shared somatotopy between movement-evoked and ICMS-evoked activity in participant C1. A| Rendering of the extrema of thumb and ring flexion in virtual reality. B| Z-scored difference in firing rate during attempted flexion of the thumb (left) and ring finger (right) vs. the mean activation during attempted flexion of each of the 5 digits. The green square indicates the posterior-medial corner of the array (Figure 3.1A). C| The green regions on the hand diagrams denote the projected fields reported by participant C1 when stimulated through one channel in the lateral and medial sensory array, respectively (indicated by a black dot in the array maps). Channels shaded in green on the array diagram denote electrodes with projected fields on the thumb and ring finger, respectively. Channels shaded in gray denote unwired electrodes. Pink and orange squares in the top right indicate the posterior and medial corner of the medial and lateral sensory array, respectively (Figure 3.1A). D| Average M1 activity evoked by stimulation through S1 channels with projected fields on the thumb (left) and the ring finger (right). Motor channels that respond strongly to attempted thumb or ring finger movements tend to also be strongly activated by stimulation of electrodes with projected fields on the thumb or ring finger, respectively. Green squares indicate the posterior and medial corner of the array (Figure 3.1A).

Examination of the spatial patterns of M1 activation suggested a coordinated progression of effects across the S1 arrays. In participant C1, for example, lateral stimulating electrodes tended to activate neurons on the lateral aspect of the M1 array and medial stimulating electrodes tended to activate more medially located M1 neurons (Supplementary Figure S3.9A).

We hypothesized that this progression reflects the respective somatotopic organizations of S1 and M1. For example, stimulation through electrodes in the S1 thumb representation might preferentially activate neurons in the M1 thumb representation. To test this hypothesis, we mapped the somatotopic organization of M1 by measuring, on each motor channel, the evoked activity when the participant attempted to move each digit. For each motor channel, we computed the difference between the activation evoked during attempted movement of each digit and the mean activation during movement of each of the five digits (motor map Figure 3.4A,B). This analysis gauged the extent to which a motor channel responded more during attempted movement of some digits than others. We mapped the somatotopic organization of S1 by identifying the digit on which the participant reported the sensation when stimulation was delivered through each electrode (the projected field, PF, Figure 3.4C). Having constructed these motor and sensory maps, we then derived the pattern of M1 activation when ICMS was delivered through electrodes with PFs on each digit in turn (sensory projection map, Figure 3.4D). Finally, we assessed the degree to which the motor map matched the sensory projection map. To this end, we compared the activation evoked in individual M1 channels by stimulation through somatotopically matched S1 electrodes, that is those with PFs on the digit that maximally activated the M1 channel during attempted movement, to the activation evoked by stimulation through unmatched electrodes. We found the M1 activation was greater for somatotopically matched than unmatched pairs ($p < 0.001$, Wilcoxon Rank-Sum test) for participants C1 and P3 (Figure 3.5A, Supplementary Figure S3.11).

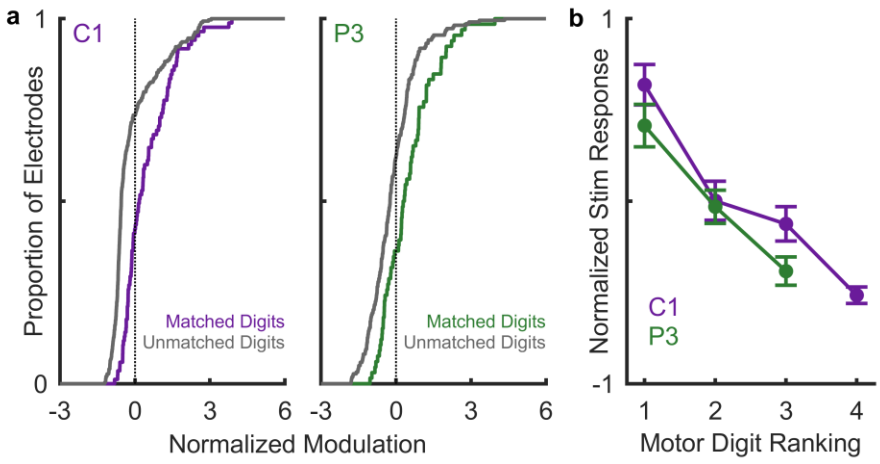

Figure 3.5. M1 is somatotopically linked to S1. A| In participants C1 and P3, M1 electrodes are more susceptible to ICMS delivered through S1 electrodes whose projected fields match the movement fields. B| When the dominant movement field matches the dominant digit in the projected field, the susceptibility is strongest; when the second most dominant movement field matches the dominant digit projected field, the susceptibility is weaker; etc. Lines denote the mean, error bars the standard error of the mean, n=96 channels.

As most M1 channels responded to multiple digits and could be activated even by unmatched S1 channels, albeit to differing degrees, we next assessed whether the full pattern of M1 activity evoked during attempted single-digit movements was predictive of the digit dependence of the ICMS-evoked activity. For example, would an M1 channel that responded most to attempted movement of the thumb, then index, then middle finger be most susceptible to stimulation through S1 channels with thumb PFs, less susceptible to stimulation through S1 channels with index PFs, and least susceptible to channels with middle finger PFs? For participants C1 and P3, we observed the hypothesized result across M1 channels (Figure 3.5B, Kruskal-Wallis $p < 0.001$) and in single M1 channels (Supplementary Figure S3.12). These results are consistent with the hypothesis that electrical activation of S1 neurons leads to preferential activation of M1 neurons with matching movement fields in participants C1 and P3.

The somatotopic link between S1 and M1 was much weaker and, in fact, non-significant in participant P2. Note, however, that ICMS-driven M1 activation in this participant was sparse (Figure 3.2A), weak (Figure 3.2B), and unpatterned (Supplementary Figure S3.9C,D). We attribute the lack of spatial patterning to the fact that this participant's most lateral M1 array, more medial than its counterparts in the other two participants, was located in the proximal limb representation as evidenced by robust arm- but weak digit-related activity. The M1 arrays in participant P2 are also much older than are those in participants C1 and P3, which may have contributed to the observed differences, though robust movement-related signals could still be harnessed from this array (Supplementary Figure S3.13).

3.3.4: Stimulation-evoked activation in motor cortex differs across tasks

The analyses shown above were carried out on M1 responses collected when the participants were not engaged in any motor task. Because manual touch typically occurs in the context of active interactions with objects, we next examined whether the signaling between S1 and M1 might depend on motor behavior. To this end, we measured ICMS-evoked responses in M1 as participants C1 and P3 performed two tasks. In the first task ('squeeze'), they attempted to squeeze a cylinder in a virtual reality environment (i.e., without making any overt movement). In this task, contact with the virtual cylinder triggered ICMS (frequency = 100 Hz) through two electrodes delivered at one of four amplitudes (20, 32, 44, and 56 μA), presented in random order. The participants were instructed to report the magnitude of the percept evoked by the ICMS train to ensure their engagement. In the second task (grasp and transport), the participants observed and attempted to mimic the actions of a virtual limb as it reached for and grasped the cylinder in one location and transported it to a different location. Upon grasp, the same ICMS

trains were delivered as in the squeeze task (again ordered randomly across trials) until the object reached the target location. For this task, we analyzed the responses during the grasp phase and the transport phase separately. We reasoned that the grasp epoch involved the same behavior as did the 'squeeze' task, whereas the transport phase involved a different behavior. We then compared M1 responses to ICMS across the three conditions ('squeeze,' 'grasp,' and 'transport').

We first verified that M1 was engaged in the two behavioral tasks by examining the task dependence of the M1 activity. We found that activity on most motor channels differed across task conditions (squeeze vs. grasp vs. transport, >80% of the electrodes exhibited significant task modulation according to a multi-way ANOVA, $p < 0.05$ in both participants). Moreover, the observed reach endpoint could be decoded during the grasp and transport task from the M1 population activity (84 and 87% classification accuracy for two sessions with participant C1 and 26% accuracy for participant P3; chance = 12.5%; in participant P3, the motor arrays were much more strongly modulated by hand/wrist than shoulder movements, thus the poor performance).

Examining the dependence of the M1 activity on ICMS amplitude, we found that many motor channels were modulated in an amplitude dependent way, generally exhibiting higher firing rates at higher ICMS amplitudes (across participants and pairs of stimulating electrodes, 31% and 78% for two sessions with participant C1 and 54% for one session with participant P3; $p < 0.05$ multi-way ANOVA, Supplementary Figure S3.14). Surprisingly, however, the effect of ICMS varied across tasks: the responses of some M1 neurons were strongly modulated by ICMS during some tasks but not others. Even the 'squeeze' and 'grasp' conditions sometimes yielded

different ICMS-evoked M1 activations, even though the behavior is nearly identical – the only difference being that grasp occurs at the end of a reach and just before transport whereas squeeze is a single, isolated movement. To quantify the task dependence, we computed the interaction between task and ICMS amplitude and found that a large number of M1 units yielded a significant interaction (17% and 42% for the two sessions with participant C1 and 19% for the session with participant P3, $p < 0.05$) (Figure 3.6A, Supplementary Figure S3.15A).

To further demonstrate the task dependence of the ICMS effects, we built a classifier of ICMS amplitude based on responses obtained in one of the three conditions (squeeze, grasp, transport) and attempted to use it to decode ICMS amplitude from the responses in the other two conditions. We found that, while we could decode ICMS amplitude on held-out data within condition with up to 69% accuracy in C1, performance was worse across conditions (Figure 3.6B, Supplementary Figure S3.15B). In particular, the effects of ICMS during transport were very different from during squeeze or grasp as evidenced by the poorer performance of classifiers built on the former and tested on the latter (33% accuracy).

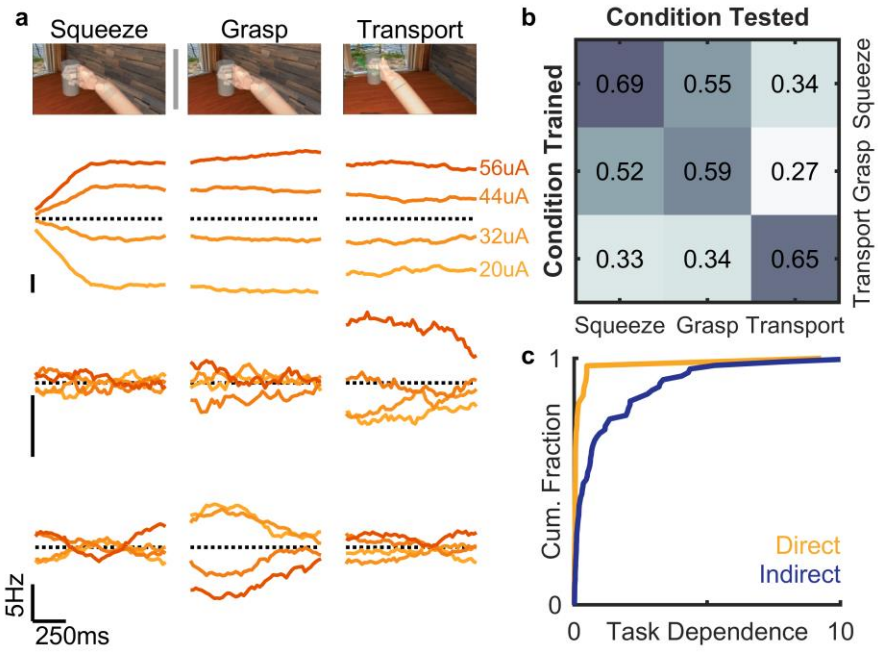

Figure 3.6. ICMS-evoked activity depends on behavior. A| Top: Squeeze, grasp, and transport in the VR environment. Bottom: Three example motor channels from Participant C1 exhibit different responses to four levels of ICMS across three motor conditions (squeeze, grasp, transport). Traces denote the firing rate evoked by stimulation at the four levels after subtraction of the mean across conditions. B| Stimulation amplitude classifier performance. Classifiers were trained from M1 activity on one of the three conditions and tested on activity in each condition (cross-validated within condition). C| Task dependence – gauged by the strength of the condition/amplitude interaction divided by the strength of the main effect of amplitude – is nearly zero for the pulse-locked responses (direct) but varies widely for the non-pulse locked (indirect) ones. The response of units with direct input from somatosensory cortex respond the same way to ICMS across behavioral conditions.

The task dependence of ICMS-evoked M1 activity varied idiosyncratically across M1 channels. For example, one M1 channel was susceptible during the transport phase but not the grasp phase while another channel showed the reverse pattern of responses (Figure 3.6A). This heterogeneity suggests that the task-dependence of the modulation was not driven by array-wide differences in the baseline activity across conditions, for example, reflecting saturation due to higher baseline activation in some conditions. Even at the single channel level, the modulation

strength was not systematically related to the (task-dependent) baseline firing rate ($p > 0.05$ for both participants, Friedman's Test, Supplementary Figure S3.16). This heterogeneous pattern of task-dependent susceptibility to ICMS implies that ICMS-evoked activity in M1 cannot be straightforwardly distinguished from intrinsic motor-related activity.

Interestingly, the task dependence of the susceptibility to ICMS was not observed for M1/S1 pairs that exhibited pulse-locked responses Figure 3.6C), suggesting that this dependence does not reflect a change in the direct input from S1 but rather a change in the impact of this input on M1.

3.3.5: ICMS-EVOKED M1 ACTIVITY CONTAMINATES MOTOR DECODING

In BCIs, signals from M1 are often used to infer motor intent and control the bionic limb[10]. The observed contamination of these intrinsic signals about intended movement with contact-related signals stemming from ICMS to S1 is thus liable to interfere with motor decoding and degrade the function of the bionic limb. To investigate this possibility, we trained a decoder (Optimal Linear Estimator)[9] to control a virtual arm across three translational degrees of freedom to enable C1 to reach to an object, grasp it, and transport it to a new location. The grasp was automatically triggered once the hand reached the object's location, to decouple the ICMS from the grasp kinematics, thereby ensuring that the ICMS was identical across grasps. During object contact, ICMS at 100 Hz and 52 μA was delivered through two electrodes (with PFs on the thumb and index), evoking a sensation whose strength was commensurate with the grasp force required to maintain object grasp (i.e., sufficient to evoke a moderately strong tactile sensation). The stimulation led to significantly more trials on which the participant was unable to complete the transport within the allotted 10-second window (38% and 12%, with and without

stimulation, respectively, $p < 0.001$, chi-squared test; Figure 3.7A). These failures were primarily due to increases in path length – the distance travelled to reach the target – during transport with stimulation compared to without (4.6 m vs. 1.4 m, both $p < 0.001$, two-sample Kolmogorov-Smirnov test; Figure 3.7B). In other words, the ICMS contaminated the M1 activity used by the decoder to infer on-going motor intent. The disruption is likely to be far stronger when decoding hand (rather than arm) movements given that ICMS-driven activity in M1 is strongest for somatotopically linked segments.

3.3.6: Biomimetic somatosensory feedback rescues decoder performance

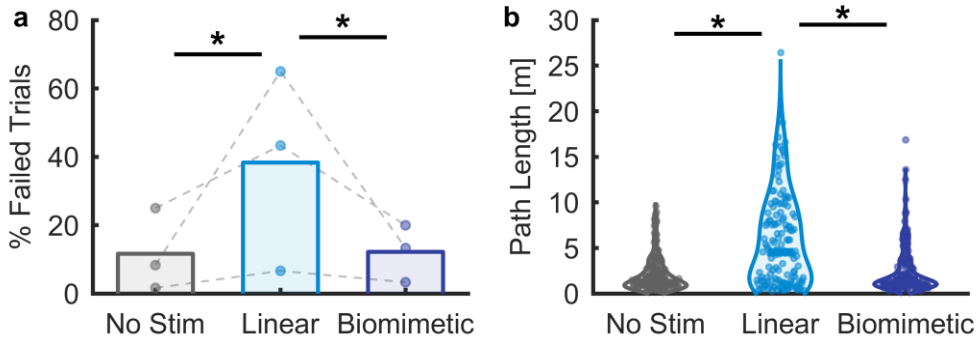

Figure 3.7. Decoder performance with and without sensory feedback (from participant C1). A| Failure rate for the three conditions. Rates collected during a single session are connected by a dotted line. B| Path length during the transport phase with different stimulation conditions. Linear stimulation caused the path length of the transport phase to be significantly longer than without stimulation ($p = 10^{-12}$, K-S Test, two-sided). In contrast, biomimetic stimulation was significantly more efficient than its linear counterpart ($p = 10^{-10)}$ and not significantly different from the no-stimulation condition ($p = 0.4$).

Importantly, because ICMS-evoked activity in M1 is task dependent, its influence on a decoder cannot be easily predicted and eliminated. However, we reasoned that reducing the intensity of ICMS would reduce its deleterious effects. With peripheral nerve interfaces, biomimetic somatosensory feedback – characterized by high-amplitude phasic stimulation at the

onset and offset of contact, and far weaker stimulation during maintained contact[11,12] – has been shown to elicit more natural and intuitive sensations[13,14]. In the present context, we reasoned that this feedback might offer the additional benefit of reducing the total amount of stimulation and thus be less deleterious to decoding. To test this possibility, we had the participant perform the reach, grasp, and transport task but provided information about grasp force using biomimetic ICMS-based feedback. With biomimetic feedback, the onset and offset transient amplitudes were higher than the highest amplitude used in the standard trains – termed 'linear' because they track the applied force – but sustained stimulation was weaker (32 vs. 52 μA). With this feedback, the participant transported objects with a third as many failures compared with linear stimulation (12% vs. 38%, $p < 0.001$, chi-squared test; Figure 3.7A). This improved performance was characterized by shorter movements during the transport phase (1.4 m vs. 4.6 m $p < 0.001$, two-sample Kolmogorov-Smirnov test; Figure 3.7B). In fact, performance with the biomimetic feedback was nearly identical to that with no stimulation (12% vs. 12% failure rate, $p = 0.87$, chi-squared test; mean path length was numerically identical for both conditions at 1.4 m; Figure 3.7). Note that ICMS-feedback did not have any beneficial effects on performance (as it has been previously shown to do[15]) because grasping was automated and therefore did not require or allow for any online correction.

3.4: Discussion

We show that ICMS of S1 evokes widespread activity in M1. Some of this activity takes the form of short-latency responses to ICMS that are time-locked to individual ICMS pulses. Most of the ICMS-driven activation in M1 is not pulse-locked, however, and seems to reflect an indirect effect of S1 input. In both cases, the spatial pattern of evoked activity in M1 depends

systematically on the location of the S1 stimulating electrode: an M1 channel is susceptible to being modulated by an S1 channel to the extent that they both encode a matching part of the hand. The signals that are directly transmitted from S1 to M1 are consistent across tasks, but their indirect impact on M1 activity is highly task dependent and varies widely across pairs of S1/M1 channels. Finally, ICMS-evoked M1 activity is relevant to prosthetics as it disrupts the ability to decode motor intent. However, this disruption can be minimized with a more biomimetic form of somatosensory feedback, which emphasizes the transient phases of object contact (its onset and offset) and minimizes sustained ICMS, mirroring the patterns of neuronal activity during object interactions.

In both humans and macaques, Brodmann's area 1 and M1 have been shown to be connected anatomically[3,4]. In macaques, tracer injections in area 1 reveal reciprocal connections with M1[3,5], albeit sparse ones. In humans, probabilistic diffusion tractography reveals strong connections between area 1 and M1[4]. Microstimulation of human somatosensory cortex with either surface or penetrating electrodes has been shown to evoke field potentials in motor cortex[6,7], revealing a functional correlate to the anatomical findings. However, neither the time course of these signals nor their spatial specificity could be gleaned from these measurements of aggregate neuronal activity in M1. While short latency ICMS-evoked responses have been found across sensorimotor cortex in other organisms[8,16–20], the present report is the first to document systematic signaling between somatosensory and motor cortices of humans at the cellular level. In macaques, surface stimulation of S1 was shown to evoke responses in M1 with latencies ranging from ~1 to 7 ms[8], consistent with our results. Because we discard the first 2 ms of the response after pulse onset to avoid contamination from the stimulation artifact, we likely missed

some responses that occurred at shorter latencies. Some of the short-latency, low-jitter M1 responses to ICMS in S1 may reflect antidromic activation[21,22], but the latency, jitter, and spiking probabilities of the pulse-locked responses were smoothly distributed over a range, offering no hint of a separation between two classes of activation (antidromic vs. orthodromic) (Supplementary Figure S3.6).

We found that the functional connectivity between S1 and M1 is patterned: neighboring electrodes in S1 produce similar spatial patterns of activation in M1. Moreover, this patterning follows somatotopic maps in S1 and M1: a given channel in S1 is liable to activate a given channel in M1 to the extent that these encode overlapping parts of the hand. The somatotopic patterning in M1 seems at odds with the observations that individual M1 neurons encode movements of joints distributed over the entire hand[23–25], resulting in a coarse somatotopic organization. Nonetheless, we observed a somatotopic progression over the sampled cortex, even within the M1 hand representation. The pattern of digit preferences in the movement fields of an individual M1 channel mirrored the pattern of digit preferences in the S1 channels that were most effective in activating that channel. The somatotopic organization of the S1-M1 connectivity is consistent with the interpretation that sensory feedback from a given digit preferentially informs the ongoing motor control of that digit. Note, however, that we were also able to decode reaching movements from the putative hand representation in M1, arguing this somatotopic organization is not absolute, consistent with prior findings[26]. The somatotopically linked connectivity observed here accounts for the observation in macaques that M1 neurons receive tactile input on the associated hand segment[27], the provenance of which had not been established. The anatomical substrates for this somatotopically linked connectivity have been

previously established at the level of arm vs. hand[5,28], but our observation at the level of fingers suggests an even more specific somatotopic link. Analysis of the nature of these signals during natural manual interactions in intact humans and monkeys will shed further light on the functional role of this cortico-cortical signaling.

ICMS of hand S1 has been shown to elicit vivid sensations that are experienced on the hand[10,29–32]. These sensations can be used to provide tactile feedback about object interactions and have been shown to improve the functionality of a brain-controlled robotic hand[15]. In the one demonstration of the benefits of somatosensory feedback on object manipulation, however, the participant's motor arrays, which were located in the proximal limb representation of M1, were only weakly impacted by ICMS to hand S1 (P2 in this study, see Supplementary Figure S3.1). When M1 and S1 arrays are both in the respective hand representations, as in C1 and P3, ICMS has a deleterious effect on decoding, thereby counteracting – at least in part – any benefits of sensation. The fact that the majority of ICMS-induced activity in M1 is dependent on behavior implies that mitigating the impact of ICMS on decoding will be challenging. Indeed, training a decoder based on combined observation and stimulation will work only (1) if the decoder is trained on tasks that span the space of possible behaviors and (2) if the subspace of ICMS-evoked activity in M1 is largely non-overlapping with that involved in motor control[33]. The first condition will be difficult to meet given realistic time constraints, and we have evidence that the second condition is not met (Supplementary Figure S3.17). Fortunately, we were able to eliminate the impact of ICMS on decoding by implementing phasic biomimetic feedback, designed to mimic natural cutaneous responses in cortex. Indeed, throughout the somatosensory neuraxis, neural populations respond more strongly at the onset and offset of

object contact and much more weakly to maintained contact[34,35]. Sensory feedback with this property entails weaker ICMS during maintained grasp, thereby resulting in weaker and thus less disruptive effects of ICMS in M1 (Supplementary Figure S3.12). In studies on electrical interfaces with the peripheral nerve, biomimetic sensory feedback has been shown to be more intuitive and naturalistic[13,14,36]. In studies with BCIs, we have shown that biomimetic ICMS yields more precise force feedback[37]. Here, we show that biomimetic stimulation also alleviates the disruptive effect of ICMS on decoding performance for brain-controlled bionic hands.

ICMS in S1 reveals strong signaling from S1 to M1 that is patterned such that S1 neurons with projected fields on one hand region preferentially activate M1 neurons that are implicated in moving that part of the hand. While the (seemingly) direct connection between S1 and M1 is fixed, the overall impact of ICMS to S1 on M1 activity is task dependent. This channel of communication between S1 and M1 disrupts the decoding of motor intent from M1 signals, but this disruption can be minimized using biomimetic feedback.

3.5: Methods

This study was approved by the institutional review boards at the University of Chicago and the University of Pittsburgh (Pittsburgh, PA, USA), and was carried out under an investigation device exemption (IDE) from the FDA.

3.5.1: Participants

The three participants, part of a multi-site clinical trial (registered on clinicaltrials.gov, NCT01894802), provided informed consent including prior to any experimental procedures. The primary eligibility criterion for the clinical trial was paralysis of at least one hand following spinal cord injury or brain-stem stroke. The primary exclusion criteria were any health concerns that

were likely to be exacerbated by surgery or brain stimulation (e.g. chronic pressure sores or a history of seizures). All three participants were male between the ages of 28 and 57 at time of implant and presented with SCI that occurred between 10 and 35 years prior. The primary outcome of the ongoing trial is that the implant is safe for at least one year; all enrolled participants have exceeded this goal. The secondary outcome was functional use of the device; assessment of this outcome is still active. The results presented here do not contribute to the assessment of these outcomes. Participant C1 presented with a C4-level ASIA D spinal cord injury (SCI). He had no spared control of the intrinsic or extrinsic muscles of the right hand but retained the ability to move his arm with noted weakness in many upper limb muscles. Filament tests revealed spared deep sensation but diminished light touch in the right hand (detection thresholds ranged from 0.6 to 2.0 g across digit tips). Data were collected 1-1.5 years after implant. Participant P2 presented with a C5 motor/C6 sensory ASIA B SCI. He had no spared control of the intrinsic or extrinsic muscles of the right hand but had limited control of wrist flexion and extension. Proximal limb control at the shoulder was intact, as was elbow flexion. However, he had no voluntary control of elbow extension. He was insensate in the ulnar region of the hand (digits 3-5) on both the palmar and volar surfaces but retained both diminished light touch and deep sensation on the radial side (digits 1-2) (thresholds were 1.4 g to 8 g on the thumb and index, respectively, and 180 g on the middle finger). Data were collected 6.5 years after implant. Participant P3 presented with a C6 ASIA B SCI. He had no functional control of the intrinsic or extrinsic muscles of the right hand but retained the ability to move his arm with noted weakness in many upper limb muscles. He was insensate in the ulnar region of the hand on both the palmar and volar surfaces but retained diminished light touch and deep sensation on

the radial side (thresholds were 0.07 g and 1.6 g on the thumb and index and 8 g on the middle finger). Data were collected 1.5-2 years after implant. All participants were compensated for time spent on the study, receiving $1080 per month that the devices were implanted for testing.

3.5.2: Statistics & Reproducibility

This project was part of an ongoing clinical trial where blinding was not possible. All enrolled subjects at the time of data collection were included, but there was no statistical method used to predetermine sample size. No data were excluded from analyses.

3.5.3: Array implantation

We implanted four NeuroPort microelectrode arrays (Blackrock Neurotech, Salt Lake City, UT, USA) in the left hemisphere of each participant. Two of the arrays, implanted in somatosensory cortex (Brodmann's area 1, S1), were 2.4 mm x 4 mm, each with sixty 1.5-mm electrode shanks wired in a checkerboard pattern such that 32 electrodes could be stimulated. The other two arrays, implanted in motor cortex (M1), were 4 mm x 4 mm with one hundred 1.5-mm electrode shanks, 96 (participants C1 and P3) or 88 (participant P2) of which were wired (active). Four inactive shanks were located at the corners of all arrays (with an additional 8 for participant P2). In P2, the motor cortex arrays were metalized with platinum while the somatosensory arrays with coated in sputtered iridium oxide. In participants C1 and P3, all electrodes were coated with sputtered iridium oxide. Most of the electrodes (74/96) on the medial array of participant C1 were too noisy to yield useful data and deactivated. Each participant had two percutaneous connectors placed on their skull, with each connected to one sensory and one motor array. We targeted array placement during surgery using functional neuroimaging of the participants attempting to make movements of the hand and arm, and

imagining feeling sensations on their fingertips[29], within the constraints of anatomical features such as blood vessels and cortical topography (Figure 3.1A and Supplementary Figure S3.1). Array locations, shown in Figure 3.1A and Supplementary Figure S3.1 on structural MRI models of each participant's brain, were confirmed using intraoperative photographs after insertion.

3.5.4: Neural stimulation

Stimulation was delivered using a CereStim microstimulator (Blackrock Neurotech, Salt Lake City, UT, USA). Stimulation pulses were cathodal first, current controlled, and charge balanced, over a range that has been previously deemed safe[38]. Each pulse consisted of a 200-µs long cathodal phase, then a 100-µs interphase period followed by a 400-µs long anodal phase at half the cathodal amplitude. Stimulation pulses could be presented at up to 300 Hz. Further details on selection of stimulation parameters can be found in ref[29].

3.5.5: Neural recordings

Neural signals in M1 were recorded at 30 kHz using the NeuroPort system (Blackrock Neurotech, Salt Lake City, UT, USA). Each stimulation pulse triggered a 1.6 ms sample-and-hold circuit in the preamplifier (hardware blanking) to avoid saturating the amplifiers and to minimize transient-induced ringing in the filtered data. The data were high-pass filtered with a 1st order 750-Hz filter[39]. Whenever the signal crossed a threshold (-4.25 RMS, set at the start of each recording session), a spiking event was recorded and a snippet of the waveform was saved. Spikes were binned in 20-ms bins for decoding. To confirm that the observed effects reflect neural activity and not an electrical artifact, we sorted units offline using Plexon Offline Sorter and repeated many of the analyses described below on isolated single units.

3.5.6: Stimulation protocol – passive condition

To study the effects of stimulation on M1 activity, we stimulated through each S1 channel a minimum of 15 times at 60 μA and 100 Hz in 1 second trains. Electrode order within each array was shuffled and stimulation was interleaved across arrays. The interval between pulse trains was 3 seconds in participant C1 and a random duration between 3 to 4 seconds in participants P2 and P3 to counteract any anticipatory effects.

3.5.7: Gauging the strength of ICMS-driven activity in motor cortex

To understand the effects of ICMS in S1 on activity in M1, we compared the fluctuations in firing during baseline to those during the stimulation interval. For each motor channel, we sampled the difference in firing rate between two consecutive 1-sec intervals during the intertrial periods, computed the mean, and repeated this process 1000 times to generate a null distribution of baseline fluctuations over the course of a recording session. For each stimulating channel, we calculated the change in firing rate between a 1 second interval preceding the stimulation train and the firing rate during the stimulation train itself, which gauged the effect of stimulation on each motor channel. For these analyses, we discarded the first 2 ms of the response after each pulse to eliminate any potential electrical artifacts that extended beyond the initial 1.6-ms hardware blanking window. We simulated this blanking in the baseline response to generate the null distribution. Motor channels were considered to be modulated by stimulation if their average change in firing rate during stimulation was significantly different from the null distribution ($p < 0.001$). To gauge the sign and magnitude of the effect of stimulation on a motor channel, we expressed the change in firing rate during stimulation for each motor/stimulation channel pair as a z-score based on the null distribution for that motor channel. Positive

modulation values indicate an excitatory effect while negative modulation values indicate an inhibitory effect.

3.5.8: Gauging the timing of ICMS-driven activity in motor cortex

To determine if motor units were phase locked to the stimulation pulses, we computed the pulse triggered average (PTA). Specifically, we binned the spikes evoked during each inter-pulse interval into 0.5-ms bins and computed the probability of spiking in each bin (i.e., the proportion of times a pulse evoked a spike in that bin). To assess whether there was a significant peak in the PTA, indicating a pulse-locked response, we first identified the time at which the probability of a spike occurring was highest and averaged the spiking probability across it and the two adjoining time bins. We computed the median probability of a spike occurring across all bins in the inter-pulse interval, to quantify the component of the response that was not pulse-locked. We computed the difference between these two values to create a phase-locking index. We sampled 20% of the PTAs for each motor and stimulation channel pair, shuffled the spike times, thus obtaining PTAs that were matched in spike count, and computed the same phase-locking index above for PTAs generated from the shuffled data. We repeated this shuffling procedure 5000 times to create a null distribution of pulse-locking indices. PTAs were considered to be significantly pulse-locked if the index was greater than that 99% of those obtained by chance (i.e., $p < 0.01$). We also estimated the latency and jitter of significantly pulse-locked responses. To this end, we randomly sampled 20% of the inter-pulse intervals and computed the PTA for this sample. We then identified the bin with the maximum spiking probability thus determining its latency. We repeated this procedure 5000 times to get a distribution of latencies, the mean and variance of which were the latency and jitter estimate for that stimulation/recording pair.

3.5.9: Quantifying somatotopically mapped connectivity

We sought to determine whether motor channels that encode information about specific digit movements also respond to stimulation in somatosensory cortex that evokes a touch sensation on the same digit. To this end, participants performed an attempted digit movement task. On each trial, a digit was cued and the participant attempted to flex then extend the digit before the next digit was cued. Participant C1 was cued by the name of the digit being spoken, then attempted to move his own paralyzed digit in synchrony with a virtual hand (MuJoCo, DeepMind Technologies, London, UK) performing the same instructed movement. He completed 125 trials of this task in one session. Participants P2 and P3 were cued by watching a set of 5 colored circles displayed on a monitor in front of them. The circles were arranged to mimic the distribution of digit tips resting open on a table or keyboard. When a circle was filled by a gray dot the participant would attempt to flex the corresponding digit until the gray dot disappeared. Following a chime, he then attempted to extend the same digit. Each participant completed 50 trials of this task.

Motor maps. To generate a map of digit selectivity across M1, we first computed the mean peri-event time histogram (in 20-ms bins) for each motor channel across a two second period centered on the start of movement for each digit flexion. From these, we then identified, for each motor channel, the response window during which the difference between the maximum response and the minimum response (each corresponding to flexion of different digits) was maximal. We used different time windows for different M1 channels because some units were most strongly active during preparation and others during movement. The modulation value for each digit was then calculated by subtracting the mean firing rate across all

digits from the average firing rate for one digit, and then dividing by the mean firing rate across all digits. Plotting this modulation value across all channels for one digit provides a map of selective activation for that digit.

To generate sensory projection maps, we first computed the modulation values for each motor channel when stimulation was delivered through stimulation channels that evoked a sensation on the palmar side of a given digit. For example, we computed the modulation value for each motor channel when all the stimulation channels with projected fields on the thumb were stimulated. We then averaged these modulation values to obtain the thumb projection map. We repeated this procedure for all the digits (excluding the little finger for participant C1 and the ring and little finger for participant P3, because they never reported sensations there).

Reasoning that the motor maps and sensory projection maps reflect individually noisy estimates of the digit preference of individual motor channels, we convolved the maps with a 2D Gaussian whose standard deviation was equal to the spacing between two adjacent electrodes, to reinforce local patterns of digit preference. Note that the subsequent analyses were also performed without spatial filtering and yielded weaker but similar results.

To test for somatotopic linkage between S1 and M1, we first compared, for each motor channel, the activation evoked when ICMS was delivered through S1 channels whose projected field matched the digit that evoked the strongest response during attempted movement to the activation evoked when ICMS was delivered through S1 channels whose projected field did not match the movement field of the M1 channel. For this analysis, the ICMS-evoked activity was normalized within digit: For example, the activation on a given M1 channel evoked by ICMS through all S1 channels with projected fields on the thumb was normalized by the mean

activation across all M1 channels evoked by ICMS through all S1 electrodes with projected fields on the thumb. This normalization was implemented to remove incidental digit-specific differences in the efficacy of stimulation array-wide. For example, thumb electrodes might be more effectively drive stimulation across the array than index electrodes. We could then compare the activation on a given motor channel when ICMS was delivered through S1 channels with PFs that were predominantly on the digit that most strongly activated that motor channel to the activation evoked by non-matching S1 channels (using a Wilcoxon rank sum test). To visualize the array-wide somatotopic organization of the motor map, we calculated the Spearman correlation between the motor activation of each electrode and the corresponding digit (thumb = 1, index = 2, …, pinky = 5). Accordingly, channels that responded preferentially to the lateral digits (ring and little finger) yielded positive correlations; channels that responded preferentially to the medial digits (thumb and index) yielded negative ones. To visualize the array-wide somatotopic organization of the sensory projection map, we calculated the Spearman correlation between ICMS-evoked activation by digit and digit. Accordingly, channels that were most activated by S1 channels with projected fields on the lateral digits yielded positive correlations; channels that were preferentially activated by S1 channels with projected fields on the medial digits yielded negative correlations. The resulting maps revealed preference gradients across the arrays (Supplementary Figure S3.11).

Next, we assessed whether the strength of the ICMS-evoked activity could be predicted from its digit preference profile. The activation of each M1 channel during attempted movement of each digit provided a digit preference profile for that channel's motor signals. The ICMS-evoked activation of individual M1 channels by stimulation across all channels with PFs on each

digit provided a digit preference profile for that channel's S1 projections. We could then test whether these two profiles matched. For example, is an M1 channel that responded most to D1 flexion, second most to D3 flexion, and third most to D2 flexion most activated by S1 channels with PFs on D1, then D3, then D2. First, we computed the mean activation on the digits, ordered by preference, to assess the mean effect across M1 channels. We also assessed the effect at the level of single motor channels by computing the Pearson correlation coefficient for the motor and sensory projection digit preference profiles. To assess significance, we computed a null distribution of correlations by shuffling both the electrode and digit assignments of the responses 10,000 times and computing the resulting correlations. Both the motor and sensory digit preference profiles were computed from the spatially smoothed motor and sensory projection maps. The null distributions were also computed after shuffling and then smoothing, to ensure that our findings were not artifacts of the smoothing.

P2 exhibited a different pattern of results than did C1 and P3. Given that P2's arrays had been implanted for much longer than the C1's and P3's, we verified that the different pattern was not due to array malfunction. To this end, we measured the activity of P2's lateral motor array during a task requiring movement of the proximal arm muscles. We asked the participant to perform overt center-out planar reaches to eight targets (10 reaches per target) on a smooth surface, with his hand supported. On each trial, we cued the target location and reach timing on a screen in front of the participant. Each trial comprised a half-second presentation phase followed by an approximately one and a half second reach. To analyze the resulting neural data, we first binned threshold crossings into 20-ms bins and convolved these with a Gaussian kernel (std = 100ms) to achieve a smooth estimate of the firing rate. We averaged these rates across

repetitions for each target and normalized them so that each channel ranged from 0 (minimum firing rate) to 1 (maximum firing rate). For presentation purposes, we estimated the preferred direction of each channel using a cosine model and sorted the channels accordingly. We also confirmed that the modulation carried significant information by classifying the movement target. We first took the average firing rate of each channel on the lateral array during the reach phase of each trial. We then trained a linear discriminant analysis classifier on the top 10 principle components and tested it using leave-one-out cross-validation.

3.5.10: Assessing the task dependence of ICMS-evoked activity in M1

We sought to determine whether the effects of ICMS to S1 on M1 activity depended on the task. To this end, we had participants C1 and P3 perform two tasks while we delivered ICMS to S1.

In the squeeze task, the participant squeezed a virtual object and reported the intensity of the ICMS-evoked touch sensation. On each trial the participant attempted to squeeze a virtual object with a medium amount of force, following the trajectory of a virtual hand observed through a VR headset. Upon contact with the object, stimulation was delivered on two electrodes at one of four amplitudes (20, 32, 44 or 56 μA). The hand continued to grasp the object for one second before a release cue appeared. Once the hand released the object, the participant reported the perceived intensity of the stimulation using a scale of his choosing, with the following instructions. If he did not feel the stimulus, he ascribed to the sensation a rating of zero. If a stimulus on one trial felt twice as intense as that on another, he ascribed a rating that was twice as high (other such examples were provided). He was encouraged to use decimals or

fractions. The main goal of the magnitude estimation component was to keep the participant engaged in the task.

In the grasp and transport task, an object appeared at one corner of an invisible cube centered on the starting point of the virtual hand. The participant then attempted to reach to the object, following the movement of the virtual hand. Once there, the participant attempted to grasp the object with medium force. During the grasp, ICMS was delivered at one of four amplitudes, as in the squeeze task. The participant then attempted to bring the object back to the center of the cube and release it there, again following the movements of the virtual limb.

Participant C1 completed 208 trials of each task in each of two sessions. Participant P3 completed 160 trials of each task in one session.

To confirm that the participant was attending to the grasp and transport task, we classified the intended target during the reach phase of the task. A naïve Bayes classifier was trained using one second of data from all active motor channels (>5 Hz mean firing rate across whole task) starting 400 ms before movement onset. This classifier was tested using leave-one-out cross-validation.

To assess whether the ICMS-evoked M1 activity varied across tasks, we analyzed the firing rates across all motor channels during three distinct phases across the two tasks: The 1-sec period after contact during 'squeeze' task; the 1-sec period after contact during the grasp and transport task, and the first second of the transport phase in the grasp and transport task. In all three of these phases, the ICMS was identical but the movements were different (squeeze/grasp vs. transport) or their context was different (squeeze vs. grasp). We performed a multivariate ANOVA on the firing rates to determine which channels were significantly modulated by changes

in task phase, stimulation level, and the interaction of the two. As an index of task dependence, we computed the ratio of the F-statistic for the interaction effect to that for the main effect of stimulation. This value was high to the extent that the interaction effect was strong compared to the main effect. This index was only computed for significantly modulated channels.

To assess whether task-dependent differences in susceptibility to stimulation reflected differences in task-dependent baseline firing rate, we investigated the relationship between ICMS-induced modulation and the baseline firing rate for each phase for each M1 channel. Baseline firing rates for the squeeze and grasp phases were calculated during the half second preceding object contact, during which time the hand was moving but no ICMS was delivered. The baseline firing rate for the transport phase was calculated using the first half-second during the reach phase, a similar movement without ICMS. The baseline firing rate in each phase for each neuron was then normalized by the mean baseline firing rate across phases. The index of modulation was the average firing rate during stimulation at the highest amplitude (56 μA) minus the average firing rate during stimulation at the lowest amplitude (20 μA) for each channel and phase, divided by the mean baseline firing rate across phases (computed as described above). We then plotted the modulation against the baseline firing rate for each channel and phase. To the extent that differences in modulation strength reflected a saturation effect, we expected a negative relationship between modulation strength and baseline firing rate.

To further determine how different the ICMS-evoked M1 activity was across tasks, we performed a linear discriminant analysis to identify stimulation amplitude based on the M1 activity during squeeze, grasp, and transport phases separately (during the half second after

contact initiation during the squeeze and grasp and during the first half second of transport), after subtracting the baseline activity for each phase (as described above) to remove task-dependent activity. These classifiers were tested on all three conditions. Within-condition accuracy was calculated using leave-one-out cross-validation, while cross condition accuracy was calculated using a decoder built from all available trials in each condition.

3.5.11: Quantifying the impact of ICMS on motor decoding

We sought to determine whether the M1 activity evoked by ICMS would disrupt the ability of the participants to control a virtual arm. In 3 sessions, participant C1 attempted to make the movements of a virtual hand and arm displayed in his VR headset. On each trial, the virtual hand reached to an object, grasped it, transported it to a new location, and released it. After completing 60 trials, we trained a decoder for three-dimensional translation of the hand using these data. The decoder used throughout this project was an indirect Optimal Linear Estimator with ridge regression[9,15]. Next, we measured neuronal activity as the participant-controlled translation, but with the computer preventing deviations from the path to the target (for an additional 60 trials). A new decoder was then trained from these data, and that decoder was used for the rest of the session. Throughout the session, the hand grasped automatically under computer control to ensure that stimulation was applied consistently across all trials while the participant-controlled hand translation. The decoders were trained without stimulation but with blanking applied at 100 Hz during object contact to simulate the neuronal signal available during online decoding with ICMS-based feedback.

Once the decoder was trained, performance was tested under three conditions. In the 'no stimulation' condition, the participant performed the same task that was used during

training; no stimulation was provided but a 1.6-ms window of neuronal data was blanked at 100 Hz to match the data available during stimulation. In the two stimulation conditions, ICMS was delivered on two electrodes, one with projected fields on the thumb and one with projected fields on the index finger. In the linear condition, the ICMS frequency was 100 Hz and the amplitude was 52 μA. In the 'biomimetic stimulation' condition, 100-Hz ICMS comprised onset and offset transients at 72 μA for 200 ms and sustained stimulation at 32 μA during maintained contact. The order of the test blocks was randomized in each session, with each condition used for two sets of ten trials before the next condition was tested. Conditions were repeated three times to obtain a total of 60 trials for each.

If the participant was unable to place the hand at the target location within 10 seconds during either the reach or the transport phase, the trial was terminated and marked as a failure. To determine the causes of failure, we computed the path length during the transport phase (when stimulation was provided and the participant had control of the arm) for every trial, even if the trial failed during that phase. The median path lengths were compared across stimulation conditions using the Wilcoxon rank-sum test to determine significance.

3.6: References

1. Brochier, T., Boudreau, M.-J., Paré, M. & Smith, A. M. The effects of muscimol inactivation of small regions of motor and somatosensory cortex on independent finger movements and force control in the precision grip. *Experimental Brain Research* 128, 31–40 (1999).
2. Sobinov, A. R. & Bensmaia, S. J. The neural mechanisms of manual dexterity. *Nat Rev Neurosci* 1–17 (2021) doi:10.1038/s41583-021-00528-7.

3. Pons, T. P. & Kaas, J. H. Corticocortical connections of area 2 of somatosensory cortex in macaque monkeys: A correlative anatomical and electrophysiological study. *J. Comp. Neurol.* **248**, 313–335 (1986).

4. Rosen, B. Q. & Halgren, E. A Whole-Cortex Probabilistic Diffusion Tractography Connectome. *eNeuro* **8**, ENEURO.0416-20.2020 (2021).

5. Ghosh, S., Brinkman, C. & Porter, R. A quantitative study of the distribution of neurons projecting to the precentral motor cortex in the monkey (*M. fascicularis*). *J of Comparative Neurology* **259**, 424–444 (1987).

6. Entz, L. *et al.* Evoked effective connectivity of the human neocortex: Evoked Effective Connectivity of Neocortex. *Hum. Brain Mapp.* **35**, 5736–5753 (2014).

7. Osborn, L. E. *et al.* Intracortical microstimulation of somatosensory cortex generates evoked responses in motor cortex. in *2021 10th International IEEE/EMBS Conference on Neural Engineering (NER)* 53–56 (2021). doi:10.1109/NER49283.2021.9441123.

8. Ghosh, S. & Porter, R. Corticocortical synaptic influences on morphologically identified pyramidal neurones in the motor cortex of the monkey. *The Journal of Physiology* **400**, 617–629 (1988).

9. Wodlinger, B. *et al.* Ten-dimensional anthropomorphic arm control in a human brain-machine interface: difficulties, solutions, and limitations. *Journal of neural engineering* **12**, 016011 (2015).

10. Pandarinath, C. & Bensmaia, S. J. The science and engineering behind sensitized brain-controlled bionic hands. *Physiological Reviews* **102**, 551–604 (2022).

11. Okorokova, E. V., He, Q. & Bensmaia, S. J. Biomimetic encoding model for restoring touch in bionic hands through a nerve interface. *J. Neural Eng.* **15**, 066033 (2018).

12. Saal, H. P. & Bensmaia, S. J. Biomimetic approaches to bionic touch through a peripheral nerve interface. *Neuropsychologia* **79**, 344–353 (2015).

13. Valle, G. *et al.* Biomimetic Intraneural Sensory Feedback Enhances Sensation Naturalness, Tactile Sensitivity, and Manual Dexterity in a Bidirectional Prosthesis. *Neuron* **100**, 37-45.e7 (2018).

14. George, J. A. *et al.* Biomimetic sensory feedback through peripheral nerve stimulation improves dexterous use of a bionic hand. *Science Robotics* **4**, (2019).

15. Flesher, S. N. *et al.* A brain-computer interface that evokes tactile sensations improves robotic arm control. *Science* **372**, 831–836 (2021).

16. Hao, Y., Riehle, A. & Brochier, T. G. Mapping Horizontal Spread of Activity in Monkey Motor Cortex Using Single Pulse Microstimulation. *Front. Neural Circuits* **10**, (2016).

17. Kraskov, A., Prabhu, G., Quallo, M. M., Lemon, R. N. & Brochier, T. Ventral Premotor-Motor Cortex Interactions in the Macaque Monkey during Grasp: Response of Single Neurons to Intracortical Microstimulation. *Journal of Neuroscience* **31**, 8812–8821 (2011).

18. Kaneko, T., Caria, M. A. & Asanuma, H. Information processing within the motor cortex. I. Responses of morphologically identified motor cortical cells to stimulation of the somatosensor cortex. *J. Comp. Neurol.* **345**, 161–171 (1994).

19. Jiang, W., Chapman, C. E. & Lamarre, Y. Modulation of somatosensory evoked responses in the primary somatosensory cortex produced by intracortical microstimulation of the motor cortex in the monkey. *Exp Brain Res* **80**, (1990).

20. Bundy, D. T. *et al.* Mesoscale corticocortical connectivity corresponds with intracortical microstimulation-evoked neural activity. 2022.03.03.482925 Preprint at https://doi.org/10.1101/2022.03.03.482925 (2022).

21. Chomiak, T. & Hu, B. Axonal and somatic filtering of antidromically evoked cortical excitation by simulated deep brain stimulation in rat brain. *The Journal of Physiology* **579**, 403–412 (2007).

22. Girard, P., Hupé, J. M. & Bullier, J. Feedforward and Feedback Connections Between Areas V1 and V2 of the Monkey Have Similar Rapid Conduction Velocities. *Journal of Neurophysiology* **85**, 1328–1331 (2001).

23. Schieber, M. H. & Hibbard, L. S. How somatotopic is the motor cortex hand area? *Science* **261**, 489–492 (1993).

24. Schieber, M. H. Constraints on somatotopic organization in the primary motor cortex. *Journal of Neurophysiology* **86**, 2125–2143 (2001).

25. Goodman, J. M. *et al.* Postural Representations of the Hand in the Primate Sensorimotor Cortex. *Neuron* 566539 (2019) doi:10.1016/j.neuron.2019.09.004.

26. Willett, F. R. *et al.* Hand Knob Area of Premotor Cortex Represents the Whole Body in a Compositional Way. *Cell* **181**, 396-409.e26 (2020).

27. Rosén, I. & Asanuma, H. Peripheral afferent inputs to the forelimb area of the monkey motor cortex: Input-output relations. *Exp Brain Res* **14**, 257–273 (1972).

28. Tokuno, H. & Tanji, J. Input organization of distal and proximal forelimb areas in the monkey primary motor cortex: A retrograde double labeling study. *J. Comp. Neurol.* **333**, 199–209 (1993).

29. Flesher, S. N. *et al.* Intracortical microstimulation of human somatosensory cortex. *Science Translational Medicine* **8**, 361ra141-361ra141 (2016).

30. Salas, M. A. *et al.* Proprioceptive and cutaneous sensations in humans elicited by intracortical microstimulation. *eLife* **7**, 1–11 (2018).

31. Hughes, C. L. *et al.* Perception of microstimulation frequency in human somatosensory cortex. *eLife* **10**, e65128 (2021).

32. Hughes, C. L. *et al.* Neural stimulation and recording performance in human sensorimotor cortex over 1500 days. *J. Neural Eng.* **18**, 045012 (2021).

33. Jiang, X., Saggar, H., Ryu, S. I., Shenoy, K. V. & Kao, J. C. Structure in Neural Activity during Observed and Executed Movements Is Shared at the Neural Population Level, Not in Single Neurons. *Cell Reports* **32**, 108006 (2020).

34. Callier, T., Suresh, A. K. & Bensmaia, S. J. Neural Coding of Contact Events in Somatosensory Cortex. *Cerebral Cortex* **29**, 4613–4627 (2019).

35. Suresh, A. K. *et al.* Sensory computations in the cuneate nucleus of macaques. *Proceedings of the National Academy of Sciences* **118**, e2115772118 (2021).

36. Bensmaia, S. J., Tyler, D. J. & Micera, S. Restoration of sensory information via bionic hands. *Nat. Biomed. Eng* **7**, 443–455 (2020).

37. Greenspon, C. M. *et al. Biomimetic Multi-Channel Microstimulation of Somatosensory Cortex Conveys High Resolution Force Feedback for Bionic Hands*. http://biorxiv.org/lookup/doi/10.1101/2023.02.18.528972 (2023) doi:10.1101/2023.02.18.528972.

38. Rajan, A. T. *et al.* The effects of chronic intracortical microstimulation on neural tissue and fine motor behavior. *J. Neural Eng.* **12**, 066018 (2015).

39. Weiss, J. M., Flesher, S. N., Franklin, R., Gaunt, R. A. & Collinger, J. L. Artifact-free recordings in human bidirectional brain–computer interfaces. *Journal of Neural Engineering* **16**, 016002–016002 (2018).

3.7: Appendix: Chapter 3 Supplemental Figures

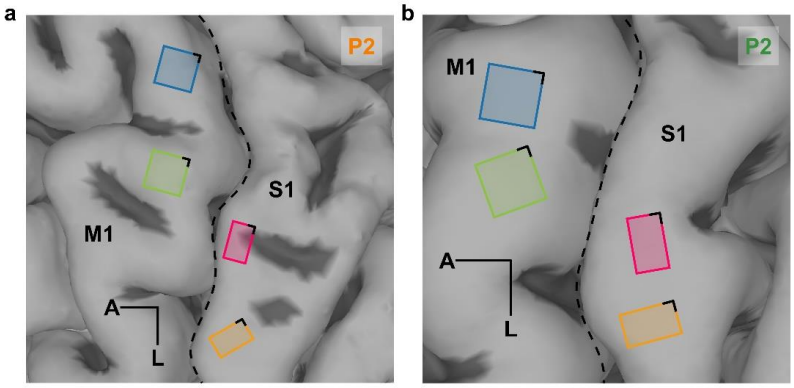

Supplementary Figure S3.1. Implant locations for other participants. Participant P2 (A) and P3 (B). See Figure 4.1 for C1.

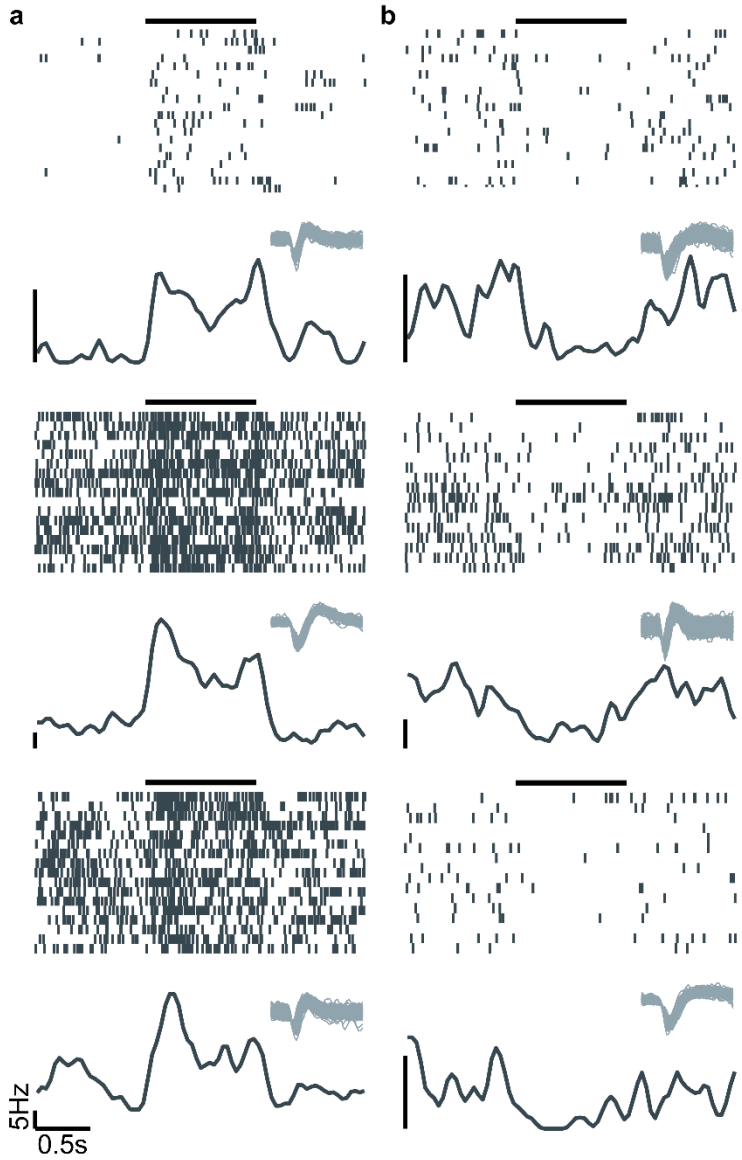

Supplementary Figure S3.2. Single unit responses in M1 during ICMS delivered to S1. A) Responses of three example neurons (inset: sorted waveforms) that were excited by stimulation (from top to bottom: C1, P3, P3). B) Responses of three example neurons that were inhibited by stimulation (C1, P2, P3).

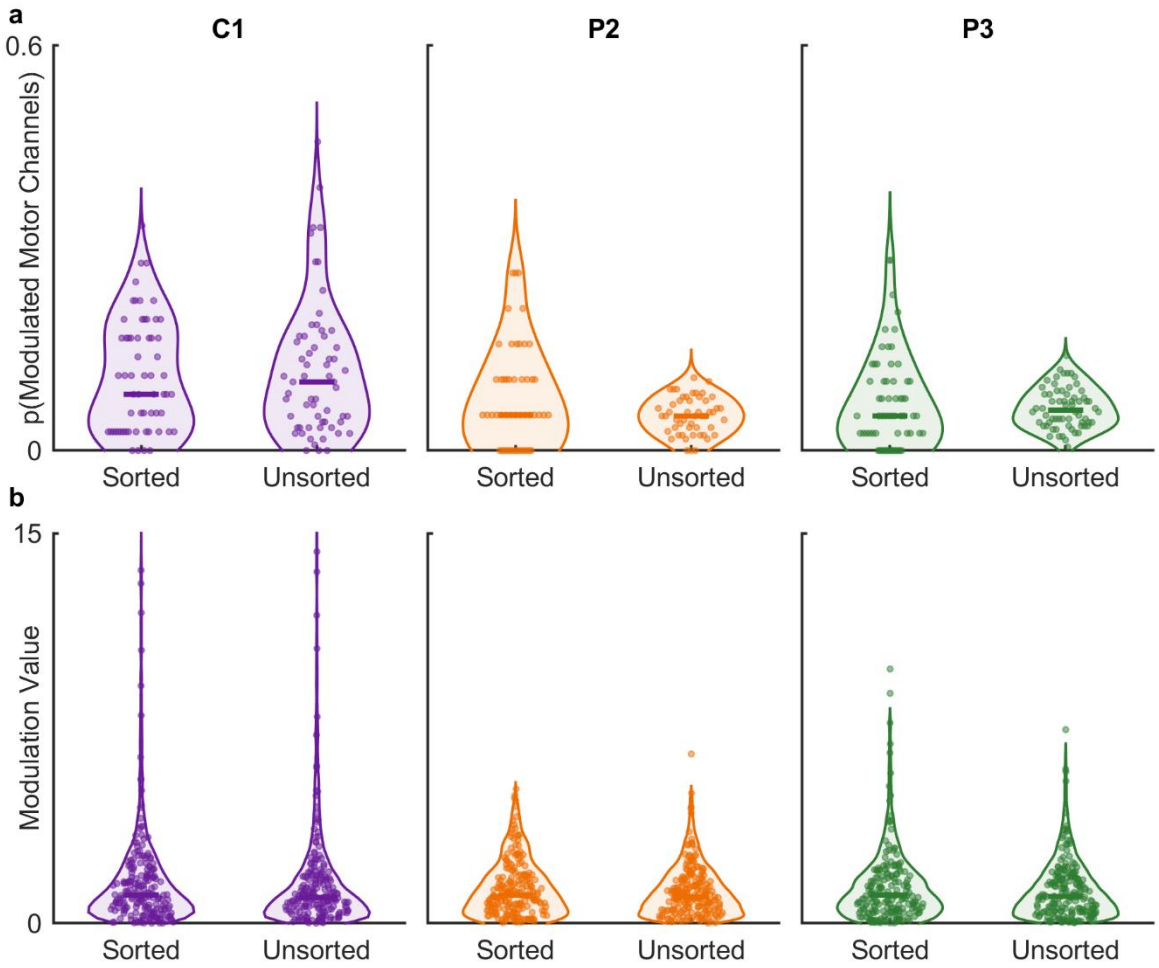

Supplementary Figure S3.3. Prevalence of ICMS-evoked activity in motor cortex is similar for sorted and unsorted units. A| Proportion of motor channels significantly modulated by stimulation channels (each dot represents a stimulation channel) for sorted and unsorted units (N = 36, 19, and 39 sorted units for participants C1, P2, and P3, respectively). B| Distribution of absolute modulation values for all pairs of motor and stimulation channels. Unlike in **Figure 3.2**B, where modulation values are averaged for each motor channel, the modulation value for each motor-sensory pair is shown separately given the small number of sorted units.

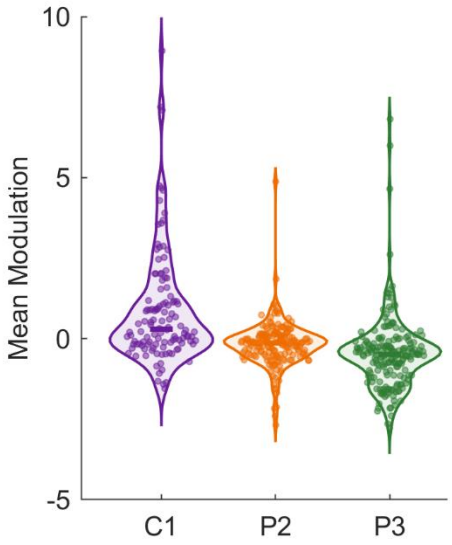

Supplementary Figure S3.4. Mean ICMS-driven modulation for each motor channel. This figure shows the raw (signed) modulation values rather than the absolute ones.

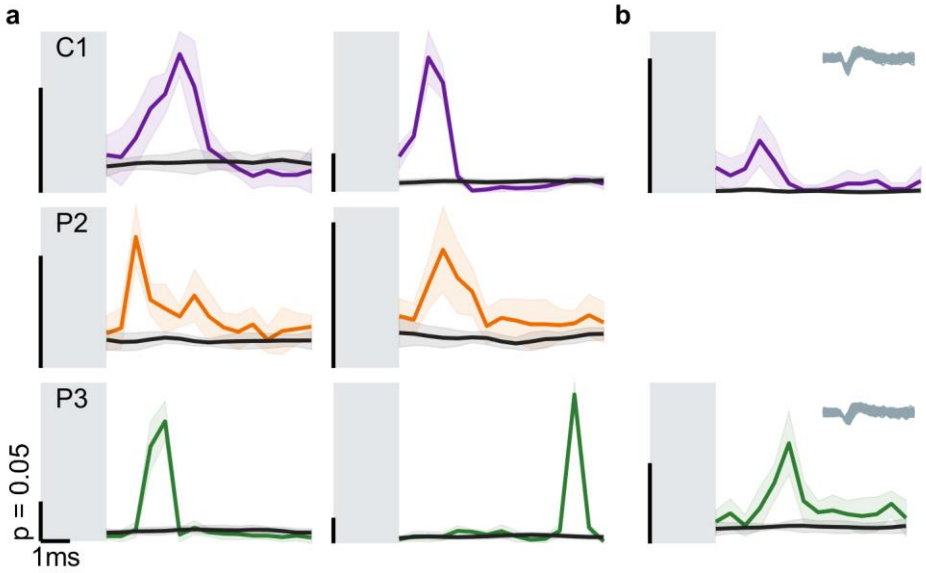

Supplementary Figure S3.5. ICMS to S1 evokes short-latency, pulse-locked responses in M1. A| Pulse triggered average (PTA) of the M1 responses evoked ICMS to S1 (colored). As a control, we computed a sham pulse triggered average (at the same pulse frequency) during baseline (black). Temporally precise responses occur at varying latencies across motor channels and participants. Each row shows two example PTAs from different S1-M1 electrode pairs for each participant (C1, P2, P3). The probability of a spike occurring in each 0.5 ms bin is shown on the y-axis Error bars represent bootstrapped standard error. B| Example PTAs for sorted units from participants C1 and P3. No sorted units with phase-locking were observed in P2.

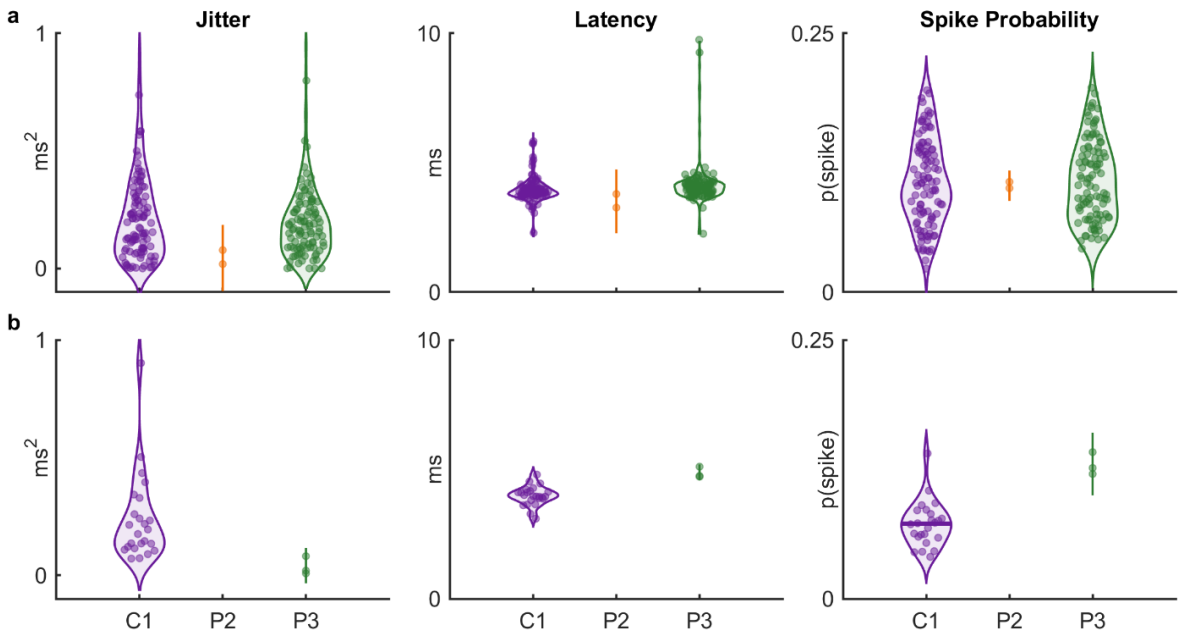

Supplementary Figure S3.6. Characteristics of pulse-locked responses. A| Characteristics of pulse-locked responses of unsorted units for each participant. Each dot represents a motor channel-stimulation channel pair. The three metrics – jitter, latency, and spiking probability (the proportion of times a pulse evoked a spike within a 1-ms window centered at the time of highest spiking probability) – were distributed unimodally, precluding classification of pulse-locked responses as reflecting antidromic or orthodromic activation. If spikes with jitter less than 0.1 ms^2 are considered to reflect antidromic activation (cf. refs.[21,22]), these responses reflect both antidromic and orthodromic activity, with a far greater prevalence of orthodromic activity. B| The same metrics in sorted units are consistent with responses of unsorted units.

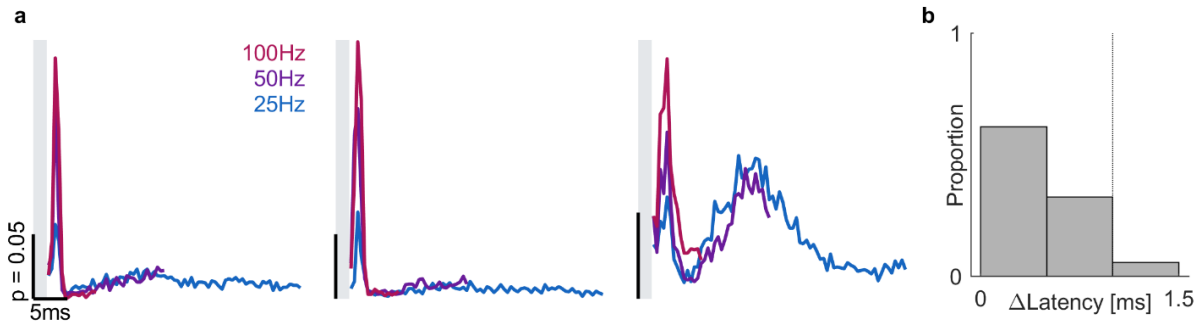

Supplementary Figure S3.7. Pulse-triggered average (PTA) of the responses evoked by ICMS at three frequencies in C1. A| Three example motor channels show the preserved initial response latency regardless of stimulation frequency. Some channels demonstrate a secondary, longer latency but lower probability response that is obscured during high frequency stimulation. B| Distribution of the differences in peak latency times across the 3 frequencies. Vertical line indicates the temporal resolution of the analysis. All latency differences fall within the temporal resolution of the analysis.

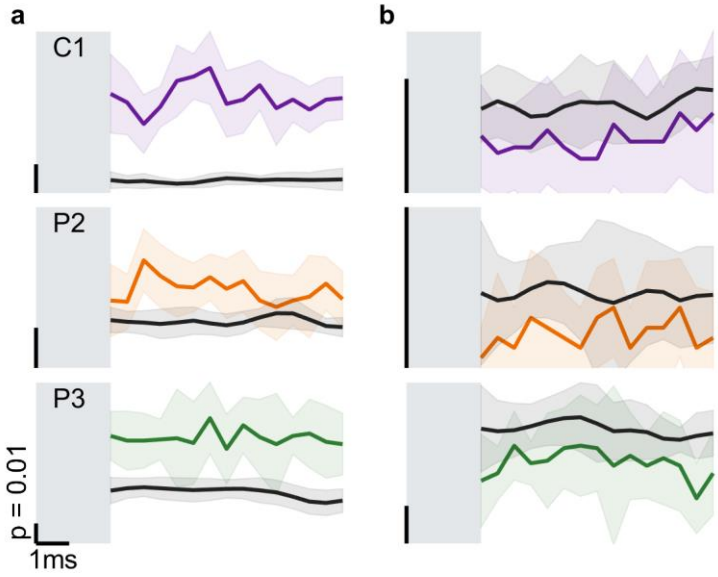

Supplementary Figure S3.8. Pulse triggered average (PTA) during ICMS (colored, mean +/- bootstrapped standard error) from channels that were modulated by stimulation but did not exhibit pulse locking in their response. As a control, we computed a sham pulse triggered average (at the same pulse frequency) during baseline (black). The gray area indicates time during which recording was blanked to eliminate the stimulation artifact. The y-axis denotes the probability of a spike occurring in each bin. A| Channels that were significantly excited by stimulation. B| Channels that were significantly inhibited by stimulation. Each row shows example PTAs for each participant (C1, P2, P3).

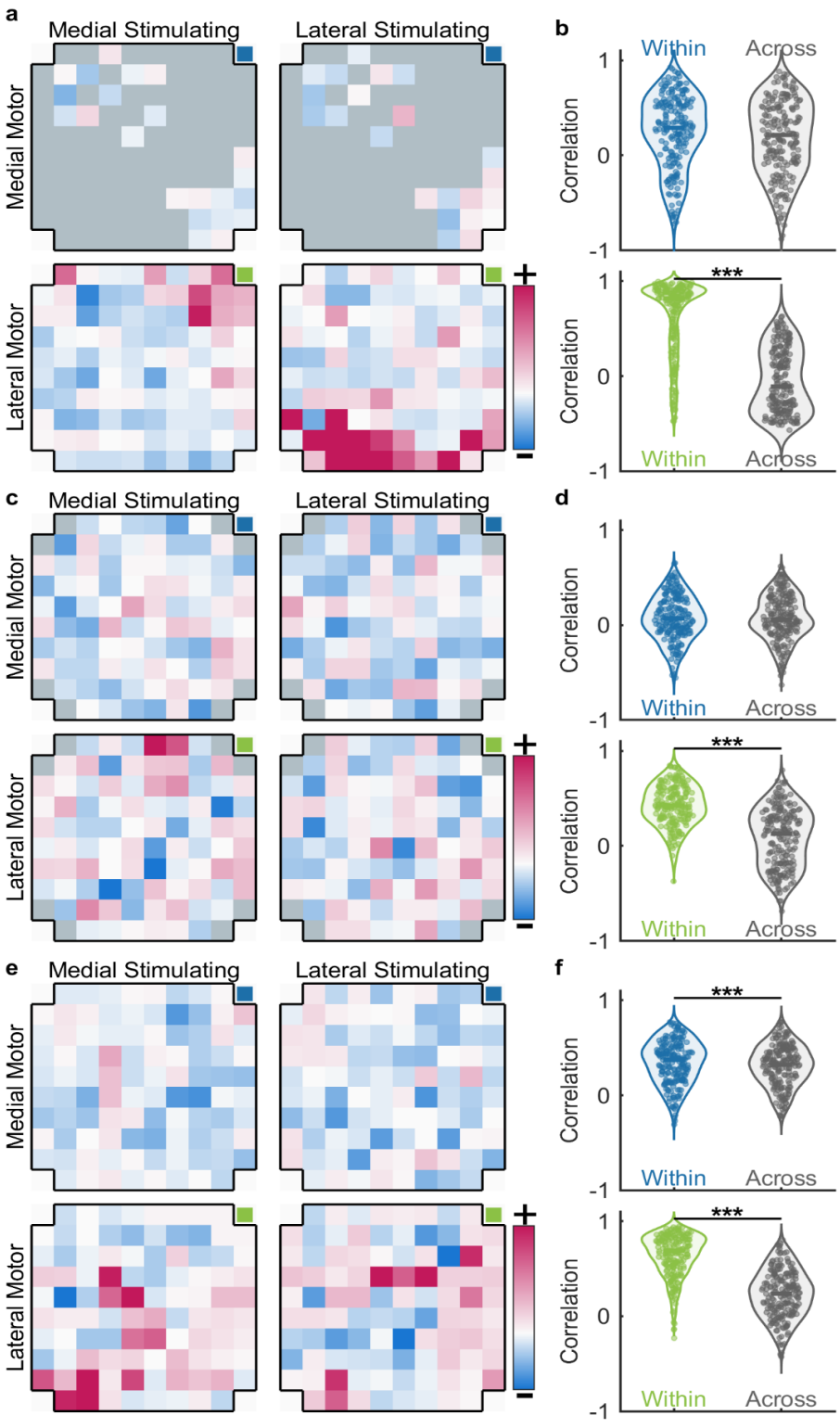
a
Medial Stimulating
Lateral Stimulating
Medial Motor
Lateral Motor
+
−
b
Within
Across
Correlation
1
0
-1
***
Within
Across
c
Medial Stimulating
Lateral Stimulating
Medial Motor
Lateral Motor
+
−
d
Correlation
1
0
-1
***
Within
Across
e
Medial Stimulating
Lateral Stimulating
Medial Motor
Lateral Motor
+
−
f
Correlation
1
0
-1
***
Within
Across

Supplementary Figure S3.9. Spatial patterning of ICMS-evoked M1 activation. A| Stimulation through an example channel on the medial somatosensory array and lateral sensory array for C1. Adjacent channels are separated by 400 µm. Blue and green squares in upper right of arrays indicate their orientation on the brain (Figure 3.1A). Grey squares denote inactive motor channels. The color bars represent the z-scored stimulation-related modulation scale (-5 to 10). B| Correlation between the spatial pattern of activation evoked in M1 by pairs of stimulation channels belonging to the same stimulation array (within array) or different arrays (across array) for C1. Asterisks indicate significance ($p < 0.001$ rank-sum test). C| Same as A for P2. D| Same as B for P2. E| Same as A and C for P3. F| Same as B and D for P3. The lateral motor arrays for all three participants show significantly higher correlation between pairs of stimulation electrodes on the same sensory array than on different sensory arrays, but this patterning is much stronger in C1 and P3 than in P2.

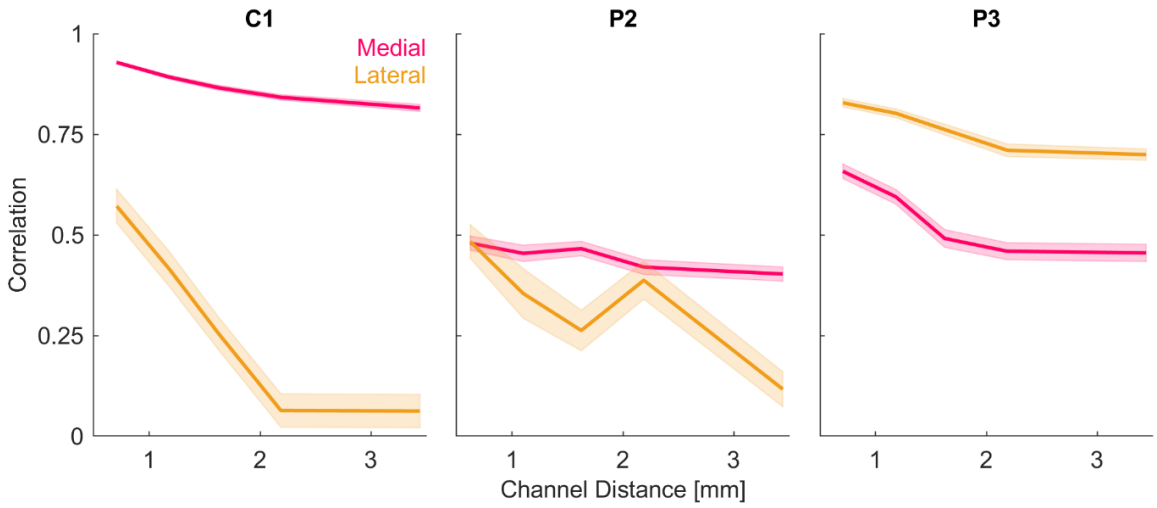

Supplementary Figure S3.10. Correlation between the spatial pattern evoked in the lateral motor array as a function of distance between two stimulating electrodes in the medial (pink) and lateral (orange) sensory arrays (mean +/- SEM). The spatial pattern of activation evoked by two electrodes tends to be more similar when the two electrodes are nearby. Correlations were lower for participant P2 overall.

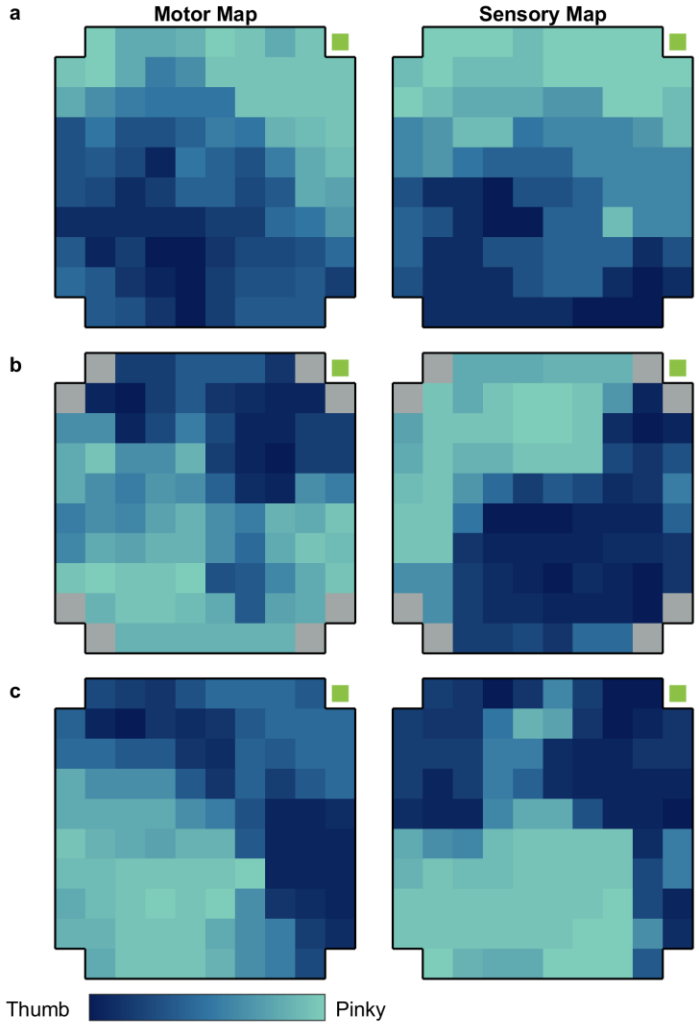

Supplementary Figure S3.11. Gradients of digit preference for motor and ICMS-evoked activity. For C1 and P3, the gradient in the motor map resembles the gradient in the sensory projection map. Left: the hue denotes, for each motor channel, the Spearman correlation between the strength of the response when attempting to move each digit and the digit identity (thumb = 1, …, pinky = 5). Dark blue indicates channels that preferentially respond during attempted thumb and index finger movements, while light green indicates channels that respond preferentially to attempted movements of the ring and pinky fingers. Right: the hue denotes, for each motor channel, the Spearman correlation between the strength of the response when ICMS-activity is delivered through S1 electrodes with PFs on each digit and the digit identity (thumb = 1, …, pinky = 5). Dark blue indicates channels that preferentially respond when ICMS is delivered through S1 channels with PFs on the thumb and index finger, while light green indicates channels that respond preferentially when ICMS is delivered is S1 channels with PFs on the ring and pinky fingers. Each row shows motor and sensory projection maps for a different participant.

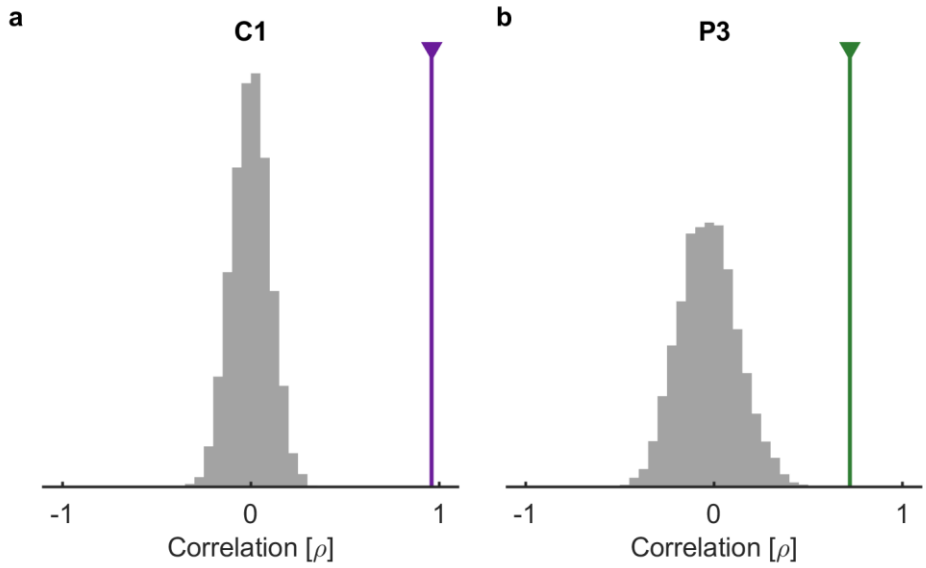

Supplementary Figure S3.12. Digit preference correlation between motor task and ICMS. A| In participant C1, the strength of motor modulation to imagined movement of a digit was highly correlated with the modulation due to ICMS of sensory channels with projected fields on the same digit (median across all channels in purple) when compared to the same responses shuffled across digits and channels before calculating the correlation 10,000 times (distribution of medians in grey). B| Same as panel A but for participant P3.

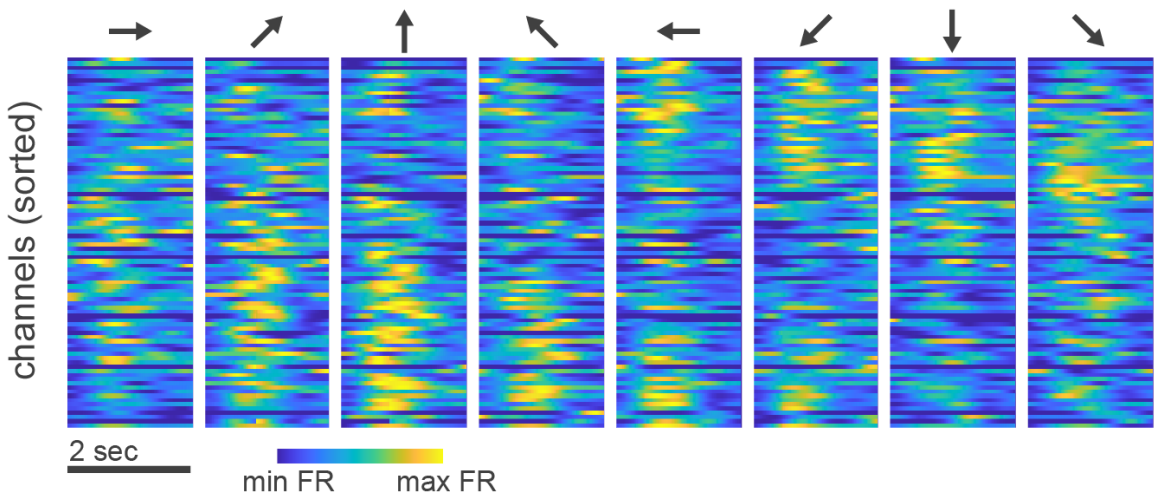

Supplementary Figure S3.13. The lateral motor array in participant P2 exhibited modulated responses during center out movements. In this task, P2 rested his hand on a horizontal surface and slid it out to one of 8 peripheral targets when prompted. Channels exhibit tuning to a variety of directions across the population and enable classifying the target with 87.5% accuracy (chance = 12.5%). Thus, the lack of strong and patterned ICMS-related modulation in this participant cannot be attributed to array failure.

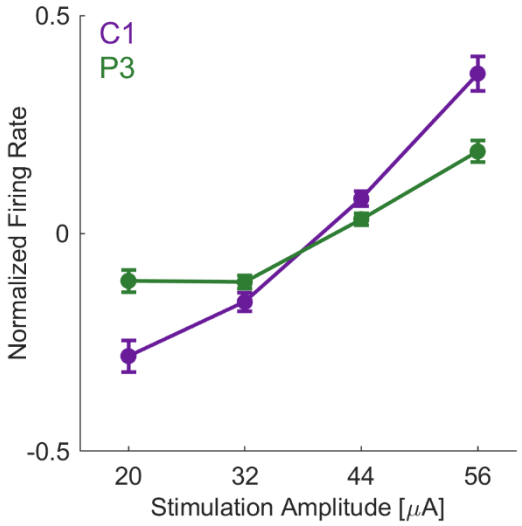

Supplementary Figure S3.14. Population firing rate increases with stimulation amplitude. During the squeeze task, firing rates recorded in motor cortex generally increased with increasing amplitude of stimulation in somatosensory cortex for both participants. Plot shows mean and SEM for two participants. ($p < 0.001$ for both, Kruskal-Wallis).

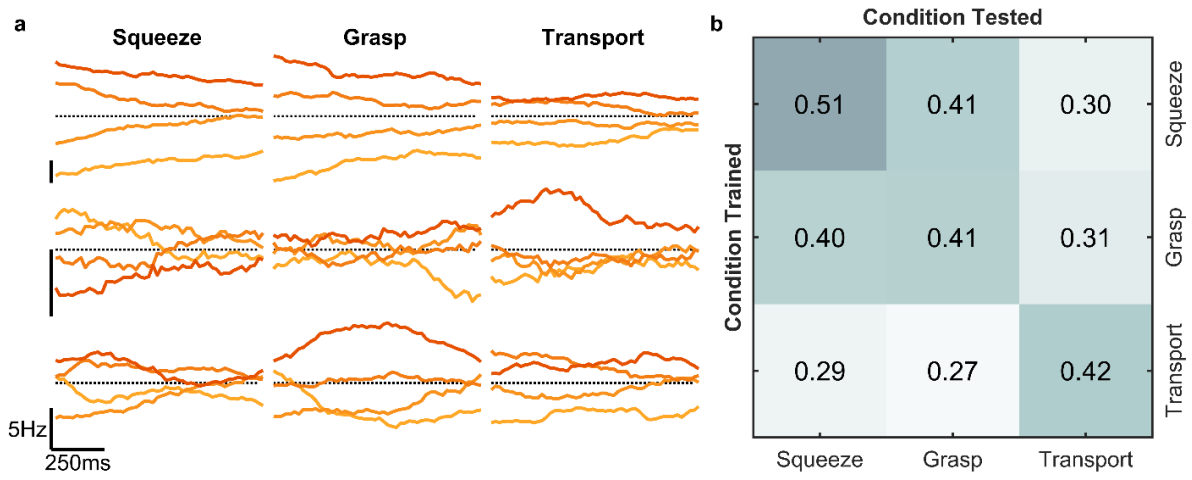

Supplementary Figure S3.15. Behavioral modulation of stimulation response in P3. A| Three example motor channels exhibit different responses to four levels of ICMS across three motor conditions (squeeze, grasp, transport). B| Stimulation amplitude classifier performance. Classifiers were trained on one of the three conditions and tested on each condition (with cross-validation for within-condition classification).

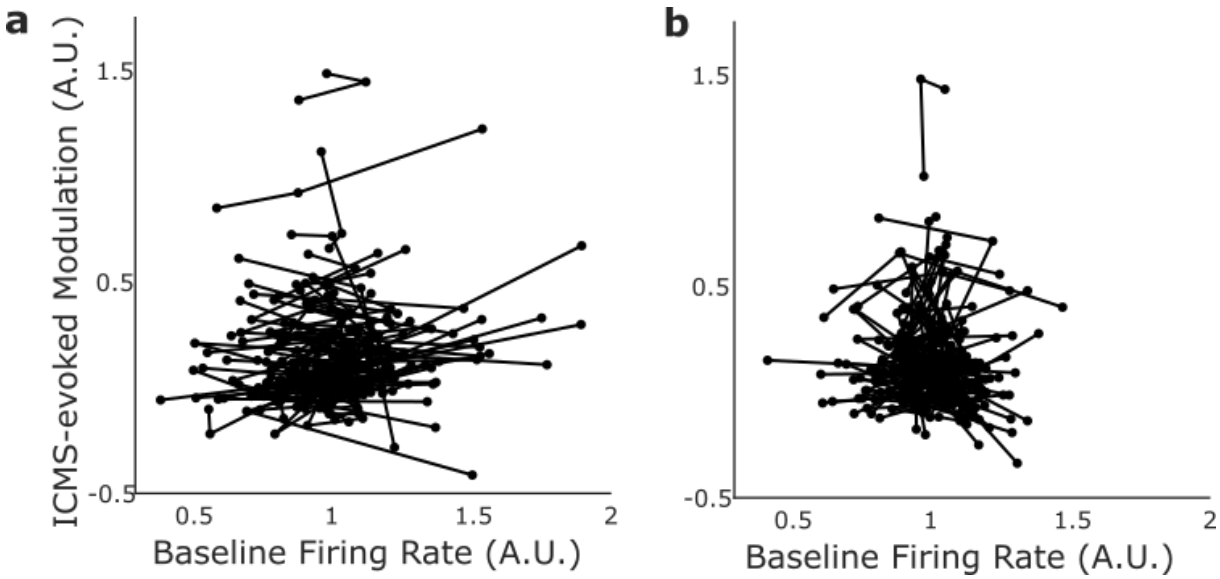

Supplementary Figure S3.16. Modulation of M1 activity by ICMS amplitude vs. M1 activity evoked by the attempted movement. A| For C1 the ICMS-evoked modulation is the mean firing rate at the highest amplitude minus mean firing rate at the lowest amplitude in each task phase, divided by the average of the baseline firing rate across phases. The baseline firing rate within each task phase is divided by the baseline firing rate across task phases. Lines connect the three phases for each channel. The strength of modulation is independent of the baseline M1 activity (R2 = 0.012), so the task-dependence of the ICMS-evoked activity does not reflect response saturation in M1. B| The same relationship as shown in panel A but for participant P3 (R2 = 0.004).

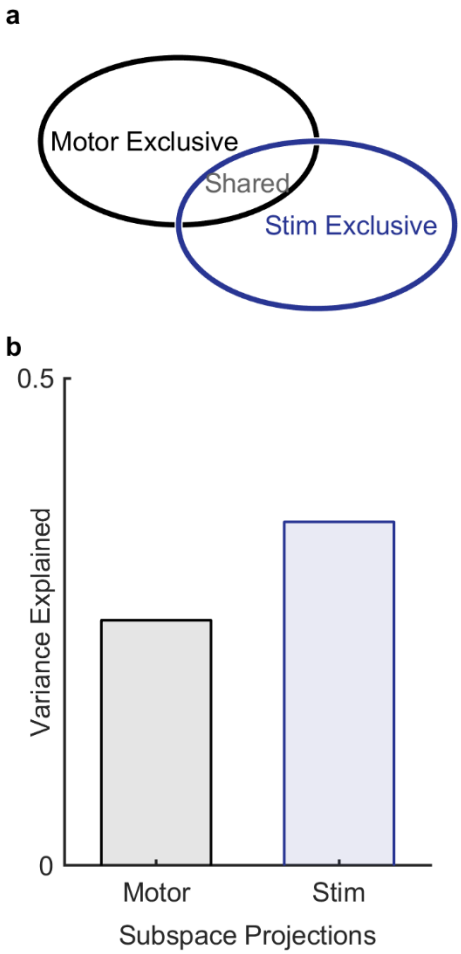

Supplementary Figure S3.17. To quantify overlap between motor and stimulation subspaces, we ran two tasks. In one, we instructed the participant to attempt to grasp a virtual object at one of 4 force levels, hold it for 1 second, then release it. No stimulation was delivered during the task. In the second task, we delivered stimulation trains that were identical in duration and shape to the grasp profiles in the first task. The participant was blinded to the level of stimulation and was instructed to report the magnitude of stimulation to maintain engagement in the task. By comparing the M1 activity in the two conditions, we can extract subspaces in M1 population activity that is exclusive to the motor task (related to volitionally moving the hand) or to stimulation, as well as the subspace shared by the two tasks. A| Three subspaces were extracted: One that contains variance of the motor task, one that contains variance of the stimulation task, and one that contains the variance that is common to the two tasks (using methods from ref. [33]). B| The shared subspace captures significant variance of both motor and stimulation tasks. In other words, the activity evoked in M1 by ICMS to S1 occupies a largely overlapping subspace as does the activity evoked in M1 during attempted grasp.

CHAPTER 4 : Future Directions and Conclusion

4.1: Summary of Previous Work

Throughout this work, I have demonstrated the viability of using ICMS to restore sensory feedback with bionic limbs and as a tool to study sensorimotor interactions in humans. In Chapter 2, I established that the location of projected fields is stable over the span of multiple years and can be reliably used to convey the location of contact, especially when stimulation is delivered through multiple electrodes. Additionally, the underlying somatotopy revealed by these findings has significant relevance to the post-injury reorganization literature. In Chapter 3, I demonstrated, using ICMS, that S1 and M1 are somatotopically connected at the resolution of individual digits. Furthermore, I demonstrated that linear stimulation impeded performance in a closed loop task, while biomimetic stimulation allowed us to provide sensory feedback while decoding motor intent. Together, these two chapters provide starting points for further studies that are crucial for understanding how sensorimotor interactions impact behavior and how these insights can be used to advance the development of BMI applications.

4.2: Future Considerations

During the closed-loop task in Chapter 3, our goal was to provide the subjects with a similar sensory experience using the linear and biomimetic trains in order to demonstrate the functional aspects of this approach. To this end, we constructed stimulus trains that either directly represented the force exerted by a virtual hand or a biomimetic train that resembled the patterns of neuronal activity observed during natural grasp. We concluded that the biomimetic stimulation paradigm was less disruptive to the decoding of motor intent, likely as a result of less current being injected into the system, especially during the hold phase of the grasp where

biomimetic stimuli have lower current profiles. Future experiments could address whether the improved performance was due to the use of different temporal structure in the protocols (biomimetic vs linear) or due simply to differences in total current. To test this, one could use linear trains where the total current is equal to that of the biomimetic trains and then compare performance between these conditions. If reducing the total current in the linear stimulation paradigm results in improved decoding performance, this confirms that total current is the key change that disrupts the neural code, and future stimulation protocols should be designed with this over-stimulation problem in mind.

Although we were able to reduce the ICMS evoked signal in M1 to an extent where it no longer interfered with our ability to decode motor intent, we were not able to provide sensory feedback in a manner that improved performance compared to the no stimulation condition. This raises a concern: if the solution to reducing disruption is to minimize the ICMS-evoked signal in the motor cortex, this implies that the motor cortex may work best when it is not receiving any tactile signals from the somatosensory cortex, at least in a way that is detectable by our decoder. Yet, we know that motor cortices receive extensive inputs from somatosensory structures in intact individuals without seemingly disrupting movement. We must better understand the way in which sensory information influences the motor cortex, and how we should address this, especially for participants whose motor cortices might not get this input if not for ICMS.

Anecdotally, S1 ICMS does not affect our participants' ability to perform non-BCI motor actions; they are able to communicate and interact with their environment regardless of the amount of current being delivered. This is in stark contrast to the impact that stimulation has on

our decoder's ability to predict motor intent. Consequently, we must ask ourselves exactly what we are decoding from M1, the extent to which the nature of our participants' injuries might influence these signals, and how decoders should be adapted and improved to address these answers. To resolve these discrepancies, future experiments where participants are asked to perform voluntary movements in the presence and absence of ICMS can be used to assess the impact that it has on their behavior and the efficacy of our decoding models.

First, whether or not we observe perturbations in movement would provide a preliminary insight into the ways M1 is able to isolate the signal introduced by ICMS from that of motor intent. This knowledge can be used to build better decoders in the future that are able to flexibly incorporate sensory feedback. If we do observe perturbations in behavior as a result of ICMS, the extent to which these deviations match those produced by decoders, can be used to validate their ability to accurately decode motor intent. If the perturbations are different from those predicted by our decoder, we can use this to understand what aspects of behavior our decoder does or does not capture to inform better design in the future.

Overall, these studies will require more careful dissection of stimulation patterns, trials with and without these perturbations, more sophisticated decoders, and possibly access to larger neural populations, potentially distributed across many brain areas.